UNIVERSITÀ DEGLI STUDI DI PAVIA

Dipartimento di Biologia e Biotecnologie

"L. SPALLANZANI"

Identification of TFIIH-dependent transcriptional impairments in skin fibroblasts from patients affected by trichothiodystrophy

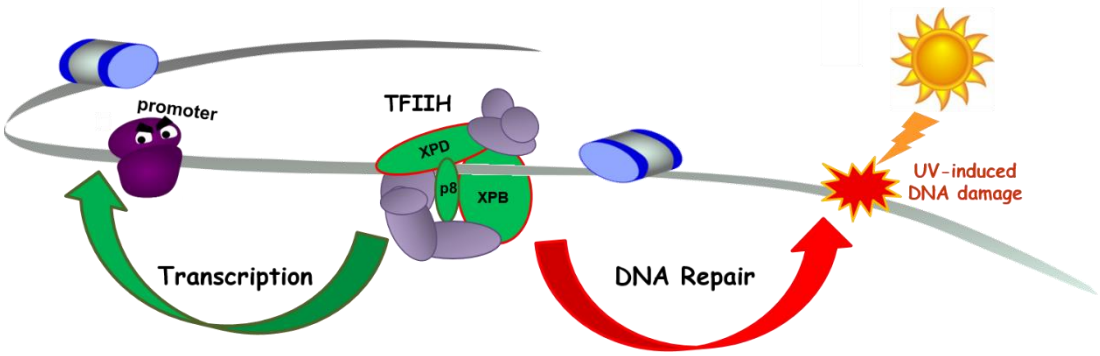

Anita Lombardi

Dottorato di ricerca in
Genetica, Biologia Molecolare e Cellulare
XXIX Ciclo (2013-2016)

UNIVERSITÀ DEGLI STUDI DI PAVIA
DIPARTIMENTO DI BIOLOGIA E BIOTECNOLOGIE
"L.SPALLANZANI"

Identification of TFIIH-dependent transcriptional impairments in skin fibroblasts from patients affected by trichothiodystrophy

Anita Lombardi

Supervised by Dr. Donata Orioli

Dottorato di ricerca in
Genetica, Biologia Molecolare e Cellulare
XXIX Ciclo (2013-2016)

Table of contents

ABSTRACT

The transcription factor IIH (TFIIH) is a multi-protein complex involved in basal transcription, gene expression regulation and nucleotide excision repair (NER), the only pathway in human cells devoted to the removal of DNA lesions induced by ultraviolet (UV) light. Mutations in genes encoding two TFIIH subunits, namely XPB and XPD, result in distinct autosomal recessive disorders, including the cancer-prone xeroderma pigmentosum (XP) and the multisystem disorder trichothiodystrophy (TTD), the latter one characterized by physical and mental retardation, premature ageing but no cancer. To explain how mutations in the same gene may result in distinct clinical phenotypes, it has been suggested that pathological features of XP are associated with mutations that mainly affect the repair activity of TFIIH, whereas those typical of TTD impair also transcription. Thus, XP and TTD patients represent a valuable model system to elucidate the TFIIH-dependent signalling pathways relevant to prevent carcinogenesis, developmental alterations and ageing.

To elucidate the causal relationship between gene expression alterations and TTD pathological phenotype, we took advantage of next-generation sequencing (NGS) technology to compare the RNAseq-based transcriptional maps of primary fibroblasts from one TTD patient female mutated in *XPD* (TTD7PV) and her healthy mother. In addition, we investigated how the transcriptional map is altered following UV irradiation in normal as well as in TTD fibroblasts. A detailed clustering analysis and functional classification of the genes that resulted to be deregulated in TTD revealed a large impairment of the transcriptional machinery, both in basal condition as well as after UV-induced DNA damage. Moreover, upon UV exposure, TTD fibroblasts fail to up-regulate the expression of several genes involved in transcriptional regulation processes. This finding is consistent with the idea of TTD being a transcriptional deficiency disorder.

The expression of the 176 genes showing the highest transcriptional deregulations in TTD7PV cells was further investigated by real time RT-PCR in primary fibroblasts from several TTD patients mutated in the *XPD* gene and with severe or moderate phenotype. By comparing gene expression profiles between TTD and their healthy parents, we identified a subset of genes whose transcriptional deregulation is associated to *XPD* mutations and therefore to TFIIH alterations. Next, we extended the analysis to primary fibroblasts from XP patients, thus defining transcriptional deregulations accounting for the TTD phenotype or common to TTD and XP. Since TFIIH complex plays a key role both in DNA repair and transcriptional regulation, we investigated whether the transcriptional

alterations previously identified in TTD fibroblasts are due to the persistence of unrepaired DNA lesions in specific genomic loci and the subsequent interference with the transcriptional apparatus activity or to a direct failure of transcriptional regulation. To clarify this issue, the distribution of γ-H2AX, a histone modification marking the sites of DNA damage, was investigated by ChIPseq analysis in fibroblasts from the TTD7PV patient and her healthy mother. We found that after UV irradiation there is a differential occupancy of γ-H2AX mainly at sub-telomeric or intrachromosomal regions of the genome. No specific enrichment of γ-H2AX is found in the loci of the transcriptionally deregulated genes, thus strengthening the hypothesis that TTD clinical features are caused by a direct transcriptional impairment of specific subset of genes and not by the interference of unrepaired DNA lesions.

Finally, the consequence of such transcriptional deregulations in TTD fibroblasts was further investigated at the protein level by immunoblot analysis. We observed that among the deregulated genes, few gave rise to an altered protein content, suggesting that protein synthesis or protein stability may compensate for a transcriptional impairment. Relevant of note, we demonstrated that all TTD fibroblasts contain reduced levels of PTGIS, a gene involved in vasodilation and inhibition of platelets aggregations as well as in adipocytes homeostasis. The finding that *PTGIS* down-regulation is a common feature of all TTD, suggests its possible involvement in TTD etiopathogenesis. Moreover, it opens the possibility of a novel diagnostic biomarker for this disorder.

Overall, our results identify specific transcriptional impairments that define the TTD expression profile, in basal condition as well as after UV-irradiation, and that contribute to explain in part the TTD pathological phenotype.

Acknowledgements

At the end of this work of thesis I want to thank all the people that have contributed in some way to the realization and have support me during my PhD years.

Foremost, I am grateful to my PhD supervisor Dr. Donata Orioli, to have chosen me the first time we met, for her great patience, the capacity to transmit her passion for that work, and also to share her immense knowledge. She is a fundamental guide and she supported me in any moment. I am aware of how like I was to have a boss like her.
I would like to thank the members of my group, which during the years, became also my friends. They contributed to render the laboratory day life very funny. I am grateful to Dr Lavinia Arseni, which is a super researcher, but most of all a dear friend. She has touched me how to behave in the lab, she shared all her knowledges and she was a constant reference for all the problems. Thank you to Dr. Martina Uggè for all the things that we have shared and just to be completely out of schemes!!! I want to thank Dr. Manuela Lanzafame which is always ready to solve my scientific doubts and to transmit her joy and enthusiasm for the research. Many thanks to Dr. Tiziana Nardo, the unique referee for the cells and the patients; she always renders the environment in lab very cool!!!!Thank you to Dr. Elena Botta for her infinite patience and a great capacity to tolerate some extrovert behaviours. Thanks to Dr. Fiorenzo Peverali for his kindness and his stimulating discussions. Thanks to all the other past and present members of the lab and the people I have had the pleasure to work with.

I want to thank also Dr. Margherita Bignami and Dr. Emmanuel Compe to have accepted to be the external referees for the thesis. They kindly contribute to improve the manuscript and they give me an important and meaningful outcome for my work.

Ed ora passiamo ai ringraziamenti meno formali, ma allo stesso modo importanti. Ringrazio di nuovo e per altri motivi Martina e Bart, i miei compagni di viaggio, senza i quali avrei fatto fatica a immaginare un percorso così divertente e stimolante.

Ringrazio i miei amici di sempre, per il fatto di esserci e di rappresentare una parte fondamentale e irrinunciabile della mia vita.

Ringrazio la mia famiglia per tutto quello che ha fatto per me, sostenendomi in ogni momento e in qualsiasi situazione. Un ringraziamento particolare va a mio padre, per avermi sempre incoraggiata in tutto ed aver creduto in me; a mia madre, per essere il mio punto di riferimento costante, e a mia sorella, che a modo suo, riesce a sopportarmi e supportarmi.

Abbreviations

6-4 PPs	pyrimidine(6-4)pyrimidone photoproducts
4FeS	iron-sulfur cluster binding domain
aa	aminoacids
AfXPB	*Archaeoglobus fulgidus* XPB
ATP	adenosine triphosphate
BSA	bovine serum albumin
CAF1	Chromatin assembly factor 1
CAK	CDK activating kinase
CBP	CREB binding protein
Cdc	Cyclin
CDK	Cyclin-dependent kinase
cDNA	complementary DNA
ChIP	chromatin immunoprecipitation
COFS	Cerebro-oculo-facial-skeletal syndrome
COL	collagen
CPDs	cyclobutane pyrimidine dimers
CRL	cullin-RING E3 ligase
CS	Cockayne syndrome
CSB	Cockayne syndrome type B protein
CSN	COP9 signalosome
Ct	Treshold cycle
CTBP	C-terminal binding protein
CTCF	CCCTC-binding factor
CTD	carboxy-terminal domain
CYP24	Cytochrome P450 family 24
Da	Dalton
DMSO	dimethylsulfoxide
DNA pol	DNA polymerase
dsDNA	double-stranded DNA
DTT	dithiothreitol
E3-ub ligase	E3-ubiquitin ligase; CSA
ECM	Extracellular matrix
EDTA	ethylenediaminetetraacetic acid
ER	estrogen receptor
FBP	FUSE-binding protein
FBS	fetal bovine serum
FC	Fold change

FCP1	TFIIF-associated CTD phosphatase 1
FEN1	I-flap endonuclease 1
GAG	glycosaminoglycan
GGR	Global genome repair
GTF	general transcription factor
HBV	Hepatitis B virus
HBX	Hepatitis X protein
HD	Helicase domain
HEPES	4-(2-hydroxyethyl)-1-piperazineethanesulfonic acid
HGF	Hepatocyte growth factor
HMGN1	high-mobility group nucleosome-binding domain-containing protein-1
HRP	Horseradish-peroxidase
IP	immunoprecipitation
lncRNA	Long non coding RNA
LOX	Lysyl oxidase
LTBPs	Latent transforming growth factor beta binding protein
m7G	7-methylguanosine
miRNAs	microRNAs
MMP	Matrix metalloproteinase
mRNA	messenger RNA
MTA1	Metastasis-associated protein 1
NER	nucleotide excision repair
NMSC	nonmelanoma skin cancer
NP-40	Nonidet P40
NRs	Nuclear receptors
NSC	Neural stem cell
nt	nucleotide
NTP	nucleoside triphosphate
PAGE	polyacrylamide gel electrophoresys
PBS	phosphate buffer saline
PCNA	Proliferating Cell Nuclear Antigen
PCR	Polymerase chain reaction
PDGF	Platelet-derived growth factor
PGC1α	PPARγ co-activator 1α
PH	Pleckstrin homology
PIC	Pre-initiation complex
PMA	Phorbol myristate acetate
pTEFb	Positive transcription elongation factor b
PTM	Post-translational modification
RNApol	RNA polymerase

RPA	Replication protein A
RPAP2	RNApol II-associated protein 2
rRNA	ribosomal RNA
RT	Reverse transcription
SDS	sodium dodecyl sulfate
snRNA	small nuclear RNA
SREBP-1	Sterol regulatory element-binding protein-1
ssDNA	single-stranded DNA
Ssl1	Suppressor of stem–loop protein 1
TAF	TBP-associated factor
TAFs	TBP Associated Factors
TBP	TATA binding protein
TCR	transcription-coupled repair
Tfb	Trascription factor b
TFIIH	transcription factor for II H
TGF	Transcription growth factor
TIE	TGF-β inhibitory element
TMB	3,3’,5,5’-tetramethylbenzidine
Tris	tris(hydroxymethyl)aminomethane
tRNA	transfer RNA
TSS	transcription start site
TTD	tricothiodystrophy
TTDN1	TTD non-photosensitive 1
UDS	UV-induced DNA repair synthesis
UPL	Universal probe library
UV	ultraviolet
UV-DDB	UV-light damaged DNA binding protein
VEGF	Vascular endotelial growth factor
VP16	Virion protein 16
XP	xeroderma pigmentosum
XRCC1	III-X ray repair cross-complementing protein 1

1. INTRODUCTION

DNA is organized into complex structure by folding it into chromatin fibers, made up of strings of nucleosomes. They represent the basic unit of DNA packaging, which consists of DNA wound around a protein structure formed by histones (Figure 1). The nucleosomes represent one of the features that allow eukaryotic cells to tightly regulate gene expression. Although the organization of nucleosomes appears rigid, these repeating subunits of chromatin are very dynamic. DNA replication, transcription and DNA repair occur within the chromatin structure and are important for cellular homeostasis, cell proliferation but also to prevent accumulation of mutations.

A rigid regulation of chromatin structure is exerted by epigenetic perturbations, by means of post-translational modifications (PTMs) such as phosphorylation, acetylation, methylation and ubiquitylation as well as displacement of histones or entire nucleosomes (Bannister et al, 2011; Sidoli et al, 2012; Dinant et al, 2008) (Figure 2).

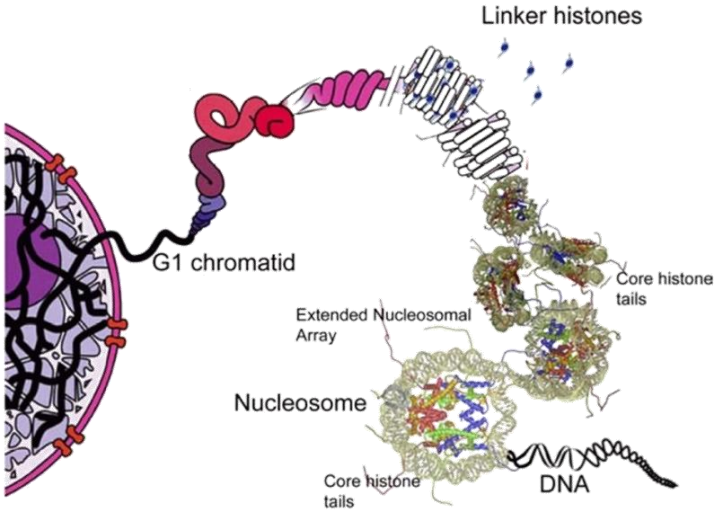

Figure 1. Schematic representation of chromatin and its different organization levels.

In addition, architectural chromatin proteins (ACPs), ATP-dependent chromatin remodellers and histone chaperonins could alter the chemical nature and the physical properties of nucleosomes, either by acting individually or in combination with one another. There are two proposals for the mechanistic function of these modifications.
One is that the chromatin packing is altered by regulating the electrostatic charge or the internucleosomal contacts directly, thus controlling the accessibility of DNA polymer and the binding of DNA signalling molecules. The other is that the attached chemical moieties alter the nucleosome surface and promote the association of chromatin binding proteins. Thus, replication and transcription come close to chromatin dynamic structure and require a constant cross-talk to other basic cellular processes to facilitate their coexistence.

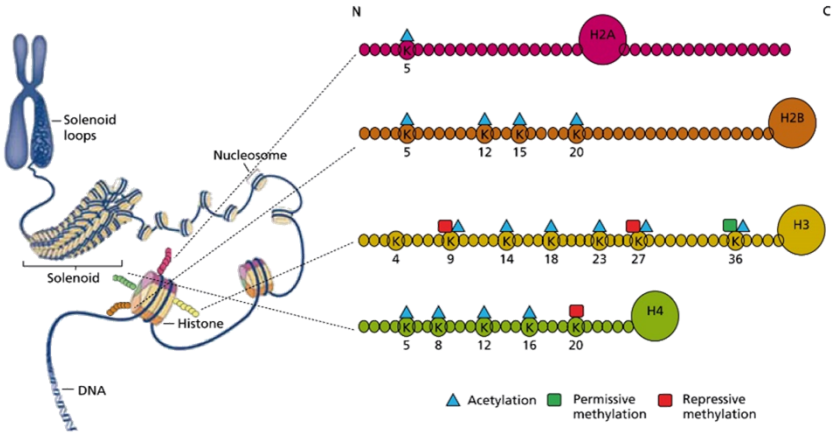

Figure 2. Schematic representation of most relevant histone modifications.

Next to a clear function in transcription regulation, chromatin dynamic is also involved in DNA damage detection and DNA repair. In the context of chromatin, the double helix of DNA is connected to a core histones made up of H2A, H2B, H3 and H4. Histone fold undergoes several types of hydrophilic modifications, which control many functions. Despite the highly conservation of histones among species, many organisms produce several variant histones, which have a crucial role in many chromatin processes. Thus, histone modifications and chromatin remodelling are

well characterized in the context of DNA repair. The hallmark of DNA damage response (DDR) related to epigenetic change is phosphorylation of H2AX. It is known that γ-H2AX marks the accumulation sites of DNA damage and carry on the activation of many signalling damage molecules. In addition, the acetylation of several histones participates in the global chromatin relaxation to allow access of proteins to the damaged DNA, whereas the methylation of histones serve as a sensor to detect an abnormal chromatin relaxation state.
Besides these epigenetic changes, a relevant key player factor in different DNA processes is the TFIIH complex (Figure 3), which is involved in basal transcription, transcription regulation and DNA repair. TFIIH is a good example of cross-talk between two different DNA-metabolic processes, whose regulation is crucial for development. In addition, defects related to TFIIH mutations can lead to human deseases.

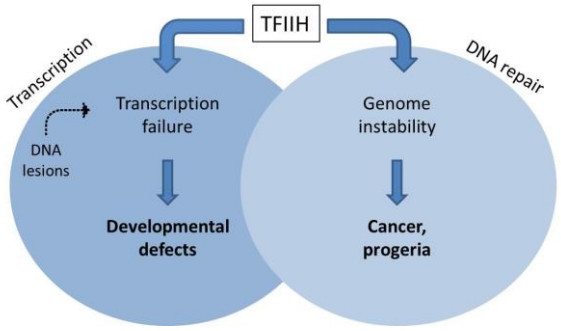

Figure 3. TFIIH defects and their impact on development and disease.

The broad spectrum of mutations in genes encoding the different subunits of TFIIH are responsible of several disorders, known as xeroderma pigmentosum (XP), trichothiodystrophy (TTD) and Cockayne Syndrome (CS) that are characterized by neurological dysfunction, immunodeficiency, reproductive and growth defects, premature ageing and in some cases cancers.

2. Review of the literature

The transcription factor IIH (TFIIH) is a multi-protein complex involved in several fundamental cellular processes. First studied for its implication in RNA polymerase (RNApol) II transcription initiation and regulation, it was then demonstrated to have a fundamental role in nucleotide excision repair (NER), the only pathway in mammalian cells that removes bulky DNA adducts induced by ultraviolet (UV) light or electrophilic chemicals. Therefore, TFIIH is a key factor acting at the cross-talk between transcription and NER, likely involved in coordinating the events that take place at the beginning of NER pathway with the repression of transcription. Moreover, it is becoming more and more evident that TFIIH plays an essential role also in regulating the expression of specific sets of genes, in supporting the RNApol I transcription and in regulating the cell cycle progression.

2.1 THE GENERAL TRANSCRIPTION FACTOR IIH (TFIIH)

2.1.1 The structure

Mammalian TFIIH is a multi-protein complex made of ten subunits organized in two main functional sub-complexes: the core-TFIIH, composed of six subunits (XPB, p62, p52, p44, p34 and p8) and the CAK (CDK-activating kinase complex), containing the cyclin dependent kinase (CDK) 7, cyclin H and Mat1 subunits (Schultz et al., 2000). The core and CAK sub-complexes are bridged by the XPD subunit, which interacts with p44 and Mat1 of the core and the CAK sub-complex, respectively (Compe and Egly, 2012). The eleventh subunit of TFIIH, named Tfb6, was identified in yeast but no human homolog has been found so far. It dissociates from the complex together with Ssl2, the yeast homolog of XPB, as transcription activation by RNApol II occurs (Murakami et al., 2012). Electron microscopy (EM) and image processing revealed that TFIIH complex has a total mass of 0.5 MDa and its structure appears as a slightly elongated flat particle 16 × 12.5 × 7.5 nm in size (Schultz et al., 2000). In particular, the core-TFIIH is organized into a ring-like structure with a 2.5-3.5 nm wide central hole sized to accommodate a double-stranded DNA (dsDNA) molecule (Figure 4).

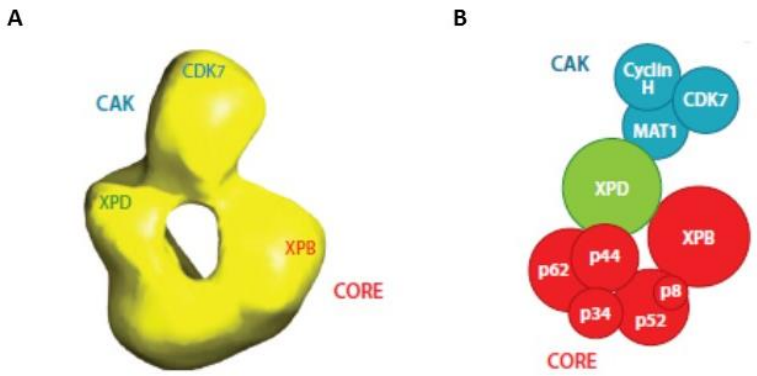

Figure 4. The TFIIH complex: model of the quaternary organization of TFIIH **(A)**, indication of the positions CDK7, XPB and XPD subunits **(B)** and schematic representation of the complex (adapted from Compe and Egly, 2016).

Intrinsically, TFIIH possesses several enzymatic subunits: CDK7 is a cyclin-dependent kinase acting during transcription and cell cycle progression; XPD is an ATPase/helicase subunit and the XPB is an unconventional ATPase/helicase, which has been proposed to act as double-stranded DNA (dsDNA) translocase (Fishburn et al., 2015). The various enzymatic activities of TFIIH are tightly modulated by interactions with many components of the transcription machinery, including general and regulatory transcription factors as well as by contacts within the TFIIH complex. These enzymatic activities are regulated for local DNA unwinding, either around the promoter to allow the mRNA synthesis by RNApol II, or around a damaged site to permit DNA cleavage on either side of the lesion by specific nucleases. Mutations in TFIIH subunits that interfere with the biochemical functions of this complex may contribute to the pathogenesis of TTD, XP and combined phenotypes (XP/CS, XP/TTD).

Consistent with its key roles in fundamental cellular processes, TFIIH is an evolutionarily well-conserved complex, whereas some subunits (XPB, XPD and CDK7) exert a significant amino acid conservation among species, and other ones (such as p8, p34, CyclinH, and p62) show the highest interspecies variability. We will proceed by describing in detail the various TFIIH subunits, that are summarized in Table 1, their PTM and the protein-protein interactions (Stefanini et al., 2010).

Table 1. Composition of the TFIIH complex

TFIIH	Human	Yeast	Function	Human genetic disorders
Core	XPB	Ssl2	3′ to 5′ ATP-dependent traslocase	TTD and XP/CS
	p62	Tfb1	Structural function and interacts with transcription factors and NER factors	
	p52	Tfb2	Regulates the ATPase activity of XBP	
	p44	Ssl1	In yeast, E3 ubiquitin ligase	
	p34	Tfb4	Structural function and strong interaction with p44	
	p8	Tfb5	Regulates the ATPase activity of XBP	TTD
XPD	XPD	Rad3	5′ to 3′ ATP-dependent helicase. Forms a bridge between CAK and core	TTD, XP and XP/CS XP/TTD
CAK	CDK7	Kin28	Kinase activity	
	Cyclin H	Ccl1	Modulates the CDK7 kinase activity	
	MAT1	Tfb3	In yeast, stabilizes CAK and regulates cullin neddylation	

Abbreviations. CAK, cyclin-dependent kinase-activating kinase subcomplex; Ccl1, cyclin C like 1; CDK7, cyclin-dependent kinase 7; MAT1, ménage à trois 1; NER, nucleotide excision repair; Ssl, suppressor of stem-loop protein; Tfb, RNA polymerase II transcription factor b; XPB, xeroderma pigmentosum group B complementing protein; TTD, trichothiodystrophy; XP, xeroderma pigmentosum; CS, Cockayne syndrome.

2.1.1.1 The core-TFIIH sub-complex

XPB (782 aa) is the largest subunit of the core-TFIIH with a molecular weight of 89 kDa. With its seven conserved ‘helicase motifs’ (Walker motifs I, Ia, II, III, IV, V, and VI) structurally organized in two helicase domains, HD1 and HD2, it belongs to the SF2 superfamily of monomeric helicases. In addition to helicase motifs, one of which being the ATP binding site, XPB contains two additional motifs: the well-

conserved R-E-D residue loop (at amino acids 472-474) and the positively charged thumb (ThM) region (at amino acids 514-537). The RED motif is proposed to introduce a wedge in the dsDNA that is then gripped by the ThM domain.
It has been suggested that the ATPase activity of XPB induces a conformational change in the pre-initiation complex (PIC), leading to an open-complex formation. Alternatively, another study suggests that XPB acts as a dsDNA translocase to exert its function in DNA opening (Compe et al., 2016).
Moreover, XPB contains a conserved DNA-remodeling domain, the HepA-related protein (HARP) domain, which is able to recognize the distortion of double strand DNA (dsDNA) molecules and facilitate the DNA unwinding (Mason et al., 2014). Within the TFIIH complex, XPB is located in the ring structure, in close proximity to the p44 subunit and on the opposite side of XPD. XPB is an ATP-dependent 3'-5' DNA helicase that is required for anchoring TFIIH to chromatin around the transcription start site. In NER the helicase activity of XPB is dispensable whereas its ATPase activity, in combination with the helicase activity of XPD, is needed to remove the DNA lesions (Coin et al., 2007). XPB activity is post-transcriptionally regulated, indeed the C-terminal region of XPB protein is phosphorylated *in vivo* on Ser751 and it has been shown that this PTM inhibits the TFIIH DNA repair activity (Coin et al., 2004). Moreover, previous studies have demonstrated that the fusion protein p210 BCR/ABL1 interacts directly with XPB, and that XPB is phosphorylated in cells expressing p210 BCR/ABL1. More recently, it has been shown that a p210 BCR/ABL1 mutant lacking the XPB-binding site show decreased *c-MYC* expression and reduced ability to drive myeloproliferation and lymphoproliferation in murine models for CML and B-cell acute lymphoblastic leukemia (B-ALL). However, this mutated form of p210 BCR/ABL1 still maintained its ability to regulate the NER pathway. Since cells expressing the XPB-binding mutant show lower levels of XPB phosphorylation on tyrosine, it is possible that p210 BCR/ABL1 transformation is influenced directly by XPB-associated activities, which may be altered by phosphorylation (Pannucci et al., 2013).
p62 (548 aa) is a subunit of the core-TFIIH complex. Probably located at the basis of the ring, it interacts with both XPD and p44 subunits of the TFIIH complex.
The relevance of p62 in the NER pathway is highlighted by the use of yeast cells. Deletion of the C-terminal region (residues 532-642) of Tfb1, the yeast homolog of p62, leads to a mutant (*tfb1-1*) with decreased resistance to both temperature and UV irradiation. Tfb1 directly interacts with Rad2, the yeast homolog of the NER factor XPG, and the binding involves several segments of Rad2 spacer region as well as the pleckstrin homology (PH) domain of Tfb1 (residues 1-108). Indeed, deletion of the PH domain of Tfb1 leads to a reduced DNA repair activity of XPG *in vitro* (Lafrance-Vanasse et al., 2012). The PH domain of p62 subunit interacts also with Rad4, the yeast homolog of the XPC NER factor, and this supports the hypothesis

that a competition occurs between Rad4 and Rad2 to bind the PH domain (Lafrance-Vanasse et al., 2013). Moreover, the PH domain of p62 binds the acidic-rich domains of several transcriptional regulatory proteins, including the alpha subunit of the general transcription factor IIE (TFIIEα), the tumor suppressor protein p53 and the Herpes Simplex Virion protein 16 (VP16, Di Lello et al., 2008; Langlois et al., 2008). It was reported that p62 is a substrate for mitotic phosphorylation *in vitro* and that it is a potential target for Cdc2 phosphorylation (SPEGK, amino acids 56-60). In addition, the p62 subunit is also essential for TFIIH functioning in transcription, it is required for the recruitment of TFIIH to the pre-initiation complex (PIC) through TFIIE and mediates the interaction of TFIIH with transcriptional trans-activators.

p44 (395 aa) is a well-characterized subunit of the core-TFIIH. It is part of the ring structure and is located in close proximity to the bulge region, flanked on either side by the XPD and XPB helicases. The essential role of p44 in NER was sustained by the discovery that a mutation in its yeast counterpart (Ssl1) conferred UV sensitivity. Mutations in the N-terminal moiety of p44 or in the C-terminal end of XPD prevent p44 interaction with XPD thus affecting the optimal XPD helicase activity and resulting in TFIIH instability. Indeed, through the crystal structure of the N-terminal regulatory domain of *S. cerevisiae* Ssl1, Kim and colleagues demonstrated that the β4-α5 loop structure of Ssl1/p44 is important for the binding and stimulation of Rad3/XPD, and it is well known that the interaction between Rad3/XPD and Ssl1/p44 is critical for cell viability (Kim et al., 2015).

Moreover, the C-terminus region of p44 contains a highly conserved cysteine-rich domain (residues 252-395) that, by NMR studies, hold a RING finger motif (Fribourg et al., 2000). Mutations within the C4 zinc finger motif (residues 291-308) prevent incorporation of the p62 subunit within the core-TFIIH whereas double mutations in the RING finger motif (residues 345-385) allow the synthesis of the first phosphodiester bond by RNApol II, but prevent its escape from the promoter. The solution structure of p44-(321-395) shows that its topology differs from that of other reported RING domains (Kellenberger et al., 2005). It has been suggested that p44 nucleates the formation of TFIIH complex through interaction with p34, p62, XPB and XPD; the tight binding to p34 is mediated by the p44 C-terminal domain. In addition, the C-terminal region of p44 was found to interact with SCL, a hematopoietic transcription factor containing a basic helix-turn-helix motif (Fribourg et al., 2000). Thus, the p44 subunit plays a central role within TFIIH, by interacting with almost all the other subunits of the core-TFIIH both in human and in yeast (Tremeau-Bravard et al., 2001). In yeast, p44 has an E3 ubiquitin ligase activity that is important for the transcription of DNA damage-response genes. This activity confers to TFIIH an additional role in regulating gene expression after DNA damage but it does not impair its activity in NER (Takagi et al., 2005). To date, no evidence of such p44 enzymatic activity has been reported in higher eukaryotes.

Finally, it has recently been shown that p44 mRNA is regulated by miR-27a during the G2-M phase, thereby modulating the cellular transcriptional shutdown observed during this transition of the cell cycle (Portal, 2011).

p52 (462 aa) is another subunit of core-TFIIH. Through its C-terminal region, it interacts and anchors XPB to the core. Integrity of p52 is a prerequisite for the presence of XPB in the core. Indeed, it has been shown that deletion of the C-terminal region of p52 is detrimental for the DNA repair and transcription activities of TFIIH. Mutations in the *Drosophila* homolog of p52, Dmp52, destabilize its interaction with XPB and result in a fly with UV sensitivity, cancer proneness, brittle-bristle with cuticular-deformation and developmental defects (Fregoso et al., 2007). Recent evidence suggests that in absence of genotoxic stress Dmp52 physically interacts with the fly p53 homologue (Dp53), whose depletion increases apoptosis and chromosome fragility in *Drosophila* cells (Villicana et al., 2013). Another role of p52 involves the modulation of XPB ATPase activity, through its interaction with TTDA/p8 (Coin et al., 2007; Nonnekens et al., 2013).

The **p34** (308 aa) subunit contains various zinc-finger motifs, which probably mediate the interaction of core-TFIIH with the DNA. It is difficult to infer the precise localization of the p34 polypeptide since it is not consistent with a simple model where each subunit should have two and only two partners. An interaction between p44 and p34 was reported, suggesting that p34 is placed on the ring next to p44 and probably on the opposite side of the bulge than XPD, close to XPB (Kellenberger et al., 2005). Recent studies clarified the structure of p34 from the eukaryotic thermophilic fungus *Chaetomium thermophilum* revealing a fundamental von Willebrand factor A-like domain. This domain is known to be generally involved in protein-protein interactions (Schmitt et al., 2014). Moreover, sequence analysis of phylogenetic distribution of core-TFIIH in different eukaryotic organisms suggested that the implication of the core-TFIIH in mRNA splicing is mediated by p34 subunit (Bedez et al., 2012).

TTDA/p8 (71 aa) is the smallest subunit of core-TFIIH. It interacts with p52 (Nonnekens et al., 2013) and XPD subunits and is present in two distinct kinetic pools: bound to TFIIH, or in a free fraction that shuttles between the cytoplasm and nucleus. After induction of NER-specific DNA lesions, the equilibrium between these two pools dramatically shifts towards a more stable association of TTDA/p8 to TFIIH. In contrast, the cellular transcriptional activity does not influence this equilibrium (Giglia-Mari et al., 2006). Following DNA damage, the nuclear TFIIH complex stabilized by TTDA/p8 stimulates the ATPase activity of XPB and promotes the local opening of the DNA around the lesion, a prerequisite for the recruitment of XPA to the site of damage (Coin et al., 2006). Thus, the major role of TTDA/p8 is to stabilize the TFIIH complex and to maintain the steady-state cellular levels of TFIIH (Aguilar-Fuentes et al., 2008). TTDA/p8 has been for long

considered as the only TFIIH subunit not essential for NER, transcription or viability. However, in a recent paper from Theil and colleagues, it has been shown that TTDA/p8 is instead a crucial component of TFIIH for life, NER and oxidative DNA damage repair (Theil et al., 2013).

2.1.1.2 The CAK sub-complex

CDK7 (346 aa), or cyclin-dependent kinase 7, is a 40 kDa protein located in the protruding domain of the TFIIH complex. It belongs to a large family of proteins exhibiting serine/threonine kinase activity and containing a typical kinase bi-lobed fold comprising the N-terminal lobe (residues 13-96) with mostly β-sheet and one α helix and a C-terminal lobe (residues 97-311) characterized mostly by α helices. The ATP is bound between the two lobes. The N-terminal lobe contains a glycine-rich region (G-loop) with regulatory function while the C-terminal lobe contains the activation segment and includes the phosphorylation-sensitive residue in the so-called T-loop, in the kinase VIII sub-domain. In the cyclin-free monomeric form the cyclin dependent kinase (CDK) catalytic cleft is closed by the T-loop, preventing enzymatic activity (Lolli et al., 2004, Malumbres et al., 2014). CDK7 restrains the enzymatic activity of CAK sub-complex and its function depends upon its association with cyclin H and Mat1, the other CAK subunits. Similarly to the other CDKs, CDK7 is activated by the binding to cyclin H and by the phosphorylation on the T-loop domain by a CDK-activating kinase. Differently from the other CDKs, CDK7 has an additional phosphorylation site on serine 164 (Ser164), but this phosphorylation is not required for the CDK7 interaction with cyclin H or for its activation *in vitro* and is detrimental for TFIIH activity during mitosis (Larochelle et al., 2001). In contrast, phosphorylation on Thr170 is essential for the CDK7 kinase activity. Also the association of Mat1 protein to the CDK7/cyclin H complex result in the *in vitro* activation of CDK7 kinase. In conclusion, for maximum activity and stability, CDK7 requires phosphorylation, association with cyclin H and association with Mat1 (Lolli et al., 2004).
Different kinases were shown to phosphorylate CDK7, namely the CDK2/Cdc2 complex, which targets both Thr170 and Ser164 in CDK7 T-loop (Garret et al., 2001) and the peculiar Protein Kinase C-iota (PKCι) that targets the Thr170 of CDK7 (Pillai et al., 2011). During transcription, BRCA1 C-terminal region was observed to interact with CAK and inhibit its activity (Moisan et al., 2004), while Myc transcription factor has been identified as a positive regulator (Cowling et al., 2007). Therefore, CDK7 plays a pivotal role in different cellular processes, such as transcription activation/regulation as well as cell cycle progression, through the tightly controlled phosphorylation of specific target proteins.

As part of the holo-TFIIH complex, CDK7 fulfills its functions in transcription by assisting the RNApol II-driven transcription. CDK7 phosphorylates the carboxyl-terminal domain (CTD) of the largest subunit of RNApol II, Rpb1, on Ser5 residues to activate transcription initiation. TFIIH-associated CDK7 is an essential part of the mechanism that establishes promoter-proximal pausing and affects pausing and termination downstream of the gene (Glover-Cutter et al., 2009). In RNApol II-driven transcription, CDK7 also phosphorylates the general transcription factors TBP (*TATA Binding Protein*), TFIIE and TFIIF. Furthermore, TFIIH-associated CDK7 participates in the regulation of hormone-dependent genes by phosphorylating nuclear receptors such as the retinoic acid receptor (RARα), the estrogen receptor (ERα), the peroxysome proliferator-activated receptors (PPARs). Even more, as part of the holo-TFIIH complex, CDK7 phosphorylates specific transcription factors, like Ets1 on the promoter of specific target genes trans-activated by the vitamin D receptor (Dranè et al., 2004), whereas as part of the CAK sub-complex, it phosphorylates the p53 transcriptional regulator protein (Ko et al., 1998). The remaining two subunits of the CAK sub-complex, cyclin H and Mat1, are both regulators of CDK7 kinase activity.

Cyclin H (323 aa) is a protein of 38 kDa. The binding of cyclin H to CDK7 results in the activation of CDK7 kinase, thus making cyclin H as a positive regulator. Structurally, cyclin H contains a highly conserved core made of two characteristic α-helical domains called Repeat 1 and Repeat 2, each containing five helices, which adopt the so-called cyclin-fold topology. Cyclin H also contains a third domain essential for the CDK7 activation formed by two long helices, the HN and HC helices that pack against Repeat 1 and are located respectively at the N- and C-termini of the molecule (Kim et al., 1996). Cyclin H is phosphorylated *in vivo* and *in vitro* on Ser5 and Ser304 by the cyclin C/CDK8 complex. These residues are located in close proximity to the HN and HC helices, which are uniquely orientated in cyclin H as compared with other cyclins. Phosphorylation of cyclin H on Ser5 and Ser304 results in the inhibition of TFIIH transcriptional activity. Furthermore, cyclin H is also phosphorylated on the Thr315 residue by the protein kinase CK2. This phosphorylation appears necessary to achieve full kinase activity of the TFIIH and CAK complex with respect to RNApol II-CTD and CDK2 phosphorylation, respectively (Schneider et al., 2002). Putative nuclear localization signals (NLSs) have been identified as responsible of the protein translocation from cytoplasm to nucleus. The presence of the PTMs in closed proximity to the NLS does not seem to affect cyclin H transport to the nucleus (Krempler et al., 2005). The role of Cyclin H is not limited to the interaction and activation of CDK7 but several other proteins have been found to be regulated by Cyclin H. Cyclin H binding to the ligand-binding domain (LBD) of the RARα is essential for TFIIH recruitment and subsequent

phosphorylation by CDK7 of the RARα N-terminal domain. This PTM is required for RARα regulated transactivation (Chebaro et al., 2013).

Interestingly, the p53 protein was shown to interact with Cyclin H in association with CDK7 and hence to reduce the CDK7 kinase activity towards CDK2 or CTD substrates (Schneider et al., 1998). Another peculiar interaction observed for cyclin H involves U1 snRNA and results in increased stability of the cyclin H/CDK7 complex along with increased kinase activity in transcription (O' Gorman et al., 2005). Cyclin H has also a critical role in maintaining embryonic stem (EC) cell identity and suggested relevant functions for Cyclin H in early embryonic development (Patel and Simon, 2010).
Both cyclin H and CDK7 have been implicated in the regulation of cancer metastasis. CDK7 appeared to promote the migration of ovarian cancer cells *in vitro* (Collins et al., 2006). Cyclin H over-expression was noted *in vivo* in endometrial adenocarcinoma with lymphvascular space invasion (Kayaselcuk et al., 2006). More recently, it has been shown that the cyclin H/CDK7 complex can influence migratory and invasive potential of cancer cells through the interaction with CtBP, a transcriptional co-repressor that determines the outcome of oncogenic transformation (Wang et al., 2013).

Mat1 (menage à trois 1, 309 aa) is a RING finger protein of 36 kDa and a characteristic C3HC4 motif located at the N-terminal region. In the central portion of Mat1 there is a coiled coil domain that was suggested to mediate the contact between the cyclin/kinase complex and the core-TFIIH, through the XPD subunit. The coiled-coil domain of Mat1 also interacts with the C-terminal half of Mat1-mediated transcriptional repressor (MMTR), which is known to inhibit the TFIIH-mediated transcriptional activity. Furthermore, MMTR has been also shown to be an intrinsic negative regulator of cell cycle progression that modulates the CAK kinase activity through the interaction with Mat1 (Shin et al., 2010).
Differently from cyclin H, no putative NLS sequences have been found in Mat1 and its nuclear import mechanism is still unclear (Krempler et al., 2005). Mat1 facilitates the assembly of the CDK7/cyclin H/Mat1 trimeric complex and is required *in vivo* to stabilize a functional CAK.
Moreover, it was shown that Mat1 is involved in defining the substrate specificity of CDK7. Deletion of Mat1 in mouse fibroblasts leads to dramatically reduced phosphorylation of RNApol II-CTD on Ser5, highlighting the role of Mat1 in general transcription (Helenius et al., 2011).

2.1.1.3 The bridging factor XPD

XPD (760 aa) is a 80 kDa subunit that has ATP-dependent DNA helicase activity. Within the TFIIH complex, XPD is located close to the CAK sub-complex and acts by bridging the CAK sub-complex to the core-TFIIH. Indeed, XPD interacts with the p44 subunit of the core and with the Mat1 subunit of the CAK, as attested by mutations in the C-terminal end of XPD that prevent the anchoring of the CAK (Coin et al., 1998). Structural studies on XPD protein revealed a four-domain structure consisting of two canonical helicase domains (HD1 containing the helicase motif I, Ia, II and III and HD2 containing the helicase motif IV, V and VI), the Arch domain (amino acids 47-49) and the fundamental as well as peculiar N-terminal 4Fe4S cluster (amino acids 82-148), coordinated by four cysteine residues. The 4Fe4S cluster is sensitive to oxidation and influences XPD protein stability (Feltes et al., 2015). It has been proposed that the 4Fe4S cluster uses DNA charge transport to verify the presence of DNA lesion during the NER process (Sontz et al., 2012). *In vitro* and *in vivo* assays demonstrate that mutations in the 4Fe4S cluster domain of XPD abrogate the TFIIH function in NER but do not affect its transcriptional activity, further supporting the idea that XPD helicase is uniquely dedicated to NER and is dispensable for transcription (Kuper et al., 2014). The Arch domain, involved in protein-protein interaction, has been shown to act as an anchoring platform for the CAK sub-complex mediated by the interaction with Mat1. The DNA molecule is thought to move through the XPD hole formed by the Arch domain, the 4Fe4S cluster and HD domain (Spies et al., 2014), in a recognition pocket scanning individual single DNA strands for the presence of bulky adducts (Mathieu et al., 2013).
Several lines of evidence suggest a function for XPD in regulating the assembly/disassembly of the CAK and core-TFIIH sub-complexes. It was shown that TFIIH disassembles into CAK and core-TFIIH during the NER pathway, a mechanism that might be involved in negatively regulating transcription during the DNA repair process. The current hypothesis suggests that XPD is repressed when CAK is part of the TFIIH complex, and that the Arch domain of XPD participates in the fine tuning of TFIIH enzymatic activities acting as molecular switch between transcription and NER (Abdulrahman et al., 2013). It has been shown that in *Drosophila* the down-regulation of XPD in mitosis results in increased CAK activity and cell proliferation whereas its overexpression negatively regulates the cell-cycle activity of CDK7 (Fuss and Tainer, 2011). The 5’ to 3’ DNA helicase activity of XPD plays a crucial role in NER, where it generates an open DNA structure around the lesion and enables the recruitment of the NER endonucleases XPG and XPF. Indeed, Mathieu and collaborators identified critical amino acids by which XPD discriminates between undamaged and damaged DNA substrates, thus the authors

proved that this DNA helicase subunit of TFIIH serves as a general damage verifier in the NER pathway (Mathieu et al., 2013). In contrast, the helicase activity of XPD resulted dispensable for the *in vitro* basal transcription even if it appears to facilitate optimal transcription by stabilizing the holo-TFIIH. Interestingly, XPD plays crucial roles in protecting mitochondrial genome stability by facilitating an efficient repair of oxidative DNA damage in mitochondria (Liu et al., 2014). Moreover, XPD was found as part of the recently discovered MMXD complex. It is composed by XPD, MMS19, MIP18, Ciao1 and ANT2, and MMXD localizes to the mitotic spindle where it is involved in the correct chromosomal segregation and nuclear shape formation. While it was proposed that the MMXD complex plays an active role in mitosis, it is also plausible to think that MMXD may sequester XPD when free CAK activity is required and TFIIH-dependent transcription needs to be silenced.
No one of the other TFIIH subunits is recruited to the MMXD complex (Ito et al., 2010). Finally, it was revealed that a specific subset of XPD alterations, which lead to the TTD and not to XP phenotype, result in higher risk of development of preeclampsia and other gestational complications possibly because they prevent XPD binding with CAK and p44 subunit, thus leading to impairment of TFIIH-mediated functions in placenta (Moslehi et al., 2012). *In vitro* studies showed that polymorphisms in the *XPD* gene influence cell proliferation, DNA repair and other responses after X-irradiation of human lymphocytes (Gdowicz-Klosok et al., 2013).

2.2 FUNCTIONAL ROLES OF TFIIH

TFIIH is an intriguing complex because it participates in transcription, NER and cell cycle regulation. The flexibility of the complex makes it able to participate in various distinct cellular processes and maintain a delicate crosstalk between transcription and DNA repair. In highly differentiated post-mitotic cells, such as neurons, hepatocytes and cardiac myocytes, TFIIH is immobilized on chromatin at sites of RNApol I and RNApol II transcription. Although statically bound, TFIIH can be rapidly remobilized in response to genotoxic or environmental stresses that requires a rapid adaptation of the transcriptional program (reviewed in Stefanini et al., 2010).

2.2.1 TFIIH in NER

Our genome is vulnerable to an array of DNA-damaging agents that affect fundamental cellular processes, such as DNA replication and transcription. To counteract the deleterious effects of these agents, cells are armed with several DNA repair pathways that protect us from cancer and accelerated aging. Each of these DNA repair pathways removes structure-specific DNA lesions (Zhovmer et al.,

2010). The nucleotide excision repair (NER), a highly versatile and sophisticated DNA damage removal pathway, counteracts the deleterious effects of a multitude of DNA lesions, including major types of damage induced by environmental sources (de Laat et al., 1999). Many of the DNA lesions recognized and repaired by NER are caused by chemicals that covalently bind a DNA base and form a so-called 'bulky DNA adduct'. The main task performed by NER is the repair of UV-induced lesions, either cyclobutane pyrimidine dimers (CPDs) or pyrimidine (6-4) pyrimidone photoproducts (6-4PPs), which makes NER the most important protection system against the carcinogenic effect of sunlight. Initially, a bulky DNA adduct is recognized by either the global genome repair (GGR) pathway or the transcription-coupled repair (TC-NER) pathway of NER. GGR is initiated by the XPC that removes DNA lesions from anywhere in the genome; whereby in the TC-NER pathway, the removal of the DNA damage located in the transcribed strand of active genes is triggered by the stalling of elongating RNApol II complexes (Spivak et al., 2016). Once the DNA lesion distorting the double helix has been recognized, the subsequent steps in NER are identical for GGR and TC-NER. The ability of both pathways to detect DNA damage is crucial for reducing the risk of mutations that can result from incorrect or incomplete DNA replication (Compe and Egly, 2012).

In the **GGR pathway**, the XPC protein initially recognizes the strand complementary to the lesion, not the chemical adduct itself but a distortion of the double helix (Alekseev and Coin, 2015) (Figure 5). This event prepares the DNA region containing the lesion for the recruitment of the other NER factors. XPC can rapidly detect various DNA lesions that do not share any common chemical structures (Clement et al., 2010; Marteijn et al., 2014) and promotes bending of the double helix, thus forming a transient recognition intermediate before a more stable repair-initiating complex is established (Sugasawa et al., 2001; Mocquet et al., 2007). XPC is the sole XP factor dispensable for TC-NER and restricted to GGR. The protein has a molecular weight of 125 kDa and is usually associated to hHR23B protein (58 kDa), which structurally stimulates XPC activity *in vitro* through its XPC-binding domain (de Laat et al., 1999) and promotes DNA damage recognition (Scharer, 2013). The XPC-HR23B complex has strong specific affinity for damaged DNA and binds directly to the lesion. XPC is poly-ubiquitinated upon DNA damage, a reversible process that does not result in protein degradation but rather increases its affinity for DNA (Nouspikel, 2009). Since HR23B contains ubiquitin-like and ubiquitin-associated domains required for efficient NER, it has been suggested that HR23B plays a role in controlling XPC ubiquitination (Dantuma et al., 2009). In mammalian cells, there are about 10 times more HR23B than XPC molecules, implying that most of HR23B is not bound to XPC and may have a second function, distinct from NER. Structural studies of Rad4, the yeast homologue of XPC, revealed

that the protein covers only the 3′ side of a DNA lesion and leaves the 5′ side almost completely free (Min et al., 2007).

In some cases, the UV light-damaged DNA-binding complex (UV-DDB), a heterodimer formed by DDB1 and DDB2/XPE proteins, promotes the recognition of lesions (Fitch et al., 2003; Wang et al., 2004). The presence of UV-DDB complex facilitates the damage recognition by inducing a kink in the DNA, which then allows the recruitment of the XPC complex. DDB2, a WD40-repeats protein, is the only protein of the UV-DDB complex to contact the DNA and interacts with CPDs through a recognition pocket. DDB1 is required for high-affinity interaction of DDB with damaged DNA, where it is targeted by DDB2 (Alekseev and Coin, 2015). UV-DDB complex is not very efficient in the case of (6-4) PPs that cause a strong distortion in DNA structure and that are promptly recognized by the XPC complex. On the contrary, UV-DDB is more relevant for proficient repair of CPDs, which cause only a modest distortion of the double helix and represent poor NER substrates (Nouspikel, 2009). DDB1 is also a member of the substrate recognition module of a cullin-RING E3 ubiquitin ligase complex (CRL), formed by cullin CUL4A and the RING finger protein ROC1 (CRL4). Under normal conditions, the CRL4-DDB2 ubiquitin ligase is inactive since it is tightly bound to the COP9 signalosome (CSN), a multi-protein complex of the ubiquitin proteasome pathway. Following UV irradiation, CRL4-DDB2 dissociates from CSN and it immediately binds the lesion through the DDB2 protein. The CRL4-DDB2 complex ubiquitinates target proteins, including histone H3, H4, and H2A, to increase damage accessibility, the XPC subunit of the XPC-HR23B complex to enhance its affinity for damaged DNA, and DDB2 itself for dislocation from the damaged site and proteasomal degradation. The temporal order of binding to damaged DNA and proteolytic removal of DDB2 by CRL4 implies an active dynamic control over the damage recognition step of GGR (reviewed in Hannah and Zhou, 2009). UV-DDB binding to the damage site results in PARP1-mediated DDB2 poly-ADP ribosylation (PARylation) that promotes PARylation of histones essential for the recruitment of a chromatin-remodeling enzyme (ALC1) to relax chromatin in proximity of the lesion (Djik et al., 2014).

Once XPC is bound to the lesion, other XPC-binding partners such as centrin 2 and/or RAD23 homologue B (RAD23B) might stabilize the complex. Centrin 2 appears to play a role in stimulating damage recognition by XPC both *in vitro* and *in vivo*, although it lacks affinity for DNA (Alekseev and Coin, 2015).

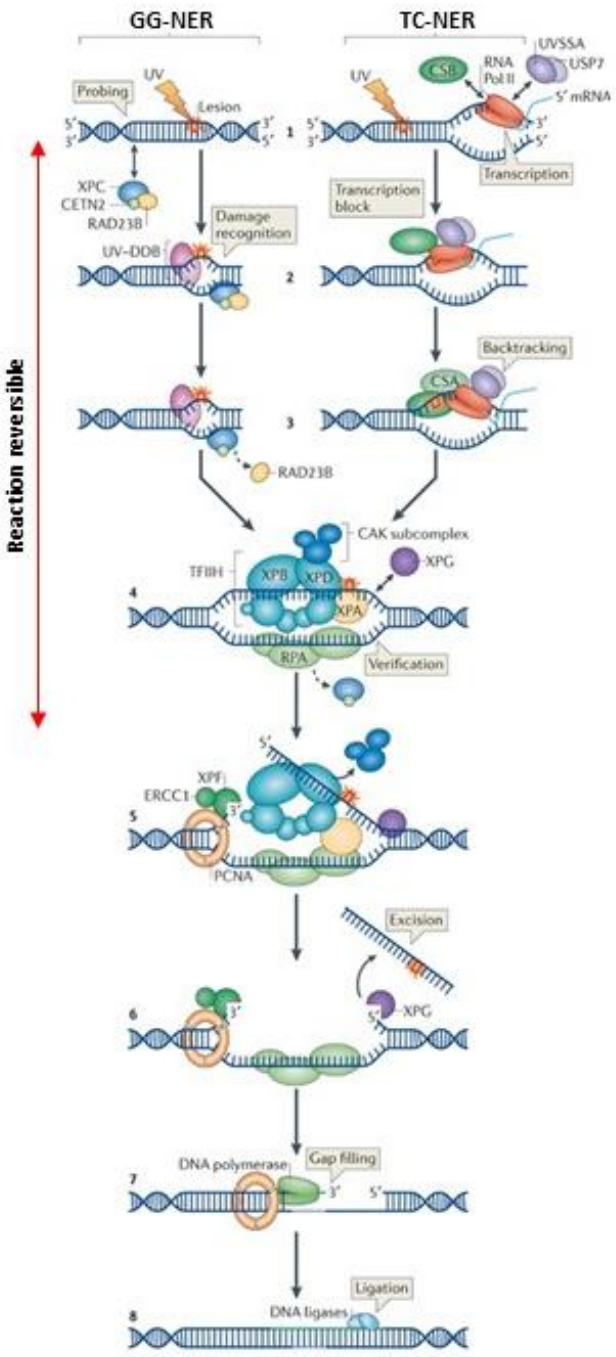
GG-NER
TC-NER
UV
Probing
Lesion
UV
CSB
RNA Pol II
UVSSA
USP7
5′ mRNA
Transcription
Transcription block
XPC
CETN2
RAD23B
Damage recognition
UV-DDB
Backtracking
CSA
RAD23B
Reaction reversible
CAK subcomplex
TFIIH
XPB
XPD
XPG
XPA
RPA
Verification
XPF
ERCC1
PCNA
Excision
XPG
DNA polymerase
Gap filling
Ligation
DNA ligases

Figure 5. Nucleotide excision repair (NER) and modalities of global genome repair (GGR) and transcription-coupled repair (TCR) in human cells (adapted from Marteijn et al., 2014).

The correct positioning of XPC is thought to be important for the subsequent recruitment of TFIIH and the excision of damaged DNA. The finding that the removal of the damaged oligonucleotide can occur *in vitro* in the absence of RAD23B, centrin 2 and the UV-DDB complex, does not exclude the possibility that these factors might contribute to the optimal positioning of XPC in a cellular context. When the XPC-damaged DNA intermediate complex is not accurately positioned (as is observed with mutated forms of XPC), XPC is rapidly degraded by a proteasome-independent mechanism (Bernardes de Jesus et al., 2008). When correctly bound to the damaged DNA, the carboxy-terminal domain of XPC might adopt a three-dimensional structure that enables the recruitment of TFIIH through the interaction of XPC with at least two subunits of TFIIH: p62, which interacts with both the C-terminal and the amino-terminal regions of XPC, and XPB that associates with the C-terminal region of XPC. A major impediment for GGR in eukaryotes is the packing of the chromatin, which is less of an impediment for **TC-NER** as the nucleosome structure is transiently opened during RNApol II translocation. As RNApol II translocates along the DNA, nucleosomes are dislodged in front of the polymerase and reassembled behind it. Transcription is arrested when RNApol II encounters an obstacle on the transcribed strand within an active gene. The stalling of RNApol II is a critical signal that activates the Cockayne syndrome (CS) proteins. Cockayne syndrome type B protein (CSB) becomes more stably bound to the arrested RNApol II and recruits factors needed to accomplish transcription-coupled repair (Figure 5). The *CSB* gene encodes a 168 kDa protein that is a member of the SWI2/SNF2 family of ATP-dependent chromatin remodelers and contains the RecA-like helicase motif found in both DNA and RNA helicases. CSB displays DNA binding activity and DNA-dependent ATPase but not helicase activity. Moreover, CSB has nucleosome remodeling activity and binds to core histone proteins *in vitro*. Different approaches provide evidence that CSB might have an impact also on transcription. Indeed, when added to a stalled RNApol II at a CPD photolesion, CSB can stimulate transcription elongation by addition of one nucleotide to the nascent transcript (Fousteri and Mullenders, 2008). UV exposure stabilizes the interaction between CSB and the RNApol II at the lesion site. Then, CSB recruits the CRL4-CSA-CSN complex, the chromatin remodeling factor p300 and the pre-incision NER core factors. In contrast to GG-NER, in which CSN dissociates from CRL4-DDB2 on damaged chromatin immediately after UV, in TC-NER the CSN complex associates with the CRL4-CSA complex immediately after UV irradiation. The CRL4-CSA complex, consisting of CSA, DDB1, Cullin4A and ROC1/Rbx1 proteins, has an E3-ubiquitin ligase (E3-ub ligase) activity that is

inhibited by the interaction with CSN and resulting in the de-neddylation of Cullin 4A. Thus, the CSA-containing (E3-ub ligase) complex engaged in TC-NER is an inactive ubiquitin ligase. In association with CSA, CSB also recruits the high-mobility group nucleosome-binding domain-containing protein-1 (HMGN1), the chromatin factor XPA binding protein 2 (XAB2), and the transcription factor TFIIS, to the damaged site.
The remaining steps are identical for GGR and TCR by requiring TFIIH. Upon TFIIH localization to the arrested elongation complex, other NER factors are recruited, namely XPG and XPA, which is possibly brought to the scene by XAB2 and replication protein A (RPA) that arrives simultaneously or shortly thereafter. The chromatin remodeling factors HMGN1 and p300 loosen the nucleosome structure behind the polymerase; RNApol II reverses direction, backtracking from the obstacle and degrading the nascent RNA product through its cryptic 3'-5' exonuclease activity, which is activated by TFIIS. TFIIH with associated XPG, XPA and RPA remain at the site of the obstacle, possibly maintaining the bubble of denatured DNA, but without the RNA-DNA hybrid. XPA and RPA bind the single-stranded DNA (ssDNA) in the vicinity of the obstruction, providing lesion verification and strand specificity before the next steps. Once RNApol II has backtracked, TFIIH extends the denatured region around the lesion to ~30 nucleotides, thus the subsequent DNA gap was filled by the structure-specific endonucleases XPG and the XPF-ERRC1 complex. CSA, as a component of a cullin-containing ubiquitination E3 ligase complex, might facilitate resumption of transcription (once the repair process has been completed) by removing or deactivating factors, including CSB (Hanawalt and Spivak, 2008). UVSSA forms a complex with the ubiquitin specific protease 7 (USP7) and plays a protective role in the early steps of NER since it stabilizes the RNApol II-CSB complex by counteracting polyubiquitination of both of them (Vermeulen and Fousteri, 2013).

As shown in Figure 5, the GGR and TC-NER sub-pathways converge into a common pathway in which TFIIH opens the DNA double helix to form a 27-nucleotide bubble asymmetrically flanking the damage (22 nt at 5' and 5 nt at 3'). The helicase activity of the TFIIH subunit XPD, which is regulated by the p44 subunit, is essential for NER, whereas the helicase activity of XPB is dispensable. Nonetheless, the ATPase activity of XPB participates in the NER pathway by anchoring TFIIH to the damaged chromatin. The XPB ATPase activity is regulated by XPC, as well as by the p8 and p52 subunits of TFIIH. XPB has also been suggested to act as a wedge that keep the two DNA strands apart allowing XPD to stand on the ssDNA (Alekseev and Coin, 2015). The relevance of the XPD helicase function during NER is attested by the numerous XPD mutations that diminish NER activity in patients cells. Mutations in the helicase motifs of XPD (abrogating the DNA unwinding activity of XPD) or in

its C-terminal end (weakening the interaction with p44) result in a decreased ability of TFIIH to unwind the damaged DNA, a crucial step in NER. Interestingly, in addition to its role as DNA helicase, it has been proposed that XPD participates in DNA damage recognition and verification (Fuss and Tainer, 2011). In addition, during NER the p8/TTDA subunit of TFIIH stimulates the ATPase activity of XPB in a DNA-dependent manner and promotes the translocation of XPA to the UV-induced photolesion (Coin et al., 2007). XPB, with the help of p8, is thereby thought to act as an ATP-driven motor that supplies the energy required to reorganize the intermediate DNA repair complex and thereby supporting the repositioning of XPC-RAD23B and the unwinding of DNA by XPD.
When TFIIH is correctly bound to the XPC-damaged DNA complex, RPA is recruited to protect the ssDNA from enzymatic hydrolysis and to prepare it for

DNA synthesis. RPA is a trimeric protein that binds ssDNA and has essential functions in replication and recombination. Since RPA is recruited prior to incision and remains associated with the site of repair after recruitment of post-incision factors until the gap-filling and ligation steps take place, it has been proposed to exert a key role of surveilling incision events, being the sole NER protein thus far reported to be present in both pre- and post-incision (Dijk et al., 2014).
Each RPA trimer has a preferred binding site of 30 nucleotides, which is strikingly similar to the size of the excised fragment in NER. It appears that RPA is recruited to the undamaged strand of DNA facing the lesion together with XPA. Within NER, RPA is so relevant that its availability, phosphorylation-dependent within dividing cells and phosphorylation-independent in non-dividing cells, constitutes a NER-bottleneck as supported by the observation that persistently stalled replication forks inhibit NER in *trans* by sequestering RPA away from sites of damage (Dijk et al., 2014). XPA is a small 273 amino acid protein originally thought to be the damage recognition factor. It was later found to have high affinity to kinked rather than damaged DNA, leading to the hypothesis that it interacts with an intermediate DNA structure in NER, subsequent to damage recognition (Fagbemi et al., 2011). Following UV irradiation, XPA undergoes phosphorylation by the checkpoint kinase ATR and resulting in the XPA recruitment to the lesion site. This event appears to mediate XPC sumoylation and complex stabilization, but the role of this post-translational modification needs to be clarified (Alekseev and Coin, 2015). Notably, XPA associates with the N-terminal moiety of XPC thus leading to the expansion of the DNA ‘bubble’ around the lesion. In addition to the potential function of XPA in maintaining the DNA structure open, the C-terminal region of XPA mediates the release of CAK from the core-TFIIH sub-complex as well as the arrival of other NER-specific factors such as XPG and XPF-ERCC1. These structure-specific endonucleases are responsible for carrying out incisions at 5′ and 3′ of the damaged

site, respectively. Concomitant to the 5′ incision, XPC, followed by XPA and TFIIH, are released from the DNA template and recycled. XPG and XPF-ERCC1 endonucleases remain on the excised DNA intermediate together with RPA, which coats the ssDNA region. Within the XPF-ERCC1 heterodimer, XPF harbors the endonuclease activity, whereas ERCC1 contains a DNA-binding domain that brings XPF into position, at the edge of the denaturation bubble. Also XPF contains a DNA-binding domain, similar to that of ERCC1, but it seems to be inactive. Conversely, ERCC1 contains a disrupted and inactive nuclease domain (Nouspikel, 2009).
The lesion is excised from chromatin *in vivo* with a higher-order structure in the same way that it is excised *in vitro* from a DNA duplex. Following the 5' incision, the proliferating cell nuclear antigen (PCNA) and replication factor C (RFC) are positioned at the 3′ primer template, and this forces the release of XPF endonuclease in an ATP-dependent manner. Then, the DNA polymerase is also recruited and repair synthesis is initiated. Thus, once lesion verification has occurred and the 5′-side incision made, the repair replication begins before the 3′-side incision is generated by XPG. This situation allows minimizing the amount of exposed single-stranded DNA during repair.
Following the release of XPG and RPA proteins, the DNA fragment of approximately 30 nucleotides, which contains the UV-induced lesion, is removed. The post-incision stage of NER consists of gap-filling DNA synthesis, ligation and restoration of chromatin structure. Recent findings have revealed the complexity of the DNA repair synthesis and ligation steps that appear depending on cell growth: in non-proliferating cells, the synthesis activity is mediated by the DNA polymerase δ (Pol δ) and Pol κ, whereas in cycling cells Pol ε is also required. The DNA nick that is formed following DNA synthesis is sealed by either the DNA ligase III-X-ray repair cross-complementing protein 1 (XRCC1) in quiescent cells or both XRCC1 and DNA ligase I-flap endonuclease 1 (FEN1) in dividing cells. Finally, the full reassembly of the repaired DNA into chromatin structure involves the histone chaperone chromatin assembly factor 1 (CAF-1). Its recruitment to sites of NER depends on the interaction with PCNA whereas its activity implies both histone recycling (as the reincorporation of the original histones at the damage site) and incorporation of the histone variant H3.1, which represents a mark for NER (Scharer, 2013). This event concludes the NER process restoring the DNA to its original undamaged state.

2.2.2 TFIIH in transcription

Initially identified as an essential factor for RNApol II-mediated transcription, TFIIH also participates in the transcription of ribosomal RNA (rRNA) by RNApol I and probably also in the synthesis of 5S rRNA, transfer RNA (tRNA) and other small

RNAs that are transcribed by RNApol III (Conaway and Conaway, 1989; Gerard et al., 1991; Feaver et al., 1991). Most of the transcription studies have focused on RNApol II that transcribes protein-encoding genes, small nuclear RNAs (snRNAs) and microRNAs (miRNAs). Although it was suggested that a preassembled holo-enzyme complex containing all the transcription components might be recruited to promoters, the initiation of transcription by RNApol II actually seems to result from the sequential recruitment of general transcription factors that assemble into a ~2-megadalton complex on core promoter DNA in an *in vitro* isolated system (Compe and Egly, 2012). This pre-initiation complex (PIC) is essential to direct accurate transcription start site (TSS) selection, promoter melting and RNApol II promoter escape (He et al., 2013).

Typically, six general transcription factors (GTFs, i.e. TFIIA, TFIIB, TFIID, TFIIE, TFIIF and TFIIH) are required for the formation of the PIC (Figure 6) with the first being TFIID, a multi-subunit complex consisting of *TATA binding protein* (TBP) and many *TBP Associated Factors* (TAFs). TBP binds to a specific DNA sequence called TATA box, located 25 nt upstream of the transcription initiation site. The binding is stabilized by the subsequent arrival of the transcription factor IIA (TFIIA), which is then involved in the recruitment of the transcription factor IIB (TFIIB). Subsequently, the RNApol II and TFIIF are recruited to form a large stable complex on the promoter. The TFIIB linker helix and the TFIIF arm domain align with each other at the promoter melting start site, probably to facilitate the separation of the two strands. Once promoter DNA melting is further extended and the RNApol II clamp closes down, the TFIIB linker helix and the TFIIF arm domain work together with the RNApol II rudder to maintain the upstream edge of the DNA bubble (He et al., 2013). This drives the assembly of TFIIE and the subsequent entry of TFIIH (reviewed by Kornberg, 2007). TFIIE and TFIIH are required for promoter DNA opening. TFIIE binds to RNApol II but not to the upstream promoter complex on the TATA box and facilitates the recruitment of TFIIH to the initiation complex, thus providing a bridge between RNApol II and TFIIH. It also stimulates the DNA-dependent ATPase and kinase activity of TFIIH (Sainsbury et al., 2015). TFIIE consists of two subunits, TFIIEα and TFIIEβ, which bind TFIIH and RNApol II. TFIIH is the last GTF to join the PIC and its activity is essential for transcription activation. Because of its large size, TFIIH can simultaneously interact with TFIIE at the base of the RNApol II stalk and position XPB on downstream DNA (He et al., 2013). TFIIH acts as a molecular ‘wrench’ that rotates DNA with respect to a fixed upstream promoter complex at the TATA box, thereby creating torque and melting DNA. As XPB was located on DNA downstream of the TATA box and did not bind to the transcription bubble, TFIIH apparently does not function as a conventional helicase. Conversely, recent studies indicated that Ssl2 - the yeast homolog of XPB - functions as an ATP-dependent, double-stranded DNA translocase and its action

on downstream DNA was suggested to lead to the threading of DNA into the RNApol II cleft. A recent EM reconstruction of a TFIIH-containing PIC revealed a distinct density of TFIIH, with two contact points to the remainder of the PIC, one near TFIIE and one near downstream DNA. XPB was located approximately 10 bp further downstream, and it was suggested that XPB 'walks' on the DNA away from the PIC, causing straining that facilitates DNA melting (Sainsbury et al., 2015). Thus, XPB uses the energy produced by ATP hydrolysis to allow the opening of the double helix at the transcription start site (*promoter melting*), to ensure the correct positioning of RNApol II on the promoter and the formation of the first phosphodiester bond. This role of XPB can be regulated by transcription factors, as illustrated by the actions of FUSE-binding protein (FBP) and FBP-interacting repressor (FIR, also known as PUF60) that during *c-MYC* gene transcription stimulate and inhibit XPB activity, respectively (Liu et al., 2001).

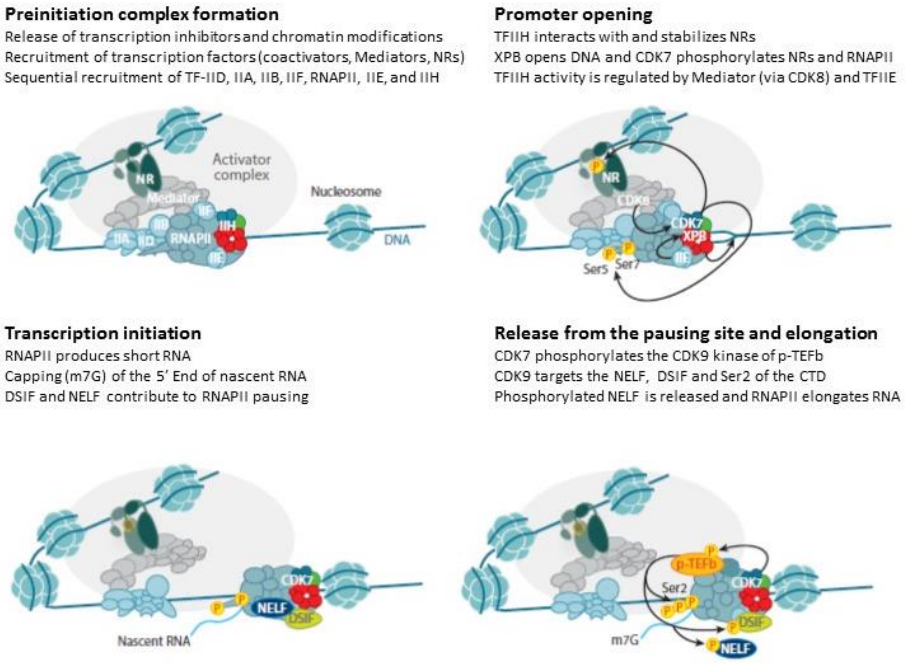

Figure 6. Assemblement of the pre-initiation complex (PIC) and transcription process regulation. Sequential recruitment of the general transcription factors on the TATA element of gene promoters and regulation of transcription through TFIIH enzymatic activities (adapted from Compe and Egly, 2016).

Following the establishment of the open complex, transcription is initiated and this event is intimately dependent on the phosphorylation status of the CTD of Rbp1, the largest subunit of RNApol II (Roy et al., 1994). The CTD of human Rbp1 contains 52 heptad repeats that can be phosphorylated on Ser2, Ser5 and Ser7. The phosphorylation of Ser5 is mediated by the CDK7 kinase subunit of TFIIH and activates the transcription initiation event. Ser5-phosphorylated RNApol II is held at promoters by two distinct pausing factors, the DRB sensitivity-inducing factor (DSIF) and the negative elongation factor (NELF), until the transcription elongation step will occur.

The CDK7 subunit is also implicated in the phosphorylation and the relieve of TFIIE from the RNApol II immediately after transcription initiation arises. After TFIIE release, DSIF would be loaded on RNApol II together with NELF and human capping enzyme (HCE) to induce RNApol II pausing and mRNA capping, respectively (Coin and Egly, 2015).

The phosphorylated CTD functions as a scaffold for the 7-methylguanosine (m7G) RNA capping machinery. These event triggers the dissociation of the RNApol II and TBP leading to the detachment of the PIC from the promoter (*promoter clearance*) (Komarnitsky et al., 2000). CDK7 phosphorylates also a subunit of the positive transcription elongation factor b (p-TEFb). P-TEFb is composed of cyclin T and a kinase subunit CDK9, which phosphorylates Ser2 of RNApol II CTD and both NELF and DSIF, leading to the dissociation of NELF, while converting DSIF to an elongation-stimulating factor to accomplish transcription elongation (reviewed in Liu et al., 2015).

As CDK7 phosphorylates CTD Ser5 and is required for CDK9-activating phosphorylation *in vivo*, it appears that CDK7 also modulates a mechanism to establish (through TFIIE and DSIF) and to relieve (through P-TEFb) barriers to elongation. This delicate modulation might create a time-frame window in which recruit RNA-processing machinery (Larochelle et al., 2012). Relevance of CDK7 regulation becomes evident from inhibition studies with a recently identified inhibitor (THZ1). CDK7 inhibition affects the global level of mRNA over time, thus revealing a reduction of RNAPII occupancy at promoters. The TFIIH kinase activity towards the CTD can be modulated by different factors, including the Mat1 and cyclin H subunits of CAK. In mouse fibroblasts deficient for Mat1, a reduced phosphorylation of RNApol II on Ser5 was observed (Helenius *et al*., 2011), whereas the cyclin H phosphorylation by CDK8 represses the CDK7 kinase activity (Akoulitchev et al., 2000). CTD phosphorylation by TFIIH also requires the contribution of non-coding RNAs, such as B2 RNA that specifically represses RNApol II CTD phosphorylation by TFIIH (Yakovchuk et al., 2009) and the core-splicing component U1 snRNA that stimulates the kinase activity of CDK7 on CTD (O'Gorman et al., 2005).

In addition to Ser5, CDK7 also phosphorylates CTD on Ser7 and this seems to be functionally important for the processing of spliceosomal snRNAs (Egloff et al., 2007). It has been demonstrated that phosphorylation of CTD by CDKs takes place in localized transcription foci of the nucleus, known as 'transcription factories' which are very stable while highly dynamic. This notion suggests that initiation and elongation of RNA transcripts take place in different nuclear compartments (Ghamari et al., 2013). If DNA is not properly de-methylated or a component of the transcriptional apparatus has been lost or even if the DNA is damaged by genotoxic agents RNA synthesis is impaired (Barreto et al., 2007).
In addition, a study conducted by Le May and collaborators (2010) showed that some NER factors are associated with the transcription machinery at the promoter of specific genes. The recruitment occurs in a sequential order after the formation of the PIC and includes XPC, CSB, XPA, and the XPG and ERCC1-XPF endonucleases. The transcriptional complex equipped with NER factors is formed in the absence of any exogenous genotoxic attack and it is distinct from a NER repair complex since it is specifically sensitive to transcription inhibitors and depends on XPC. NER factors (with the exception of CSB) located at promoters play an active role in transcription being involved in DNA de-methylation and histones post-translational modifications, in particular H3K4/H3K9 methylation and H3K9/14 acetylation.
Thus, it appears evident that TFIIH is involved in NER pathway as well as in transcription (Singh *et al*., 2015).
As mentioned before, TFIIH is also involved in the transcription of ribosomal 5.8S, 18S and 28S RNAs (rRNAs) essential for the formation of ribosomes. In support of TFIIH serving a function in RNApol I transcription, immunoprecipitation experiments and biochemical fractionation approaches demonstrated a tight association of TFIIH with a sub-fraction of RNApol I and its initiation factor TIF-IB. In contrast to RNApol II-driven transcription where the TFIIH-dependent ATP hydrolysis is indispensable both for the formation of the open complex and promoter clearance, neither the ATPase nor the helicase, or even the kinase activity of TFIIH appeared to be required for RNApol I transcription initiation (Iben et al., 2002; Assfalg et al., 2012).

2.2.3 TFIIH in transcription regulation

In addition to its 'basal' functions, TFIIH can modulate the activity of several transcriptional regulators, including p53 (Lu et al., 1997), herpes simplex virion protein VP16 (Xiao et al., 1994), Epstein-Barr nuclear antigen 2 (EBNA2, Tong et al., 1995), hepatitis B virus (HBV) X protein (HBX, Qadri et al., 1996), FIR (Liu et

al., 2000) or its *D. melanogaster* orthologous Half pint (HFP, Mitchell et al., 2010) as well as nuclear receptors. The TFIIH-mediated phosphorylation of transcription regulators accounts for the transactivation of specific target genes. CDK7 phosphorylates all nuclear receptors within their A/B domain, except vitamin D receptors (VDRs), which lack a functional A/B domain (Drané et al., 2004). However, TFIIH can still regulate some VDR-responsive genes such as cytochrome P450 family 24 (*CYP24*) by phosphorylating the VDR DNA-binding partner Ets1, which might fulfill the role of an A/B domain. In fact, Ets1 seems to promote the binding of VDR to its responsive element and trigger the subsequent recruitment of RNApol II and transcription co-activators (Drané *et al.*, 2004). TFIIH plays a pivotal role in the regulation of other nuclear receptor co-activators, as demonstrated by Traboulsi and colleagues (2015). These scientists revealed that TFIIH cooperates with PPARα co-activator 1 (PGC1-α) in an ATP-dependent manner to mediate the interaction of PGC1-α with the deacetylase enzyme SIRT1 on target gluconeogenic genes.

Nuclear receptors bound to their specific ligands become phosphorylated on the activation function-1 (AF-1) transactivation domain localized at the N-terminal end of the nuclear receptors. The phosphorylation of AF-1 domain results in the transcription activation of specific target genes. In contrast, the activity of AF-2 domain localized at the C-terminus of nuclear receptors is regulated by ligand binding (Chen et al., 2003). TFIIH directly phosphorylates the AF-1 domain likely at the time of the PIC, when TFIIH and the nuclear receptors are respectively bound to the promoter and responsive elements (Keriel et al., 2002). In the case of estrogen receptor α (ERα), AF-1 activity is modulated by the phosphorylation on Ser104 (and/or 106), Ser118 and Ser167. Mutation of Ser118 reduces ERα activity. Ser118 can be phosphorylated by CDK7 in response to the ligand-dependent interaction between TFIIH and the transactivation domain AF-2 or by the ERK1/2 mitogen activated protein kinases (MAPK) signal transduction pathway in response to cell surface signals (Chen et al., 2003). However, further regulation is mediated by phosphorylation in different sites depending on the incoming stimulus: Ser305 and Ser294 at hinge domain can carry mutually exclusive phosphorylations, the former induced by growth factors whereas the latter mediated by TFIIH upon ligand (estradiol or tamoxifen) exposure. It has been proposed that CDK-dependent phosphorylation at Ser294 differentiates ligand-dependent from ligand-independent activation of Ser305 phosphorylation, showing that hinge domain phosphorylation patterns uniquely inform on the various ERα activation mechanisms (Held et al., 2012).

Understanding the effect of TFIIH phosphorylation on nuclear receptors is complicated by the fact that CDK7 is able to influence diverse molecular processes but also because nuclear receptors might be phosphorylated by other kinases.

Nonetheless, phosphorylation by CDK7 is necessary for optimal nuclear receptor-mediated transactivation and this phosphorylation might influence the interaction of nuclear receptors with other factors. As an example, the nuclear protein vinexin-β, which participates in actin cytoskeletal organization, interacts with the non-phosphorylated form of RARγ but not with other RAR isoforms to repress gene transcription (Bour et al., 2005). CDK7-mediated phosphorylation of RARγ disrupts its interaction with vinexin-β and restores RARγ transactivation. Furthermore, TFIIH-mediated phosphorylation can regulate the turnover of nuclear receptors by triggering their ubiquitin-mediated degradation by the proteasome machinery (Compe and Egly, 2012). Indeed, the phosphorylation of androgen receptor by CDK7 directs the recruitment of the mouse homologue of the E3 ubiquitin ligase MDM2 and the proteasome to the promoter of androgen receptor-specific target genes (Chymkowitch et al., 2011).

Moreover, TFIIH might interact with partners of nuclear receptors. This was invastigate for PPARγ co-activator 1α (PGC1α, Sano *et al*., 2007; Traboulsi et al., 2014) which is a metabolic regulator and a transcriptional co-activator for several nuclear receptors and also for the metastasis-associated protein 1 (MTA1), which represses estrogen receptor-driven transcription (Talukder et al., 2003). TFIIH functioning is also influenced by the activity of the transcriptional Mediator complex, a gene expression regulator (Conaway and Conaway, 2011) that functions as an adaptor and conveys essential information from specific transcription factors that are bound at upstream responsive elements to the basal RNApol II transcription machinery. The Mediator complex promotes the positioning of TFIIH into the PIC (Esnault et al., 2008) and regulates the kinase activity of TFIIH through its CDK8 kinase subunit. Other factors participate in nuclear receptor-mediated transactivation by targeting TFIIH, as illustrated by the action of the co-chaperone Ydj1 in yeast (Moriel-Carretero et al., 2011).

Finally, recent findings revealed an additional role of TFIIH in gene expression regulation, through a transcription derepression mechanism. Indeed, it has been shown that in human primary dermal fibroblasts TFIIH triggers the removal of the sterol regulatory element-binding protein-1 (SREBP-1) from *COL6A1* promoter in order to up-regulate the expression of the gene (Orioli et al., 2013). It was also shown that in fibroblasts from TTD patients the SREBP-1 failed to be displaced from *COL6A1* promoter leading to reduce synthesis of collagen type VI. In addition, TTD-typical mutations of TFIIH that are known to impair the stability of the complex induce the over-expression of the matrix metalloproteinase-1 (*MMP-1*) gene. This event is caused by an erroneous signaling event mediated by retinoic acid receptors (RARs) on the *MMP-1* promoter (Arseni et al., 2014).

2.2.4 TFIIH in cell cycle regulation

Aside from its involvement in gene transcription and NER, TFIIH is also a regulator of cell cycle progression given that the CDK7 subunit of the CAK sub-complex is a critical activator of CDKs. CDKs regulate the cell cycle by integrating signals that derive from various checkpoints and ensuring that each event of the cell cycle occurs when the previous phase has been successfully completed. The activity of CDKs is controlled in a tightly timed manner by the availability and protein levels of cyclins, by the interaction with protein regulators and by CDK phosphorylation and auto-phosphorylation events. Amongst the most relevant targets of CDK7 so far identified as implicated in cell cycle progression are the cyclin-dependent kinases CDK1, CDK2, CDK4 and CDK6. The phosphorylation by CDK7/CAK is necessary for their kinase activation and in turn for the phosphorylation of key cell cycle substrates. Genetic analysis in flies and worms demonstrated the engagement of CDK7 in CDK1 activation, whereas a chemical-genetic analysis in human colon cancer cells revealed that acute inhibition of CDK7 prevented activation of CDK2 and CDK1 and impeded both S phase and mitosis. Therefore, Fisher and colleagues proposed a model whereby mitogenic signals trigger a cascade of CDK T-loop phosphorylation that drives cells past the restriction (R) point, when continued cell-cycle progression becomes growth factor-independent. Because R-point control is frequently deregulated in cancer, they propose the CAK-CDK pathway as a target for chemical inhibition aimed at impeding the inappropriate commitment to cell division (Fisher, 2013).

CDK7 activity is required to maintain the active state of CDK4 and CDK6, not merely to establish it as in the case of CDK1 and CDK2. In contrast, phosphatases work to dampen activation of CDK4 and CDK6 and delay G1 progression. To balance that antagonism, CAK activity towards CDK4 can be regulated by T-loop phosphorylation of CDK7 itself. This modification, previously shown to accelerate the phosphorylation of RNApol II-CTD but not of CDK2/cyclin A, stimulated CDK4 activation *in vitro*. In human cells entering the division cycle after quiescence, CDK7 and CDK4 T-loop phosphorylation increased with similar kinetics, suggesting a cell-cycle regulation of CAK activity and a rate-limiting role of CDK4 T-loop phosphorylation (Schachter et al., 2013).

Ganuza and colleagues analyzed the physiological role of CDK7 in mice by genetic targeting. They reported that loss of CDK7 causes impaired T-loop phosphorylation of cell cycle CDKs leading to cessation of cell division *in vitro* and early embryonic lethality *in vivo*. Loss of CDK7 expression in adult mice has a little effect on non-proliferating tissues whereas in proliferating tissues leads to the premature onset of age-related phenotypes most likely due to depletion of progenitor cells and exhaustion of their renewal capacity (Ganuza et al., 2012). Previous results showed

that excess of Xpd in *Drosophila* titrates CAK activity and results in mitotic defects and lethality, whereas a decrease in Xpd leads to increased CAK activity and cell proliferation (Chen et al., 2003). Because XPD anchors CAK to TFIIH, the simplest explanation is that reduced XPD levels release more CAK in a form that has more access to and/or more activity towards CDK7's cell cycle targets. At least in surviving animals such reduced XPD levels do not appear to be detrimental for transcriptional activity, suggesting that transcription requires less CDK7 kinase activity than mitosis and that one functional allele of *XPD* is sufficient, as demonstrated by the recessive nature of XPD mutant phenotypes. In contrast, elevated levels of XPD lead to the inactivation of mitotic CDK activity possibly because XPD acts as a molecular dispatcher for CDK7 by sequestering it in the holo-TFIIH complex or maybe in the XPD-CAK complex found in normal cells. Forfeiture of free CAK hampers the phosphorylation of CDKs. Therefore, under physiological conditions, oscillating levels of cellular XPD may determine the fate of the CAK complex and thereby the phosphorylation of different CDK7 substrates. In *Drosophila* cells, during the interphase (or in response to DNA damage) higher levels of XPD ensure the integrity of the TFIIH complex supporting transcription (or repair). At the same time XPD prevents improper cell division by sequestering CAK. In contrast, during mitosis the phosphorylation of CDK1, which is performed by the free CAK complex without core TFIIH, is essential. Reduced levels of XPD during mitosis may then allow the release of sufficiently high amounts of free CAK for proper phosphorylation of CDKs. Differently from *Drosophila* cells, mammalian cells do not vary the concentration of XPD subunit during cell cycle, therefore suggesting that other mechanisms may be adopted to regulate CAK activity in mitosis. Alterations in XPD that affect the interaction of the CAK sub-complex with the core-TFIIH may result in free CAK with high affinity for cell cycle substrates and reduced levels of the holo-TFIIH complex (Figure 7).

A quaternary complex containing all three CAK subunits plus XPD was described in *Drosophila* embryos as well as in mammalian cells. Its biological relevance, however, remains unknown. One possibility is that XPD sequesters CAK into an inactive quaternary complex. *Drosophila* embryos lacking XPD show several mutant phenotypes, including general loss of division synchrony, problems in spindle targeting and mitotic defects that might be due to a loss of CAK control. In the absence of XPD, embryos show increased tendency to improperly segregate chromatin. The activity of the mitotic kinase CDK1 is required to enter mitosis and its down-regulation at the anaphase transition is a prerequisite for mitotic exit. Embryos lacking XPD build up normal CDK1 activity as individual nuclei enter mitosis. In contrast, CDK down-regulation and the mitotic exit are delayed. While in normal *Drosophila* embryos CDK7 is progressively removed from the chromosomes during mitotic exit, in the absence of XPD excessive localization of

CDK7 is seen on anaphase chromosomes, which is paralleled by a persistency of phosphorylated histone 3 over the entire chromosomes through ana- and sometimes even telo-phase, indicative of mitotic kinase hyperactivity.

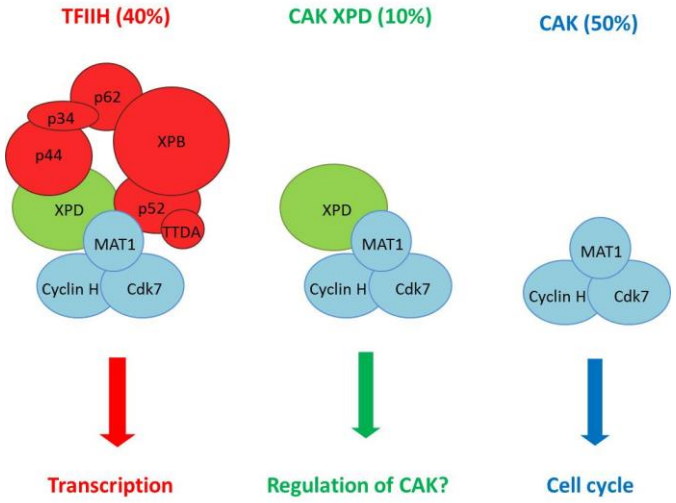

Figure 7. The three CDK7-containing complexes. CDK7 kinase can be found in three different complexes, holo-TFIIH, CAK-XPD, and free CAK, which represent 40, 10, and 50% of the CDK7-containing complexes, respectively. CDK7 acts in transcription when it is part of the holo-TFIIH, whereas it acts in cell-cycle progression when it is part of the free CAK (from Zhovmer et al., 2010).

The XPD subunit also exists in another recently discovered complex that does not contain any other TFIIH subunit: the MMXD complex, which plays an active role in mitosis. It is also possible that MMXD may sequester XPD when free CAK activity is required and TFIIH-dependent transcription needs to be silenced. Although no other TFIIH subunit besides XPD is present in the MMXD complex, MMS19 was previously shown to interact with TFIIH and to participate in DNA repair (Ito et al., 2010).
The previously mentioned MMTR complex is involved in the regulation of cell cycle progression as an intrinsic negative regulator of CAK sub-complex. In particular, MMTR over-expression delayed G1/S and G2/M transitions, whereas co-expression of Mat1 (CAK subunit) and MMTR rescued the cell growth and proliferation rate. Moreover, MMTR, whose expression level is modulated during cell cycle

progression, is required for inhibiting the CAK kinase-mediated CDK1 phosphorylation (Shin et al., 2010). Finally, another subunit of TFIIH appears involved in cell cycle progression. The XPB subunit was found to interact with the centrosomal protein γ-Tubulin and to associate with the centrosomes and the adjacent parts of the mitotic spindle from prophase until telophase. XPB re-localizes to the newly formed nuclei at the end of mitosis. Truncated forms of XPB result in an abnormal sub-cellular distribution of the protein during the interphase and abolished centrosomal association during mitosis, thus suggesting a role for XPB in cell cycle regulation (Weber et al., 2010).

2.2.5 TFIIH in development

The temporal and spatial control of differentiation and proliferation in eukaryotes occurs through regulation of fundamental processes including transcription, cell cycle control and DNA repair. The TFIIH complex that acts at the crosstalk of these processes is a good candidate for being a regulator of differentiation and proliferation (Chen et al., 2003; Fisher, 2005).
The role of CAK in development was examined through the analysis of its subunits. By examining the physiological role of CDK7 during the course of *Drosophila* development, Leclerc and collaborators demonstrated that the expression of dominant-negative forms of the kinase severely delayed the onset of zygotic transcription in the early embryo (Leclerc et al., 2000). Temperature-sensitive mutation isolated in *C. elegans* demonstrated that CDK7 is essential for both transcription and cell cycle progression in embryonic blastomeres (Wallenfang and Seydoux, 2002). Through genetic inactivation of CDK7 in mice, Ganuza and co-workers (2012) demonstrated that embryos lacking CDK7 developed to peri-implantation stages before undergoing massive apoptosis. Moreover, CDK7 has been observed to mediate CDK5 activation in brain development (Rosales et al., 2003). By investigating the function of the CDK7/cyclin H/Mat1 complex in murine embryonic stem (ES) cells and pre-implantation embryos, it was demonstrated that depletion of cyclin H leads to differentiation of ES cells independent of changes in cell cycle progression. In contrast, developmental genes resulted acutely up-regulated after cyclin H down-regulation, likely perturbing normal ES self-renewal pathways. Consistent with its function in ES cells, cyclin H depletion from mouse embryos also leads to defects in the expansion of the inner cell mass (ICM) of blastocysts. Thus, these findings indicate that cyclin H has an essential role in promoting self-renewal of pluripotent stem cells of blastocyst-stage embryos (Patel et al., 2010). A further attempt to understand CAK function during development was made by disrupting the murine *Mat1* gene. Mat1-deficient mice exhibit peri-implantation lethality, with homozygous mutant blastocysts failing to expand the

ICM in culture (Rossi et al., 2001). In culture, $Mat^{-/-}$ blastocysts give rise to viable post-mitotic trophoblast giant cells, while mitotic lineages fail to proliferate and survive (Rossi et al., 2001). Notably, cyclin H and CDK7 protein levels are also reduced in Mat1 mutant blastocyst explants. Postnatal *Mat1* deletion in the testis results in the loss of spermatagonial stem cells, whereas cardiac-specific Mat1 mutants develop heart failure secondary to mitochondrial dysfunction (Sano *et al*., 2007; Korsisaari et al., 2002). In contrast, loss of *Mat1* in mouse embryonic fibroblasts promotes adipogenesis by decreasing inhibitory phosphorylation of proliferator-activated receptor γ (Helenius et al., 2009). These different phenotypes suggest that Mat1 is not globally required for cell survival or transcription, but rather that it can modulate selected target genes in a cell type-specific manner (Patel and Simon, 2010).

Relevant of note, the CAK and core sub-complexes of TFIIH have differential dynamics in the early fly embryo. At the onset of transcription, the core components are nuclear whereas most of the CAK remains cytoplasmic. However, a small portion of CAK is positioned at promoters that are activated at the onset of transcription in the early embryos. Later in development, both sub-complexes are preferentially nuclear and co-localize in many chromosomal regions. Both the transitory complex CAK-XPD and the core are present in the cytoplasm of the syncytial blastoderm, from where they migrate into the nucleus to form the TFIIH ten-subunit complex and participate together with other components of the basal transcription machinery to initiate transcription (Aguilar-Fuentes et al., 2006). As core-TFIIH and CAK sub-complex are employed to a different extent in transcription and cell cycle progression, functional studies on core subunits revealed a different involvement of core-TFIIH in embryo development. Indeed, studies aimed at mimicking human pathologies caused by mutations in core-TFIIH subunits highlighted the fact that direct knockout approach cannot be applied to generate animal models: murine knockout of XPB and XPD helicases, as well as depletion of TTDA/P8 subunit, resulted in embryonic lethality at early stages (Andressoo et al., 2009, de Boer et al., 1998, Theil et al., 2013). *Drosophila* embryos lacking Xpd show a series of nuclear division defects, problems in spindle targeting and mitotic synchronization defects. Interestingly, in a TTD *Drosophila* model carrying TFIIH-destabilizing mutations in genes encoding the XPB or p52 subunit, overexpression of TTDA/p8 suppresses accumulated developmental defects associated with these mutations (Aguilar-Fuentes et al., 2008).

2.2.6 The dynamics of TFIIH complex

Several lines of evidence indicate that the composition of TFIIH is able to adapt its involvement in distinct cellular processes. When TFIIH is engaged in DNA repair

loses its transcriptional activity together with the release of the CAK sub-complex from the core-TFIIH. In particular, during NER the release of CAK is promoted by XPA, through its C-terminal part. XPA triggers the detachment, and not the degradation, of the CAK sub-complex from core-TFIIH complex only in the presence of DNA damage and it is responsible for the recruitment of the other repair factors on the lesion. This event promotes the removal of the damaged oligonucleotide and thereby the repair of the DNA. Following DNA repair, the NER factors are released from the complex and the CAK sub-complex reappears with the core-TFIIH on the chromatin concomitantly with the resumption of transcription. It is not clear if it is the free CAK that reassembles to the core-TFIIH previously involved in NER, or if it is a whole new holo-TFIIH complex that is recruited to the chromatin. Still open is the question on the possible role of CAK in NER before its release (Coin et al., 2008). Studies on human fibroblasts demonstrated that alterations in XPB resulted in accelerated release of CAK from the DNA damage site, whereas no effect was observed in XPD deficient fibroblasts. Thus, the authors suggested that XPB and XPD helicases differentially regulate the anchoring of CAK to core TFIIH during damage verification step of NER (Zhu et al., 2012).
As previously discussed, the detachment of the free CAK from the TFIIH complex is required in mitosis to allow the phosphorylation of the CDKs proteins by CAK-associated CDK7 and, at the same time, to inhibit the kinase activity of TFIIH-associated CDK7 in transcription. Studies in *Drosophila* embryos reveled the key role of Xpd in the assembly/disassembly of CAK and core-TFIIH. Thus, XPD incorporation into TFIIH is dependent upon the acquisition of its characteristic Fe-S cluster from the cytosolic iron-sulfur protein assembly (CIA) machinery (Vashisht et al., 2015). Relevant of note, analysis of transcription initiation dynamics directly into living mammalian tissues revealed that in highly differentiated post-mitotic cells that exit cell cycle, such as neurons, hepatocytes and cardiac myocytes, TFIIH is effectively immobilized on the chromatin during transcription. In contrast, in active proliferative cells, TFIIH has the same dynamic behavior as in cultured cells (Giglia-Mari et al., 2009).

2.3 HEREDITARY DISORDERS CAUSED BY MUTATIONS IN GENES ENCODING TFIIH SUBUNITS

The demonstration that TFIIH has various cellular functions was greatly facilitated by the fact that mutations in its XPB, XPD and p8 subunits cause autosomal recessive disorders, including trichothiodystrophy (TTD), xeroderma pigmentosum (XP) and, rarely, the combined symptoms of XP or TTD with Cockayne syndrome (XP/CS or

TTD/CS). Whereas these diseases were initially defined as DNA repair syndromes, it seems that some of their clinical features cannot be solely explained on the basis of a DNA repair defect and might be due to transcription deficiencies. For instance, the skin photosensitivity observed in some patients can be correlated with NER defects, whereas other clinical features, such as sterility or lipodystrophy, could be explained by dysfunctions in hormone-dependent transcriptional regulation. Many have tried to provide explanations for the broad range of clinical features that are observed in patients with XP and TTD. Such studies have considered the various cellular functions of TFIIH and the position of the mutations in its different subunits. The heterogeneity of the phenotypes suggests that each mutation differently affects the biochemical properties of TFIIH and consequently might disrupt distinct steps of transcription. Depending on the cellular context, TFIIH might establish specific interactions with various transcription factors. Therefore, each TFIIH mutation would specifically affect some factors and thus influence the expression of distinct genes (Compe and Egly, 2012).

The disorders caused by mutations in TFIIH are the following:

Trichothiodystrophy (TTD) is also known as sulfur-deficient brittle hair syndrome, since the main symptom involves hair abnormalities, accompanied by various other symptoms such as short stature, ichthyosis, mental retardation, abnormal nail plates, abnormal teeth, and infertility. About half of the patients present cutaneous photosensitivity but no skin cancer predisposition. Notably, over 80% of TTD patients show neurological abnormalities, namely microcephaly, mental retardation, deafness and ataxia.

Xeroderma pigmentosum (XP) is characterized by sun sensitivity and markedly increased risk of UV radiation-induced skin and mucous membrane cancers. Approximately a quarter of XP patients develop neurological symptoms, including microcephaly, mental deterioration, cerebellar ataxia, sensory deafness and peripheral neuropathy, all of which appear to involve global brain atrophy.

Cockayne syndrome (CS) is predominantly a developmental and neurological disorder. It results in a severely reduced lifespan but is not linked to an increased incidence of cancer. CS is characterized by pre or post-natal growth failure, gait defects, retinopathy and other ocular abnormalities, impaired sexual development, sensorineural hearing loss, signs of premature aging. Solar exposure in patients with CS causes mainly redness of the skin (erythema) and severe inflammation, although severe CS cases without photosensitivity have also been reported.

Cerebro-oculo-facial-skeletal syndrome (COFS) is a progressive brain and eye disorder leading to microcephaly with cerebral atrophy, severe mental retardation,

cataracts, microcornea and growth retardation. These features are very similar to those of CS, but the eye defects appear to be more severe.

Patients with the **XP/CS** complex have skin and eye disease of XP and the somatic and neurological abnormalities of CS (Lindenbaum et al., 2001; Rapin et al., 2000). Their skin is hypersensitive to sunlight and they develop the freckling and other pigmentary changes of XP but they also have the short stature, immature sexual development and the retinal degeneration of CS. About thirty patients with the XP/CS complex have been reported in the literature.

XP/TTD is a complex phenotype characterized by the acute sun sensitivity and mild pigmentary abnormalities of XP patients but no skin cancers. In addition, the XP/TTD phenotype presents hair abnormalities, ichthyosis, short stature, microcephaly and sensorineural hearing loss typical of TTD patients. Four cases have been so far described, all mutated in the *XPD* gene (Broughton et al., 2001; Boyle et al., 2008).

As shown in Table 2, the majority of patients with alterations in TFIIH present mutations in the ERCC2/*XPD* gene and clinical features of XP or TTD.

Table 2. Patients mutated in *ERCC3/XPB*, *ERCC2/XPD* or *GTF2H5/TTDA*/p8 genes and corresponding phenotype as reported by the literature

Disease	Mutated gene[a]		
	ERCC3/XPB	***ERCC2/XPD***	***GTF2H5/ TTDA/p8***
TTD	2 (1)	42(39)	4 (3)
XP	2 (1)	46 (38)	-
COFS	-	1	-
XP/CS	5 (4)	7 (7)	-
XP/TTD	-	4 (4)	-

Abbreviations. TTD: trichothiodystrophy; XP: xeroderma pigmentosum; COFS: Cerebro-oculo-facio-skeletal syndrome; CS: Cockayne syndrome

[a] In brackets the number of families.

One patient mutated in *XPD* showed the COFS phenotype and other XP features combined with either CS or TTD. In contrast, few patients have been so far described with mutations in the *XPB* gene, which included two TTD, two XP and five cases with clinical features of both XP and CS patients. This observation indicates that very few mutations in *XPB* are compatible with life and reflects the essential role of XPB in transcription and NER. On the contrary, *XPD* seems to tolerate many different mutations likely due to the fact that the helicase activity of XPD is necessary for NER but dispensable for transcription initiation where it plays a much less crucial role (Lehmann, 2003). Finally, mutations in *TTDA/P8* gene have been observed only in four patients with clinical features of TTD. The *TTDA/P8* gene encodes the only TFIIH subunit for which a complete absence is compatible with life (Giglia-Mari et al., 2004).

2.3.1 Trichothiodystrophy

Trichothiodystrophy (TTD) was first indicated as a distinct clinical entity by Price and coworkers in 1980 (Price et al., 1980) to describe a group of autosomal recessive neuroectodermal disorders whose defining feature is brittle hair with a cystein content less than half of normal. The designation derives from Greek: *tricho*, hair; *thio*, sulfur; *dys*, faulty; and *trophe*, nourishment. TTD was also known as Tay's syndrome (Tay, 1971), Pollitt syndrome (Pollitt et al., 1968), Amish hair-brain syndrome and Sabinas syndrome.
Three genes have been identified as responsible for the *photosensitive form* of TTD, namely *XPB*, *XPD* and *TTDA* (*p8* or *GTF2H5*). In 2005 it has been described *MPLKIP*, the first disease gene responsible for the *non-photosensitive form* of TTD (Nakabashi et al., 2005), and the disease locus has been designated TTDN1 (TTD non-photosensitive 1). Evidence has been provided that the non-photosensitive form of TTD is genetically heterogeneous, as previously found for photosensitive TTD and it has been found two unrelated children which harbour mutations in the *GTF2E2* and one patient shows a nonsense mutation in *RNF113A* gene. The clinical and cellular features of TTD are reported in Table 3.

2.3.1.1. Clinical features of TTD

Sparse, dry, short *brittle hair* associated with low sulfur and cysteine content (10–50% of normal) is the diagnostic hallmark of all TTD patients. The alteration affects hair from the scalp, eyebrows and eyelashes, which reveal a peculiar tiger tail pattern when investigated with the polarized light microscopy (Figure 8). A relevant and even more pronounced cysteine reduction is observed in the nail clippings from the patients (Sass et al. 2004). Nails are short, broadened and may show longitudinal ridging as well as horizontal splits (nail dysplasia). Other clinical manifestations in

TTD may affect the skin of the patients. At birth, a smooth, shiny *collodion*-like membrane frequently covers the skin of affected babies and, in the first weeks of life, the ichthyosiform erythroderma becomes manifest. The dry, scaly ichthyotic skin, which may involve also patient palms and soles, tends to become less prominent over time (Stefanini and Ruggeri, 2008). In addition, patients may manifest erythroderma, eczema, telangiectasia, hemangioma, lipoatrophy, parchment-like skin, poikiloderma, folliculitis, cheilitis, hyperpigmented eyelids and hypopigmented macules. Notably, about 50% of TTD patients exhibit cutaneous photosensitivity but not premalignant skin lesions or cutaneous tumors. Photosensitivity may be conspicuous in some patients who manifest an abnormal sun reaction on minimal sun exposure with blistering and persistent erythema. Nevertheless, in some cases photosensitivity appears to diminish with age.

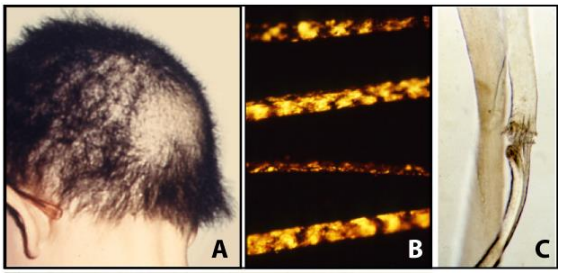

Figure 8. Hairs features in TTD patients. Short and brittle hair (A). Light microscopy findings: hair with alternating light and dark "tiger tail" bands under polarising microscopy (B), trichoschisis (C) (adapted from Stefanini and Ruggeri, 2008).

Besides skin manifestations, the clinical spectrum of TTD includes a wide range of associated signs and symptoms. Patients are frequently born prematurely with a low body weight (ranging between 2 and 2,5 kg) that, in some cases it was attributed to placental insufficiency (Happle et al. 1984, Ostergaard and Christensen 1996). Indeed, mothers of TTD patients report more complications in their pregnancy of affected children compared to those of their healthy kids. They experienced preeclampsia (pregnancy-induced high blood pressure), HELLP (hemolysis elevated liver enzymes and low platelets) syndrome and/or reduced fetal movements (Tamura et al, 2011 and 2012; Moslehi et al, 2010, 2012 and 2014).
Most of TTD children have short stature compared to peers, impaired intellectual and physical development. Skeletal deformations have been described in many cases, including genu valgum, coxa valga, pes valgus, cubital and tibial valgus

deformity, ulnar deviation of fingers, zygodactyly, clinodactyly, scoliosis, thoracic kyphosis, lumbosacral lordosis, and metacarpal bones of the thumb reduced in size. Marked osteopenia in long bones and axial osteosclerosis have been also described (Toelle et al. 2001; Wakeling et al. 2004). In addition, many TTD patients exhibit neurological and developmental defects but at present there is no evidence of progressive neurological degeneration. Mental retardation, speech delays, reduced learning ability and impaired motor control (ataxia) are frequently described. Spasticity, paralysis, tremor, hypotonia, decreased muscle tone, seizures and sensorineural hearing loss may also be observed. In addition, few TTD patients present calcification of the basal ganglia and some additional cases reveal hypomyelination of the white matter of the cerebrum likely caused by developmental delay (dysmyelination) (Yoon HK 2005; Kraemer 2007). Developmental defects also include microcephaly, congenital cataracts in the eye, delayed puberty and short stature. Delayed menarche and hypoplasia of female genitalia can be observed in affected females whereas undescended testes and bilateral or unilateral cryptorchidism have been reported in male patients. Post-pubertal patients frequently present a delayed development of secondary sexual characters and reduced fertility. The most severely affected cases of TTD lack subcutaneous fatty tissue, a feature that contributes to the progeric-like face of TTD patients (Happle et al. 1984). Indeed, the absence of subcutaneous tissue results in sunken cheeks, receding chin, beaked nose and large ears, thus contributing to the aged appearance. Other progeroid features include dental caries, osteoporosis, hearing loss and cataracts. Many TTD patients show the hematological features of β-thalassemia and reduced synthesis of β-globin (Viprakasit et al. 2001). Neutropenia, anemia and hypereosinophilia have been sporadically observed. Notably, TTD is also associated with recurrent infections, particularly respiratory infections, which can be life-threatening thus contributing to the early mortality: affected patients have a 20-fold increased risk of death before age 10. Though, the prognosis of affected patients depends on the type and severity of the features associated with the hair alterations. Finally, despite the intellectual impairment, TTD patients usually have a very social and friendly personality.

2.3.1.2 Cellular defects of TTD

The clinical photosensitivity reported in about half of TTD patients is paralleled by cellular alterations due to defects in nucleotide excision repair (NER), the only mechanism by which human cells remove the major *DNA* lesions induced by ultraviolet (UV) light. Specific functional assays on *in vitro* cultured fibroblasts are available to evaluate the cellular response to UV light, such as the measurement of UV-induced DNA repair synthesis (unscheduled DNA synthesis, UDS), recovery of RNA synthesis (RRS) at late times after UV irradiation and sensitivity to the lethal

effects of UV. The most commonly used test relies on UDS analysis, which is performed by measuring the incorporation of labelled nucleotides into the genomic DNA of UV-irradiated cell samples either by autoradiography or liquid scintillation counting or using a fluorescence assay (Lehmann et al., 2011). Reduced levels of UDS confirm the diagnosis of photosensitive form of TTD, which is also characterized by reduced RRS and survival after UV irradiation. Further tests can be applied to identify the defective gene.

The classical complementation assay for NER defects is based on UDS analysis in heterodikaryons obtained following fusion of fibroblasts of the patient under study with cells representative of each of the various NER-defective groups. The restoration after fusion of normal UDS levels in heterodikaryons allows the classification of patients into different complementation groups (i.e., they are defective in different genes) whereas the maintenance of impaired UDS levels indicates that the patients are in the same complementation group (i.e., they are defective in the same gene). In parallel to the classical complementation tests based on cell fusion, genetic analysis can be carried out also by analysing UDS or RRS levels in patient cells after microinjection with wild-type cloned NER genes or after infection with recombinant lentiviruses expressing one of the cloned NER genes (Jia et al., 2015).
An alternative approach makes use of a host-cell reactivation assay by co-transfecting a UV-treated plasmid plus plasmids each expressing a cloned NER gene (Emmert et al. 2002). In addition it was established that all the mutations responsible for the NER-defective form of TTD cause a decrease up to 70% in the cellular content of TFIIH (Vermeulen et al., 2000, 2001; Botta et al., 2002). Conversely, the non-photosensitive TTD patients carry a normal response to UV and a normal behaviour to complement the defect in NER defective TTD cells.

Table 3. Clinical and cellular features of the four TTD complementation groups

Mutated gene	Clinical symptoms[a]				TFIIH[b] level	NER[c] defect	
	Hair alterations	Skin photos.	Physical impairment	Neurol. impairment		UV-sens.	UDS (% of normal)
Photosensitive form							
ERCC3/XPD	+	+	+/++	+/++	35-65	+/++	10-50
ERCC2/XPB	+	+	-	-	40	+	40
GTF2H5/ TTDA	+	+	+	+	30	++	15-25
Non-photosensitive form							
MPLKIP/ TTDN1	+	-	+/++	+/++	normal	-	normal
GTF2E2	+	-	+	++	normal	-	normal
RNF113A	+	-	+	++	normal	-	normal

Abbreviations. NER: nucleotide excision repair; UDS: Unscheduled DNA synthesis; photos: photosensitivity; neurol: neurological; sens: sensitivity.

[a] Physical impairment: + moderate (survival beyond early childhood, delayed puberty, and short stature); ++ severe (death during childhood and/or failure to thrive/dystrophy). Neurological impairment: + moderate severity (mental development at either preschool level or primary-school level, axial hypotonia, and reduced motor coordination); ++ severe (very poor mental and motor performances and speech).

[b] TFIIH level refers to the mean steady state of the subunits CDK7, p44, and p62 in patient cells expressed as percentage of that in normal C3PV cells analyzed in parallel (Botta et al., 2002, 2007).

[c] *UV-sensitivity*: survival partially (+) or drastically (++) reduced compared with normal. UDS: the ability to perform UV-induced DNA repair synthesis is expressed as a percentage of that in normal cells.

2.3.2 Xeroderma pigmentosum

Xeroderma pigmentosum was first described by Moriz Kaposi in 1874. Nine years later Albert Neisser reported about two siblings showing cutaneous abnormalities typical of XP in association with progressive neurologic degeneration beginning in the second decade. Neurologic involvement in XP was emphasized in 1932 by the Italian physicians Carlo De Sanctis and Aldo Cacchione. DNA repair abnormalities in XP were brought to the attention of the general scientific community in 1968 by Cleaver, who reported that cultured skin fibroblasts from three patients were unable to normally repair lesions induced in their DNA by UV radiation, as a consequence of a failure of NER. XP occurs with an estimated incidence of about one in a million of live births in the United States and Europe. It is more common in Japan (from 1:40.000 to 1:100.000, Hirai et al., 2006), North Africa, the Middle East and areas where the consanguineous marriages are common (Kraemer et al., 1987). Patients have been reported worldwide in all races and, consistent with autosomal recessive inheritance, there is no significant difference between the sexes.

2.3.2.1 XP clinical features

Patients with XP are hypersensitive to UV radiation both at the clinical and cellular level. Therefore, they show cutaneous and ocular abnormalities that are usually strikingly limited to sun-exposed areas of the body (Figure 9). If aggressive UV avoidance is not introduced early, first skin cancer may appear in early childhood. There is great variability in the age at onset and in the severity of symptoms, depending on the mutated gene and the amount of sun exposure.
Approximately half of the patients with XP have a history of acute sun sensitivity from early infancy, acquiring severe sunburn with blistering or persistent erythema lasting several weeks on minimal sun exposure. Patients with a history of severe sunburn on minimal sun exposure developed their first skin cancer at an older age when compared with patients with XP-C and XP-E, but they had an increased frequency of neurological abnormalities (Sethi et al., 2013). The normal sunburn response of XP-C and XP-E patients may relate to the preservation of transcription-coupled DNA repair in these groups.

In all patients, numerous freckle-like hyper-pigmented macules appear on sun-exposed area of the skin. The median age of onset of first cutaneous symptoms is one to two years (Kraemer et al., 1994). Following continued sun exposure, most XP patients develop xerosis (dry skin) poikiloderma (the constellation of hyper- and hypopigmentation, atrophy, and telangiectasia), and premalignant actinic keratoses at an early age.

Figure 9. Skin alterations in two XP patients showing freckle-like changes with different amounts of pigmentation and precancerous lesions.

Ocular abnormalities have been reported in 80% of XP patients. Photophobia is often present and may be associated with prominent conjunctival injection. Continued UV exposure of the eye may result in severe keratitis leading to corneal opacification and vascularization. Epithelioma, squamous cell carcinoma, and melanoma of UV-exposed portions of the eye are common.

It has been estimated that all of the sites exposed to UV radiation have about a thousand-fold increased risk of developing tumors in XP patients. XP patients can develop hundreds of skin cancer. Early onset and increased frequency of both nonmelanoma skin cancer (NMSC) and melanoma has been observed in XP patients. The median age of onset of the first skin neoplasm was 9 years for NMSC, nearly 50 years earlier than that of the general population, and 22 years for malignant melanoma. In XP patients under 20 years of age, the frequencies for melanoma and NMSC were more than 1000-fold higher than in the US general population (Kraemer et al., 1987). Moreover, besides skin and eye cancer, a greatly increased frequency of cancer of the oral cavity, particularly squamous cell carcinoma of the tip of the tongue, a presumed sun-exposed area, has been reported (Kraemer et al., 1994). In XP patients there is also a smaller increase in internal tumors, predominately gliomas of the brain and spinal cord pancreatic, gastric, renal, and testicular tumors have been reported. Overall, the literature reports suggest an approximate ten to twenty-fold increase in internal neoplasms (Kraemer et al., 1994).

Neurologic abnormalities have been reported in approximately 20-30% of XP patients and are commonly observed in cases with mutations in the *XPA, XPB, XPD* or *XPG* gene. The onset may be early in infancy or delayed until the second decade. The neurologic abnormalities may be mild (e.g., isolated hyporeflexia) or severe, with progressive intellectual impairment, sensorineural deafness beginning with high-frequency hearing loss, spasticity, or seizures.

2.3.2.2 Molecular and cellular characteristics of the XP groups

DNA repair investigations performed in fibroblast strains from approximately 350 patients suggested the presence of genetic heterogeneity in the NER defective form of XP by showing different degrees in the severity of clinical symptoms and in the residual repair activity among patients (Fossihi et al., 2016). The first demonstration of genetic heterogeneity in the NER-defective form of XP was provided by de Weerd-Kastelein and collaborators (1972), by combining somatic cell hybridization procedures with UDS analysis at the single cell level. Genetic analysis in about fifty XP cases led to the identification of seven genetically different forms of XP, that were named A to G, in order of increasing residual DNA repair synthesis (de Weerd-Kastelein et al., 1973, 1974; Bootsma 1978; Cleaver 1975; Kraemer et al., 1975a, b). The clinical and cellular features of the seven XP complementation groups are summarized in Table 4.

Clinical variability of the XP-A phenotype is associated with a mutational heterogeneity. Despite a relatively homogenous mutational spectrum, mutational heterogeneity for rare cases is observed because of the high rate of consanguinity. A study of Messaoud and colleagues reported that XP-A Tunisian patients presenting an intermediate phenotype, i.e. development of skin cancers and neurological signs after the age of 10 years, shared a common mutation with a founder effect (Messaoud et al., 2010). More recently two Tunisian families with severe dermatological and neurological XP phenotypes were investigated and the results showed the presence of a novel mutation (glu111X) in three patients belonging to the same family and presenting a very severe phenotype, i.e. development of skin lesions and neurological signs before one year of age. For the other patient, they identified a nonsense mutation (arg207X) already found in a Palestinian XP-A patient (Messaoud et al., 2012).

A few other mild cases have mutations close to a splice site such that alternative splicing may allow the production of a low level of normal protein (Sidwell et al., 2006).

Table 4. Clinical and cellular features of the seven XP complementation groups

Group	Patient number [a]	Clinical symptoms [b]		Cellular response to UV [c]		
		Cancer	Neurological anomalies	UV sensitivity	UDS % of normal	RRS
XP-A	216	++	++/+	+++	<5	-
XP-B	7	+/-	++/+	++	10-40	-
XP-C	61	+	-	++	15-30	+
XP-D	44	+/-	++/-	++	2-55	-
XP-E	12	+/-	-	+	>50	+
XP-F	24	+/-	-/++	+	15-30	-
XP-G	6	+/-	++/+/-	++	2-25	-

Abbreviations. [a] Modified from Moriwaki and Kraemer (2001).
[b] Cases with different severity in terms of age at onset and frequency of skin tumours or neurological abnormalities (++, +); cases reported as cancer-free at the last clinical examination or without neurological involvement (-). See text for details between and within each complementation group.
[c] UV-sensitivity: survival partially (+) or drastically (+++) reduced compared with normal. *UDS* (Unscheduled DNA Synthesis) The ability to perform UV-induced DNA repair synthesis is expressed as a percentage of that in normal cells; *RRS* recovery of RNA synthesis rate after UV normal (+) or defective (-).

3. Aims of the research

TFIIH plays a key role both in NER and transcription, thus providing a clue to explain the clinical features of TTD phenotype, which is characterised by hair abnormalities, physical and mental retardation, neurodegeneration, ichthyosis, signs of premature aging but no cancer. At first defined as a DNA repair syndrome, nowadays TTD appears more likely ascribed to transcriptional impairments and several lines of evidence point to this statement. *In vitro* studies with recombinant TFIIH complex carrying amino acidic changes typical of TTD phenotype revealed a reduced transcriptional activity (Dubaele et al., 2003; Keriel et al., 2002). Primary cell lines derived from TTD patients exhibit a reduced cellular content of TFIIH (Vermeulen et al., 2000, Botta et al., 2002) as well as alterations in the transcriptional profile of several genes. In particular, the β-globin deficiency, the reduced levels of collagen type VI in the extracellular matrix (ECM) (Orioli et al., 2013), the over-expression of the matrix metalloproteinase-1 (*MMP-1*) gene (Arseni et al, 2015) were shown to be caused by transcriptional impairments. Also the use of the TTD mouse model contributed to demonstrate the transcriptional defects in TTD cells, including the reduced transactivation of the peroxisome proliferator-activated receptors (PPARs), which are essential for lipid metabolism and differentiation/survival of adipocytes *in vivo* as well as the selective dysregulation of thyroid hormone target genes in specific areas of the TTD mouse brain (Compe et al., 2005; Compe et al., 2007; Traboulsi et al., 2014).

In addition, a recent study on two unrelated children demonstrated that mutations in the *GTF2E2* gene encoding a subunit of the TFIIE transcription factor are responsible for clinical features typical of TTD not associated to NER defects (Kuschal *et al*., 2016). All together, these findings support the hypothesis of TTD being a transcriptional disorder.

The aim of this research study is to define the expression profile typical of TTD cells and, by so doing, to identify signalling pathways whose deregulation may account for TTD clinical symptoms.

To address this issue, we took advantage of the NGS techniques. We identified and compared the RNAseq-based transcriptional maps of primary dermal fibroblasts from the severely affected TTD7PV female patient (mutated in the *XPD* gene) with that of her healthy mother. The idea to compare family members arises from the need to minimize the expression variability caused by different genetic background. In

addition, since TTD cells are NER-defective, we also investigated how the accumulation of unrepaired DNA lesions affects the gene expression profile. By this approach, we will identify genes differentially expressed in TTD cells in basal condition as well as after UV-irradiation.
Next, to identify the expression deregulations that only depend on malfunctioning TFIIH, we extended the analysis to other TTD patients characterized by different mutations in the *XPD* gene. In addition, since mutations in *XPD* are also responsible for the cancer-prone disorder XP, we analysed the expression of the deregulated genes in XP patients. This approach will allow us to distinguish between genes whose deregulation is specific for the TTD pathological phenotype rather than common to TTD and XP.
We also asked whether the transcriptional alterations typical of TTD are the consequence of unrepaired DNA lesions in specific genomic loci, which may interfere with the transcriptional process, or if they are the result of an inefficient transcriptional apparatus as a consequence of mutated TFIIH. Therefore, we investigated by ChIPseq analysis the distribution throughout the genome of γ-H2AX, a histone modification which marks the accumulation sites of DNA damage, in TTD fibroblasts exposed to UV irradiation. By comparing the γ-H2AX distribution in TTD7PV patient with that of her healthy mother, we intend to identify the sites more exposed to the DNA damage accumulation in TTD fibroblasts and define its possible correlation with the loci of transcriptional deregulated genes.
Finally, we analysed the protein amount of the most relevant deregulated genes to discriminate weather the transcriptional alterations are paralleled by altered protein content and therefore account for the TTD pathological phenotype.
By these methods, we will hopefully identify transcriptional profile specifically related to TTD that could partially explain the different pathological features exhibited by TTD and XP disorders.

4. Materials and methods

4.1 Case reports

The study was performed on 12 patients, 7 of whom were affected by trichothiodystrophy (TTD) and 5 by xeroderma pigmentosum (XP). TTD and XP parents were used as controls. Clinical, cellular and molecular data, and related literature references of the analysed patients, are summarized in Table 4. At the time of clinical diagnosis the TTD patients analysed in this study were 9 months to 10 years of age and all exhibit the typical hair abnormalities (short, thin, brittle and dry), signs of premature aging and delayed physical and mental development of different severity. In those cases, in which detailed clinical descriptions were available, these features were frequently associated with other symptoms typical of TTD, such as ichthyosis, nail dysplasia, microcephaly, a face characterized by a receding chin, small nose, large ears, and varying degrees of proneness to infections. Photosensitivity was reported for all the analysed TTD patients, whose cellular characterization revealed a defect in the ability to repair UV-induced DNA damage with UDS levels ranging between 7 and 20% of normal (Table 4A). All the patients were mutated in the *XPD* gene; moreover, they showed a reduction by up to 30% of normal in the cellular steady-state level of TFIIH.
The 5 XP cases analysed in this study all showed hypersensitivity to sun exposure, pigmentary alterations and premalignant lesions of varying severity in sun-exposed areas of the skin (Table 4B). All the analysed patients are mutated in *XPD* gene. XP15PV, XP16PV and XP17PV show mild mental retardation, whereas XP49PV and XP1BR show a severe phenotype.

Table 4. Clinical, cellular and molecular features of the patients analysed in this study
A) Photosensitive form of trichothiodystrophy

Patient Code[a]	Clinical severity[b]	Sex	UDS[c]	TFIIH level[d]	Mutated gene		Mutated alleles[e]	Refs[f]
TTD7PV	severe	F	15	56	*ERCC2/ XPD*	m p	Arg722Trp (Arg156+Asp711) [Leu461Val; Val716_Arg730del] (Arg156)	1,2,6,8
TTD8PV	moderate	M	10	34	*ERCC2/ XPD*	m p	Arg112His (Arg156) Arg112His (Arg156)	1,2,3,4-6,8
TTD11PV	severe	M	10	43	*ERCC2/ XPD*	m p	Arg112His Val121_Glu159del	2,3,8
TTD12PV[b]	severe	M	20	65	*ERCC2/ XPD*	m p	Arg722Trp Cys259Tyr	2,3,8
TTD15PV[b]	severe	M	20	60	*ERCC2/ XPD*	m p	Arg722Trp Cys259Tyr	2,8
TTD20PV	severe	F	10	46	*ERCC2/ XPD*	m p	not expressed Arg112Cys	8
TTD23PV	severe	F	7	36	*ERCC2/ XPD*	1 2	Arg112His (Arg156) not expressed	7,8

B) Xeroderma pigmentosum

Patient code[a]	Clinical severity[b]	Sex	UDS[c]	TFIIH level[d]	Mutated gene		Mutated alleles[e]	Refs[f]
XP15PV[b]	mild	F	26	/	*ERCC2/ XPD*	m p	Arg683Gln Arg683Gln	8,9
XP16PV[b]	mild	F	25	108	*ERCC2/ XPD*	m p	Arg683Gln Arg683Gln	3,8,9
XP17PV	mild	M	13	59	*ERCC2/ XPD*	1 2	Arg683Trp Arg616Pro	3,8, 10,11
XP49PV	severe	M	12	83	*ERCC2/ XPD*	1 2	Arg683Trp [Leu461Val;Val716_ Arg730del]	8
XP1BR	severe	/	30	83	*ERCC2/ XPD*	m p	Arg683Trp Arg683Trp	9

Abbreviations. TTD: trichothiodystrophy; XP: xeroderma pigmentosum; F: female; M: male; m: maternal; p: paternal.

[a]TTD12PV and TTD15PV: brothers; XP15PV and XP16PV: sisters.
[b]Clinical severity in TTD refers to the degree of physical and mental impairment. For XP, it refers to the type and severity of skin lesions. See the quoted references for clinical details.
[c]UV-induced DNA repair synthesis (UDS) after irradiation with 10 J/m^2 observed in patient cells is expressed as percentage of that in normal cells analysed in parallel.
[d]TFIIH levels measured by immunoblot analysis are expressed as percentage of that in normal cells analyzed in parallel.
[e]Polymorphisms in parentheses.
[f]References:
1. Stefanini M, Giliani S, Nardo T, Marinoni S, Nazzaro V, Rizzo R, Trevisan G. DNA repair investigations in nine Italian patients affected by trichothiodystrophy. Mutat Res. 1992; 273:119-125.
2. Botta E, Nardo T, Broughton B, Marinoni S, Lehmann AR, Stefanini M. Analysis of mutations in the *XPD* gene in Italian patients with trichothiodystrophy: site of mutation correlates with repair deficiency but gene dosage appears to determine clinical severity. Am J Hum Genet. 1998; 63:1036-1048.
3. Botta E, Nardo T, Lehmann AR, Egly JM, Pedrini AM, Stefanini M. Reduced level of the repair/transcription factor TFIIH in trichothiodystrophy. Hum Mol Genet. 2002; 11:2919-2928.
4. Stefanini M, Lagomarsini P, Giliani S, Nardo T, Botta E, Peserico A, Kleijer WJ, Lehmann AR and Sarasin A. Genetic heterogeneity of the excision repair defect associated with trichothiodystrophy. Carcinogenesis. 1993a; 14:1101-1105.
5. Battistella PA, Peserico A. Central nervous system dysmyelination in PIBI(D)S syndrome: a further case. Childs Nerv Syst. 1996; 12:110–113
6. Dubaele S, Proietti de Santis L, Bienstock RJ, Keriel A, Stefanini M, van Houtten B, Egly JM. Basal transcription defect discriminates between xeroderma pigmentosum and trichothiodystrophy in XPD patients. Mol Cell. 2003; 11:1635-1646.
7. Orioli D, Compe E, Nardo T, Mura M, Giraudon C, Botta E, Arrigoni L, Peverali F.A., Egly JM, Stefanini M. *XPD* mutations in trichothiodystrophy hamper collagen VI expression and reveal a role of TFIIH in transcription derepression. Human Molecular Genetics, 2013 1–13.
8. Arseni L, Lanzafame M, Compe E, Fortugno P, Afonso-Barroso A, Peverali FA, Zambruno G, Egly JM, Stefanini M, Orioli D. TFIIH-dependent MMP-1 overexpression in trichothiodystrophy leads to extracellular matrix alterations in patient skin. Pnas, 2015; 112(5):1499-504.
9. Taylor EM, Broughton B, Botta E, Stefanini M, Sarasin A, Jaspers NGJ, Fawcett H, Harcourt SA, Arlett CF, Lehmann AR. Xeroderma pigmentosum and trichothiodystrophy are associated with different mutations in the *XPD* (*ERCC2*) repair/transcription gene. Proc Natl Acad Sci USA. 1997; 94:8658-8663.
10. Mariani E, Facchini A, Honorati MC, Lalli E, Berardesca E, Ghetti P, Marinoni S, Nuzzo F, Astaldi Ricotti GC, Stefanini M. Immune defects in families and patients with xeroderma pigmentosum and trichothiodystrophy. Clin. Exp. Immunol. 1992; 88:376–382.
11. Takayama K, Salazar EP, Lehmann A, Stefanini M, Thompson LH, Weber CA. Defects in the DNA repair and transcription gene *ERCC2* in the cancer-prone disorder xeroderma pigmentosum group D. Cancer Res. 1995; 55:5656–5663.

Primary fibroblasts from two genetically unrelated healthy donors were used (C3PV, C5BO). In parallel, to minimize the variability due to the different genetic background, dermal fibroblasts from TTD and XP families were also used (Table 5).

Table 5. Fibroblasts from healthy TTD and XP relatives

	Alleles TTD and XP relatives
m.TTD7PV	N / Arg722Trp
f.TTD7PV	N / [Leu461Val; Val716_Arg730del]
m.TTD11PV	N / Arg112His
f.TTD11PV	N / Val121_Glu159del
m.TTD12-15PV	N / Cys259Tyr
f.TTD12-15PV	N / Arg722Trp
m.XP15-16PV	N/ Arg683Gln
f.XP15-16PV	N/ Arg683Gln
m.XP17PV	Arg683Trp
f.XP17PV	Arg616Pro

Abbreviations. m: mother; f: father.

4.2 Cell culture and maintenance

The study was performed on primary cultures of dermal fibroblasts established from biopsies taken from sun-unexposed areas of the skin.
Cells were routinely cultured at 37°C in a humidified atmosphere conditioned with 5% CO_2. In particular, fibroblasts were grown in a 1:1 mixture of HAM's F-10 (Euroclone) and DMEM (Euroclone) supplemented with 10% fetal bovine serum (FBS, Australian Origin, Lonza), 2 mM L-glutamine (EuroClone), 100 U/ml of Penicillin and 0.1 mg/ml of Streptomicin (EuroClone). Fibroblasts were used at passages between 5 and 20 of the *in vitro* culture. All cell strains were routinely tested by staining with Hoechst 33258 and found to be mycoplasma-free.

4.2.1 Cell treatment

For UV treatment, fibroblasts were cultured under standard conditions, rinsed in phosphate buffered saline (PBS), exposed to a UV-C dose of 10 J/m^2 using a UV Stratalinger and subsequently recovered in fresh culture medium for 2hrs inside the incubator at 37°C with 5% O_2. Untreated cells were processed in parallel.

4.3 Analysis of mRNA levels

4.3.1 RNA isolation and purification

Total RNA was obtained as follows: $2x10^6$ primary dermal fibroblasts were cultured under standard conditions, rinsed in fresh PBS and purified using the RNeasy Mini Kit (Qiagen) according to manufacturer instructions. Trace DNA were removed by DNase treatment using the Turbo DNA-free kit (Ambion, Applied Biosystems), according to manufacturer instructions. RNA was quantified using the Nanodrop 1000 Spectromphotometer (Thermo Scientific) and RNA quality was evaluated by looking the 18S/28S RNA ratio following agarose gel electrophoresis.

4.3.2 RNAseq analysis

Total RNAs were isolated from $2x10^6$ fibroblasts form the compound heterozygous TTD7PV patient, who shows a severe phenotype, and from those of the patient's healthy mother (TTD7PVmother). Three biological replicates were performed for each cell strain and the 4 µg of RNAs were sent to Instituto di Genomica Applicata (IGA) in order to be sequenced and processed for the RNAseq analysis. Briefly, total RNAs were subjected to polyA+ fraction selection and transformed in a cDNA library for next-generation sequencing by the use of the TruSeq RNA Sample Prep kit (Illumina) according to manufacturer's protocol. A total of 60 million sequence reads were obtained for each cell line in three biological replicates on an Illumina HiSeq2500 instrument (60 million reads / replicate). Raw reads were subjected to standard quality control procedures with the NGSQC-toolkit software and aligned to the human genome reference sequence (NCBI37/hg19) by the TopHat alignment software. Genes were annotated and quantified according to the TopHat-Cufflinks protocol and differential gene expression analysis was performed by CuffDiff.
The most deregulated subset of genes was deeply analysed through the Integrative Genomic Viewer (IGV), a high-performance visualization tool for interactive exploration of datasets, including RNA-seq aligned sequence reads. The bioinformatic analysis was performed by Dr.ssa Roberta Carriero and Dr.ssa Silvia Bione from the CABGEN laboratory.

4.3.3 Quantitative real-time RT-PCR

Quantitative real time-RT PCR was carried out by using a fluorescent DNA binding dye (SYBR Green) or the Universal Probe library (UPL)-based RealTime Ready Custom Panels.

4.3.3.1 UPL-based RealTime Ready Custom Panels

Total RNAs were extracted from fibroblasts of 4 TTD/XP-D patients, and 4 normal donors selected among the TTD parents. Equal amounts of RNAs from dermal fibroblasts of TTD/XP-D or healthy parents were mixed together to obtain a TTD pool and control pool, respectively, in basal condition and after UV irradiation. One μg of each RNA pool was reverse-transcribed using the iScript cDNA Synthesis kit (Biorad), according to manufacturer instructions. The retro-transcribed pools were diluted 1:25 in water. Real time-PCR reactions were performed using UPL-based RealTime Ready Custom Panels (Roche) in 96-well format using the LightCycler 480 Real-Time PCR System (Roche). Each gene assay (consisting of a primer pair and a UPL probe) was chosen from the Universal ProbeLibrary (Roche) to customize the panels in order to contain 176 target genes, identified by the RNAseq analysis, and three reference genes. Each reaction was performed in 20 μl reaction mixture, containing 5 μl cDNA template (10 ng), 10 μl LightCycler 480 Probes Master mix (Roche) and 5 μl of RNAse-free water. Resupension in 20 μl reaction volumes results in a final concentration of 0.4 μM for each primer and 0.2 μM for the UPL probe. Reaction conditions were: 95°C for 10 min, 60 cycles of 95°C for 10 sec, 60°C for 30 sec and 72°C for 1 sec (with acquisition single), followed by a final cooling at 40°C for 30 sec.
The Ct was automatically given by LightCycler480 software package (Roche) and for each reaction the efficiency was 2.0±0.2. Quality of the data and quantifications were computed by applying the Relative Quantification Analysis. Using the 2-ΔΔCt method (Livak and Schmittgen, 2001). The fold change (FC) of target genes in TTD was calculated by normalizing each Ct value to the geometric mean of the three reference genes (G6PD, GAPDH and YWHAZ) and to the mean value of the corresponding gene in the control sample. By using this approach, the absence of variation is equivalent to 1.

4.3.3.2 SYBR Green I dye-based assays

Two μg of total RNA were reverse-transcribed into first-strand cDNA using the iScript Reverse Transcriptase kit (Biorad) according to manufacturer instructions.

Briefly, 10 µl of 5X iScript Reverse Transcription Supermix for RT-qPCR and 2,5 µg of iScript reverse transcriptase were added to RNA template in a final volume of 50 µl. RT-PCR was performed using the MasterCycler (Eppendorf). Samples were incubated at 25°C for 5 min and reverse transcription reactions were carried out at 42°C for 30 min. Afterwards, samples were maintained at 48°C for 15 min and then transferred at 85°C for 5 min to inactivate the enzyme, cDNAs were stored at -20°C. In each experiment, cDNAs were diluted 1:10 in water and run in duplicate. Real time-RT PCRs were performed using the LightCycler 480 Real Time-PCR System (Roche Diagnostics) in 96 well plates and analysed by the LightCycler 480 Software 3.5 (Roche Diagnostics). Each reaction was performed in 20 µl final volume containing 10 µl 2X iQ MasterMix SYBR Solution (Biorad), 1,25 µg (10 pmol) forward and reverse primers (Table 6), 3,5 µl water and 4 µl template cDNA (either diluted cDNA or a RT-reaction mix without the reverse transcriptase). The reaction was initiated by activation of Taq polymerase at 95°C for 5 min, followed by 60 three-step amplification cycles consisting of 25 sec denaturation at 95°C, 25 sec annealing at 60°C and 25 sec extensions at 72°C. A final dissociation stage was run to generate a melting curve that reveals the specificity of the amplification products. Transcript quantification was achieved using threshold cycle (Ct) measured with the second derivative maximum method. Standard curves were obtained for each primer set with serial dilutions of cDNA. Amplification of the housekeeping gene GAPDH was used as reference to normalize the cDNA amounts.

Table 6. Sequence of the primers used in real time-PCR

Assay	Gene	Position[a]	Primer	Sequence 5'-3'
	ANGPT4	+707/+725	F	GTTGACCCGGCTCACAAT
		+751/+770	R	GATTGCCAGGAGCTGTTCC
	EGR1	+563/+581	F	AGCACCTGACCGCAGAGT
		+638/656	R	CCAAACCACTCGACTGCC
	GADD4A	+345/+365	F	AGAGCAGAAGACCGAAAGGA
		+398/+417	R	TCAGCAAAGCCCTGAGTCA
	GADD4B	+352/+372	F	GTGTACGAGTCGGCCAAGTT
		+394/+413	R	GTGGTCCTCTGCCTCTTGG
	ID1	+755/+773	F	CGCTCCTCTCTGCACACC
		+802/827	R	GATTCCACTCGTGTGTTTCTATTTT
	ID3	+735/+754	F	CGTGTCCTGACACCTCCAG
		+846/+867	R	CCACTTGACTTCACCAAATCC
	IER3	+561/+579	F	GTACCTGGTGCGCGAGAG
		+611/+633	R	GAACTCAGAACACTACAGCGGA
	IL13RA2	+458/+478	F	GCAATGCACAAATGGATCAG
		+541/+562	R	AAGTTCAGGATATGGATTGCG
	IL20RB	+742/+762	F	TTCCTTGTGGCCTACTGGAG
		+795/+815	R	GGTGAGGAGTGGGGGTATTC
	JUN	+3016/+3037	F	AGGATAGTGCGATGTTTCAGG
		+3068/+3088	R	GGACAGCCCACTGAGAAGTC
	JUND	+562/+580	F	CAGCGAGGAGCAGGAGTT
		+609/+632	R	ATTTACACAAGCAGAACCAGCTC
	FOSB	+1096/+1116	F	AGCAGCTAAATGCAGGAACC
		+1147/+1168	R	GGAGACAGATCAGTTGGAGGA
	FOS	+705/+727	F	CGGAGACAGACCAACTAGAAGA
		+783/+803	R	TAGAGTTCATCCTGGCAGCT
	CLU	+1032/1051	F	GTGCCGGGAGATCTTGTCT
		+1065/+1083	R	GAATCCCTCCAGGTCGCT
	GAPDH	+855/+874	F	AGCTCACTGGCATGGCCTTC
		+952/+971	R	ACGCCTGCTTCACCACCTTC
	PCDH10	+3901/+3922	F	GCTGGATGGACTGCTGACTAA
		+3953/+3977	R	GACACGGAAAAGGATATGCTAGTC
	PTGIS	+551/+571	F	GGGTCTCCTCGACTTCTCCT
		+580/+601	R	GGCTACCTGACTCTTTACGGAA
	SFRP4	+1205/+1230	F	TGAAAAATGGAGAGATCAGCTTAGT
		+1231/+1251	R	CAGGAACAGCGGAGAACAGT
	STMN2	+620/+639	F	TCCCTGGAGGAGATCCAGA
		+669/+688	R	AGTCTCAGGAGGCCCAGG
	TBX1	+564/+583	F	GAAGCTCTTCGGCATGGAT
		+647/+666	R	CCTTCCACAGCTCCTCCTG
	WISP2	+738/+756	F	GCGACCAACTCCACGTCT
		+817/+835	R	GCAGAGGACGACAGCAGC

Abbreviations. Ampl: amplicon; F: forward; R: reverse.
[a] The position is referred to the *ANGPTL4* gene sequence (GenBank XM_005272484.3), to *EGR1* (GenBank NM_001964.2), *GADD45A* (GenBank NM_001924.3), *GADD45B* (GenBank NM_015675), *ID1* (GenBank NM_002165.3), *ID3* (GenBank NM_002167.4), *IER3* (GenBank NM_003897.3), *IL20RB* (GenBank NM_144717.3), *IL13RA2* (GenBank NM_000640.2), *JUN* (GenBank NM_002228.3), *JUND* (GenBank NM_005354), *FOSB* (GenBank NM_006732.2), *FOS* (GenBank NM_005252.3), *CLU* (GenBank NR_045494.1), *PCDH10* (GenBank NM_032961.2), *PTGIS* (GenBank NM_000961.3), *SFRP4* (GenBank NM_003014.3), *STMN2* (GenBank NM_007029.3), *TBX1* (GenBank NM_005992.1), *WISP2* (GenBank NM_003881.3) and *GAPDH* (GenBank NM_002046.4) mRNA sequences.

4.4 Chromatin Immunoprecipitation (ChIP)

For each chromatin immunoprecipitation $4x10^5$ primary fibroblasts were seeded in 10 cm dishes and incubated at 37°C until they reach 80% of confluence. Cells were exposed to a UV-C dose of $10J/m^2$ and recovered in fresh medium for 2hrs. Then, each sample was supplemented with 1% formaldehyde (Sigma) solution and after 10 min at room temperature, the cross-link was quenched by adding to each dish a glycine solution at the final concentration of 125 mM. After 5 min incubation at room temperature, cells were rinsed three times in cold PBS, collected by scraping in cold PBS additionated with 1X Phosphatase Inhibitor Cocktail, centrifuged at 1800 rpm for 10 min and resuspended in 10 volumes of Swelling buffer (25 mM HEPES, pH 7.8; 1.5 mM MgCl2; 10 mM KCl, 0.5% NP-40, 1 mM DTT, 0.5 mM PMSF, 1X Phosphatase Inhibitor Cocktail). After 10 min on ice, samples were centrifuged at 1300 rpm at 4°C for 5 min. The pellets containing the nuclei were resuspended in 10 volumes (of the original pellet) of Sonication buffer (50 mM HEPES pH 7.8; 140 mM NaCl; 1 mM EDTA; 1% Triton X-100, 0.1% Sodium Deoxycholate; 0.2% SDS; 0.5 mM PMSF; 1X Phosphatase Inhibitor Cocktail). The nuclear suspensions were distributed as 250 µl aliquots into 1,5 ml sonication tubes and sonicated 40 times using a Bioruptor Plus (Diagenode) with a 30 sec pulse followed by 30 sec of cooling. The aliquots were pooled togheter again and centrifuged at 13200 rpm for 15 min and the supernatants containing the cross-linked chromatin was isolated from the debris. The supernatants were precleared by incubation on a rotating wheel at 4°C for 2-3 hrs with 120 µl of Pierce ChIP-grade Protein A/G Magnetic Beads, which were previously rinsed in Sonication buffer and blocked by incubation on a rotating wheel at 4°C for 2-3 hrs in 450 µl Sonication buffer supplemented with 1mg/ml bovine serum albumin (BSA).Then, the magnetic beads suspension was placed in a magnetic rack, the beads were pulled apart and the

supernatants were aliquoted in INPUT (150 µl) and ChIP (420 µl) volumes. INPUT samples were stored at -20°C until the de-crosslinking procedure. ChIP samples were incubated overnight on a rotating wheel at 4°C in 450 µl of Sonication buffer supplemented with 1mg/ml BSA and 5 µg of anti-γH2AX (Ab81299, Abcam). Immunocomplexes were collected by adsorption to 40 µl of precleared magnetic beads for 2-3 hrs. The beads were pulled apart again and the supernatant was stored as flow-through. Beads were washed twice in 500 µl Sonication buffer, twice in 500 µl Wash Buffer A (50 mM HEPES pH 7.8, 500 mM NaCl, 1 mM EDTA, 1% Triton X-100, 0.1% Sodium Deoxycholate, 0.1% SDS, 0.5 mM PMSF, 1X Phosphatase Inhibitor Cocktail), twice in 500 µl Wash Buffer B (20mM Tris pH 8.0, 250mM LiCl, 1mM EDTA, 0,5% NP-40, 0,5% Na-deoxycholate, 0,5mM PMSF, 1X Phosphatase Inhibitor Cocktail) and twice in TE Buffer (1 mM EDTA, 10 mM Tris-HCl pH 8.0). All washes were performed on a rotating wheel at 4°C for 10 min followed by centrifugation at 2000 rpm for 1 min. Then, beads were incubated at 65°C for 10 min in 100 µl Elution buffer (50mM Tris-HCl pH 8.0, 1 mM EDTA, 1% SDS) and spinned at 2000 rpm for 5 min. The elution procedure was repeated twice and the supernatants collected. Both INPUT and ChIP samples were de-crosslinked by incubation overnight at 65°C with 0.2 M NaCl and 0.05 mg/ml RNase A. Samples were then incubated at 42°C for 2 hrs with 5 mM EDTA and 0.1 mg/ml Proteinase K. DNAs fragments were purified with the Qiagen QIAquick PCR purification kit (Qiagen), according to manufacturer instructions, by eluting the INPUT samples in 30 µl and the ChIP samples in 30 µl of Nuclease-Free Water. DNA was quantified using the Nanodrop 1000 Spectromphotometer (Thermo Scientific) and 20 ng of DNA for each immunoprecipitation were sent to the Instituto di Genomica Applicata (IGA) in order to be sequenced, 2x100 bp reads length. The samples were processed for ChIPseq analysis.

Briefly, DNAs were transformed in a DNA library for next-generation sequencing by the use of the TruSeq ChIP Library Preparation Kit (Illumina) according to manufacturer's protocol. A total of 60 million sequence reads were obtained for each cell line in three biological replicates on an Illumina HiSeq2500 instrument (60 million reads / replicate).

Raw reads were subjected to standard quality control procedures with the NGSQC-toolkit software and aligned to the human genome reference sequence (NCBI37/hg19) by the Bowtie alignment software. Enriched domains were annotated and quantified according to the SICER protocol and differential gene expression analysis was performed by DiffBind.

The common peaks among different samples were individually analysed by UCSC Browser.

4.5 Protein analysis by Western Blotting (WB)

Primary fibroblasts were washed twice in PBS and $5x10^5$ cells were lysed in 50 µl of 3X Laemmli Buffer (187.5 mM Tris-HCl pH 6.8, 6% SDS, 0.015% bromophenol blue, 30% glycerol, 2.25% β-mercaptoethanol) using a cell lifter. Cell lysates were boiled at 95°C for 10 min, sonicated three times using a Bioruptor Plus (Diagenode) with a pulse of 15 sec followed by 15 sec of rest and stored at -80°C. Total protein extracts (10-20 µg) were separated on a SDS-Polyacrylamide Gel Electrophoresis (SDS-PAGE), composed of a 5% Stacking gel (4X Upper Tris Buffer (0,5 M Tris, 0,4% SDS, HCl pH 6.8), 30% Acrylamide/bisacrylamide Solution, 10% APS, TEMED) and a 12% Running gel (4X Lower Tris Buffer (1,5 M Tris, 0,4% SDS, HCl to pH 8.8), 30% Acrylamide/bisacrylamide Solution, 10% APS, TEMED) and ran at 100V for 2hr. Alternatively, Mini-PROTEAN TGX™ Precast Gels 4-20% gradient (Biorad) were used, depending on the size of the analyzed proteins, and ran at 200 V for 1 hr.

Proteins were then transferred onto a 0.20 µm nitrocellulose membrane (Protran, Whatman) in Phosphate Transfer Buffer (PTB, 12.2 mM $Na_2HPO_4.2H_2O$, 7.8 mM $NaH_2PO_4.H_2O$) by applying an electrical current of 1.16 A at 4°C for 1hr or with Trans-Blot Turbo™ Transfer System, by applying the Biorad preprogrammed protocol for mixed molecular weights (7 min at 2.5 A constant, up to 25V). After the transfer, the membranes were firstly incubated at room temperature for 1 hr in milk blocking buffer (5% skim milk in 1X Magic Buffer: 50 mM Tris-HCl pH 7.5, 50 mM NaCl, 0.15% Tween-20) and then overnight at 4°C with primary antibodies (Table 7) diluted in milk blocking buffer. The dilution of each antibody is indicated in Table 7.

After three washes (10 min each) in 1X Magic Buffer, the membranes were incubated at room temperature for 1 hr with horseradish-peroxidase-(HRP)-conjugated secondary antibodies (Jackson ImmunoResearch) diluted 1/10000 in milk blocking buffer. The membranes were washed three times for 10 min each in 1X Magic Buffer and then developed using the SuperSignal West Pico Chemiluminescent Substrate (Thermo Scientific), or the LiteAblot Extended Long Lasting Substrate (EuroClone) or the Western lightning Ultra Extreme sensitive Chemiluminescent Substrate (Perkin Elmer) according to manufacturer instructions. The chemiluminescent signals were detected using the ChemiDoc XRS system (BioRad) and quantified using the *Quantity one* (BioRad) software.

Table 7. Antibodies used in this study

Antibody	Dilution by application		Origin	Reference
Anti-H3	WB	1:10000	Rabbit Polyclonal	Ab1791, Abcam
Anti–γH2AX	WB	1:10000	Rabbit Monoclonal	Ab81299, Abcam
Anti-γtubulin	WB	1/10000	Mouse Monoclonal	T 6557, Sigma
Anti-angptl-4	WB	1/500	Rabbit Polyclonal	Ab115798, Abcam
Anti-ptgis	WB	1/500	Mouse polyclonal	Ab72952, Abcam
Anti-Wisp2	WB	1/1000	Rabbit Polyclonal	Ab38317, Abcam
Anti-WNT4	WB	1/1000	Mouse Polyclonal	Ab169592, Abcam
Anti-PCDH10	WB	1/1000	Mouse Polyclonal	Ab172709, Abcam
Anti-IL13RA2	WB	1/500	Rabbit Polyclonal	Ab108534, Abcam
Anti-IL20RB	WB	1/500	Mouse Polyclonal	Ab169620, Abcam

Abbreviation. WB: western blotting

4.6 Statistical analysis

Each experiment was repeated two/three times and the values processed for statistical significance. P-values were obtained by the unpaired two-tailed student t-test. Fisher F-ratio at a probability level (p-value) of 0.05 was used to compare variances among analyzed groups. Data are reported as mean ± standard error (SE). P-values<0.05 were considered significantly different.

5.Results

In the attempt to identify deregulated signaling pathways contributing to TTD pathological phenotype, we focused our study on the following aspects: *i)* whole-genome transcriptional profile by RNAseq analysis of primary dermal fibroblasts from one TTD patient mutated in *XPD* and comparison with the expression profile of her healthy mother (section 5.1); *ii)* expression profiles changes in response to UV-induced DNA damage in normal as well as TTD fibroblasts (section 5.2); *iii)* investigation of transcriptionally deregulated genes by real time-RT PCR extending the analysis to other severely affected TTD patients mutated in the *XPD* gene (section 5.3); *iv)* definition of the TTD-specific and the TFIIH-specific transcriptional impairments by investigating primary fibroblasts from XP patients mutated in *XPD* (section 5.4); *v)* impact of the transcription deregulations on the corresponding protein levels in the attempt to provide a rationale to TTD clinical features (section 5.5).

5.1 Altered gene expression profile in TTD dermal fibroblasts

The expression profile of primary dermal fibroblasts from the TTD7PV female patient, was investigated and compared with that of her healthy mother (TTD7PVmother). By so doing, we expected to minimize the expression variability due to different genetic backgrounds. The TTD7PV patient was selected because of her severe phenotype, the fact that she is a compound heterozygous for one of the most frequent TTD alterations (Arg722Trp, Table 8) and the availability of early passage fibroblasts both from the patient and the mother. The RNAs from three biological replicates of each sample were processed for RNAseq analysis (section 5.1.1). Illumina sequencing was performed at IGA Technology Service (Udine) and, in collaboration with Dr. Roberta Carriero and Dr. Silvia Bione from the bioinformatic laboratory CABGEN (IGM-CNR, Pavia), we performed the bioinformatics analysis of RNAseq raw data, in an attempt to identify genes differentially expressed in TTD dermal fibroblasts.
To investigate the biological meaning of the output gene lists, we portrayed the enriched biological themes by performing a detailed clustering analysis and functional classifications (section 5.1.2).

5.1.1 Several hundred genes are differentially expressed in TTD7PV

Data derived from the RNAseq analysis provided a picture on the transcriptome of TTD7PV dermal fibroblasts and its distinctive expression profile from the control cells cultured in basal condition. The analysis identified 718 differentially expressed genes in TTD7PV cells, the majority of which is down-regulated in agreement with the notion that a reduced transcriptional activity may be responsible for the clinical features of this disorder (Figure 10, A and B). It is conceivable that some of these gene expression alterations may account for the multisystem nature and the developmental defects of TTD pathological phenotype.

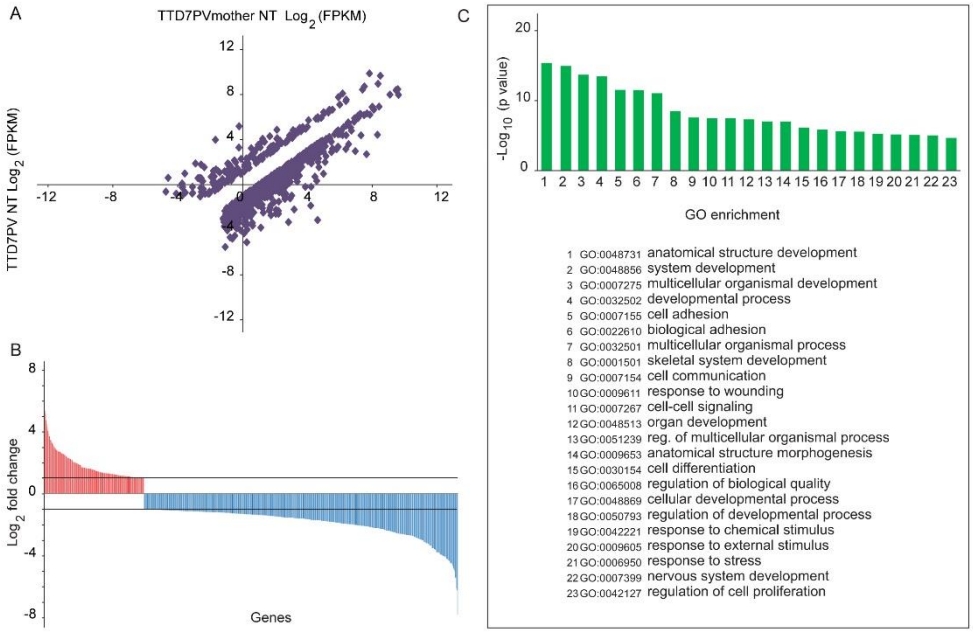

Figure 10. Differential gene expression analysis in TTD dermal fibroblasts in basal condition.
A) Scatter plot analysis showing the expression levels of the 718 genes deregulated in basal condition in TTD7PV dermal fibroblasts compared to the healthy mother (TTD7PVmother). Each dot corresponds to a different gene. 173 genes are up-regulated, 545 genes are down-regulated. FPKM: fragments per kilobase of exon per million mapped fragments. **B)** Schematic representation of the 718 genes differentially expressed in TTD7PV fibroblasts. Red and blue bars indicate up- and down-regulated genes, respectively. **C)** Schematic representation of the Gene Ontology (GO) biological processes enrichment of the 718 transcriptionally deregulated genes in TTD cells obtained by using the DAVID bioinformatics tool. The top 23 enriched pathways (FDR ≤ 0.05) are indicated based on their p values (P ≤ 0.05).

The DAVID bioinformatics tool provided a biological meaning to the 718 differentially expressed genes in TTD and among the most enriched biological themes based on Gene Ontology (GO) terms (Figure 10C), we identified several 'developmental processes' categories, in agreement with the developmental defects in TTD. In addition, several of the deregulated genes belonged to the 'cell-cell signaling' and 'cell adhesion' pathways, in agreement with our previous finding demonstrating extracellular matrix defects in TTD fibroblasts (Orioli et al., 2013; Arseni et al, 2015).

5.2 UV-induced transcriptional alterations and γ-H2AX chromatin modifications in normal and TTD fibroblasts

Photosensitive TTD cells, which are defective in NER, are unable to remove the UV-induced DNA lesions and result in the formation of bulky DNA-adducts that block cell transcription. The removal of UV photoproducts is essential to resume the inhibited transcription. Starting from this notion, we investigated whether the transcriptional alterations in TTD fibroblasts are due to the accumulation of lesions in regions of the chromatin that are more sensitive to DNA damage and therefore to the subsequent interference with the transcriptional apparatus activity or to a direct transcriptional failure caused by TFIIH mutations.
Thus, to identify global transcriptome changes in response to UV light, we irradiated primary dermal fibroblasts from TTD7PV patient and her healthy mother (TTD7mother) with UV-C rays and performed RNAseq analysis on RNAs collected after 2hrs of recovery. In this time frame, the NER pathway in normal cells has only partially removed the UV-induced DNA lesions (Figure 11).

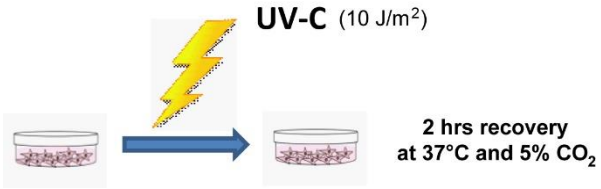

Figure 11. Schematic representation of the experimental strategy. Primary dermal fibroblasts from the TTD7PV patient or the healthy mother were exposed to UV-C (10 J/m2). After irradiation cells were maintained in fresh culture media for 2 hrs and then processed for RNAseq analysis. Three biological replicates were performed for each cell strain.

5.2.1. The normal cellular response to UV-irradiation affects the expression of 332 genes

By RNAseq and computational data analysis, we found that the expression profile of 332 genes is modified in normal dermal fibroblasts 2 hours after UV irradiation (Figure 12). This subset of genes includes an equal number of up- and down-regulated genes. Interestingly, among the upregulated ones (170 genes), the great majority belongs to the "transcriptional regulation" and "DNA-binding proteins" GO-categories, suggesting a transcriptional involvement in the primary cellular response to UV-irradiation. Notably, among the UV-responsive genes identified by RNAseq, *BTG2*, *PMAIP1* and *IL11* were previously described (Gentile et al, 2003).

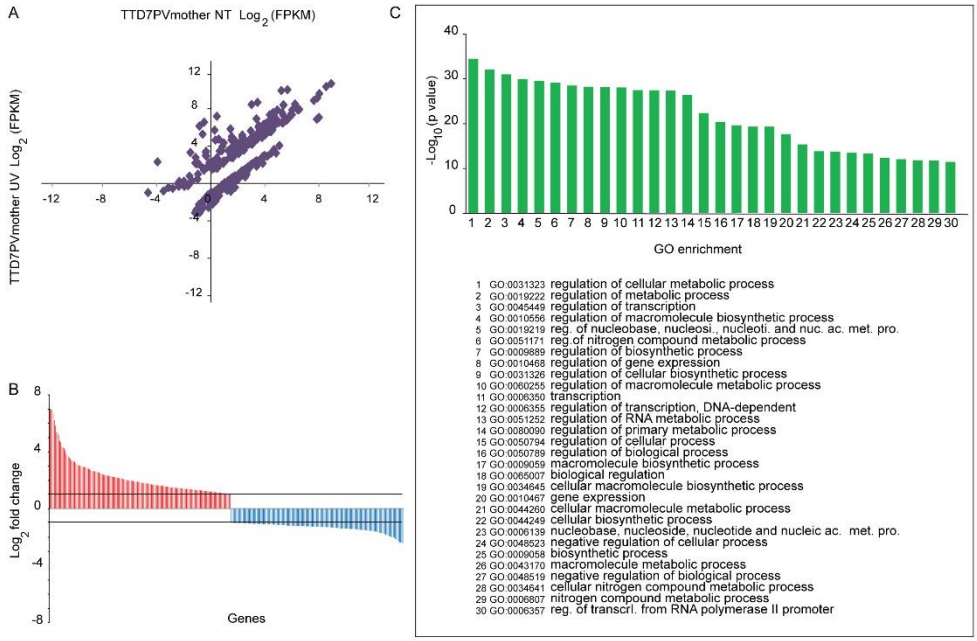

Figure 12. UV-responsive genes in normal dermal fibroblasts after UV-irradiation
A) Scatter plot analysis showing the expression levels of the 332 genes deregulated upon UV irradiation in primary fibroblasts from the healthy individual (TTD7PVmother). Each dot corresponds to a different gene. 170 genes are up-regulated, 162 genes are down-regulated. FPKM: fragments per kilobase of exon per million mapped fragments. **B)** Schematic representation of the 332 genes differentially expressed in dermal fibroblasts of TTD7PVmother after UV irradiation. Red and blue bars indicate up- and down-regulated genes, respectively. **C)** Schematic representation of the GO biological processes enrichment of the 332 transcriptionally deregulated genes in TTD7PVmother sorted by the DAVID functional annotation tool. The top 30 enriched pathways (FDR $\leq$ 0.05) are indicated based on their p values ($P \leq 0.05$).

Moreover, DAVID analysis on all 332 UV-responsive genes, highlighted that 'metabolic processes' 'transcription regulation' (including genes encoding general transcription factors, mediators and several zinc finger proteins) "chromatin organization" and "biosynthetic processes" are the most enriched GO-terms. Overall, this analysis marks the normal cellular response of dermal fibroblasts to the UV-induced DNA damage.

5.2.2. The TTD cellular response to UV-irradiation affects the expression of 502 genes

The expression profile analysis performed by RNAseq revealed that 502 genes are transcriptionally modified in TTD upon UV-irradiation. Relevant of note, among the 502 deregulated genes, 250 are in common with the normal cellular response to UV-irradiation whereas 252 are deregulated only in TTD7PV fibroblasts (Figure 13).

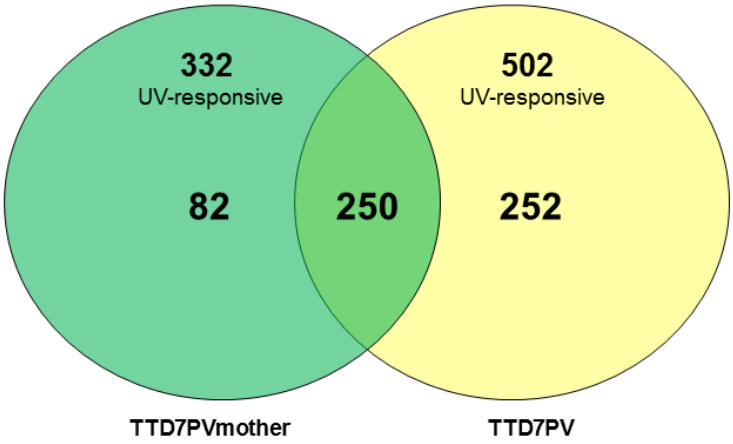

Figure 13. Venn diagram indicating the number of genes whose transcription is modified following UV-irradiation in control (TTD7PVmother, *green*) and patient (TTD7PV, *yellow*) fibroblasts. The expression of 250 genes is commonly modified in TTD and control cells in response to UV-irradiation, whereas the transcriptional modification of 82 and 252 genes occurs specifically in the control and patient fibroblasts, respectively.

While the 250 UV-responsive genes common to TTD and control fibroblasts include an equal number of up- and down-regulated genes, the large majority of the 252 TTD-specific genes are down-regulated in accordance with the TFIIH-dependent transcriptional impairment that characterized TTD cells (Figure 14, A and B).

Moreover, functional studies performed by DAVID tool revealed that most of the 252 UV-responsive genes encode transcriptional-related proteins (Figure 14 C). The identification of these signaling pathways, which seem to characterize the TTD-response to UV-irradiation, may hopefully shed light on TTD deficiencies.

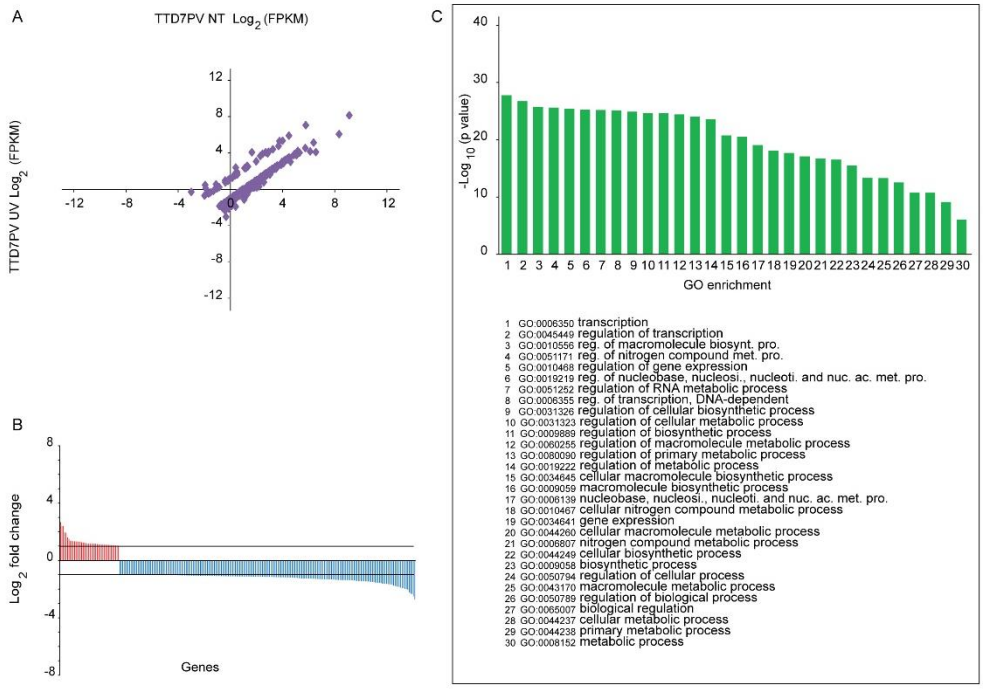

Figure 14. Expression profile in TTD dermal fibroblasts after UV irradiation
A) Scatter plot analysis showing the expression levels of the 252 UV-responsive genes specific for TTD7PV fibroblasts. Each dot corresponds to a different gene. 42 genes are up-regulated, 210 genes are down-regulated. FPKM: fragments per kilobase of exon per million mapped fragments. **B)** Schematic representation of the 252 genes differentially expressed in TTD7PV fibroblasts. Red and blue bars indicate the up- and down-regulated genes, respectively. **C)** Schematic representation of the GO biological processes enrichment of the 252 UV-responsive genes specific for TTD7PV fibroblasts sorted by the DAVID functional annotation tool. The top 30 enriched pathways (FDR $\leq$ 0.05) are indicated based on their p values ($P \leq 0.05$).

Notably, a subset of 82 UV-responsive genes fails to be regulated in TTD fibroblasts (Figure 13). The majority of these genes (57) is transcriptionally up-regulated in normal fibroblasts in response to UV-exposure and encodes proteins involved in developmental processes (Figure 15, A-D). It is tempting to speculate that the lack

of transcription up-regulation of 57 UV-responsive genes in TTD fibroblasts could be ascribed to the impaired transcriptional machinery affected by the reduced levels of mutated TFIIH (Botta et al., 2002). However, it is also conceivable that TTD transcriptional failure could arise from the persistence of UV-photolesions in specific regions of the genome thus leading to a block of transcription. Further studies are required to investigate the relevance of this transcriptional failure in TTD and its implications in TTD ethiopathogenesis.

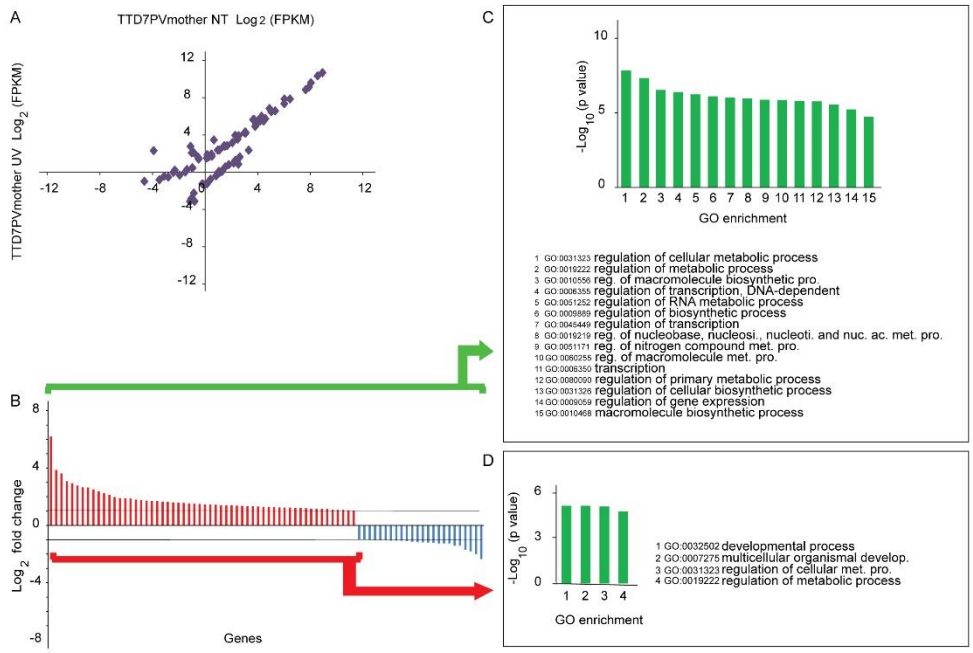

Figure 15. Functional pathways of 82 UV responsive genes specific for normal dermal fibroblasts

A) Scatter plot analysis showing the expression levels of the 82 genes that respond to UV irradiation in primary fibroblasts of the healthy individual (TTD7PVmother). Each dot corresponds to a different gene. 57 genes are up-regulated, 25 genes are down-regulated. FPKM: fragments per kilobase of exon per million mapped fragments. **B)** Schematic representation of the 82 genes differentially expressed in TTD7PV mother's fibroblasts. Red and blue bars indicate up- and down-regulated genes, respectively. **C-D**) Schematic representation of the GO biological processes enrichment obtained by using the DAVID bioinformatics tool. The analysis has been applied to the 82 UV-responsive genes (C) and to the 57 up-regulated genes (D). In C the top 15 enriched pathways are indicated (FDR ≤ 0.05) according to their p values ($P \leq 0.05$), in D all the pathways with FDR ≤ 0.05 are indicated.

5.2.3 TTD dermal fibroblasts exhibit altered protein amount and different occupancy of γ- H2AX in response to UV-irradiation

The persistence of unrepaired DNA lesions, including UV-induced photolesions, results over time in the formation of double-strand breaks (DSBs). It is known that upon DSB induction by ionizing radiation, histone H2AX in the vicinity of DSBs is phosphorylated by ATM and DNA-PKcs at Serine 139, thus generating γ-H2AX. H2AX is widely distributed and upon phosphorylation triggers the accumulation of a multitude of different DSB-repair and DNA-damage signaling molecules. In addition, it has been suggested that γ-H2AX allows the recruitment to the DSB of other chromatin-modifying complexes such as the ATP-dependent remodelers INO80 and SWR1, that act in concert to enhance DNA accessibility in order to facilitate the repair process (Kinner et al., 2008). Therefore, we investigated the presence and amount of γ-H2AX in TTD dermal fibroblasts, cultured in basal conditions or upon UV-irradiation at different time points (1, 2, 4, 6 hours) through immunoblot analysis.

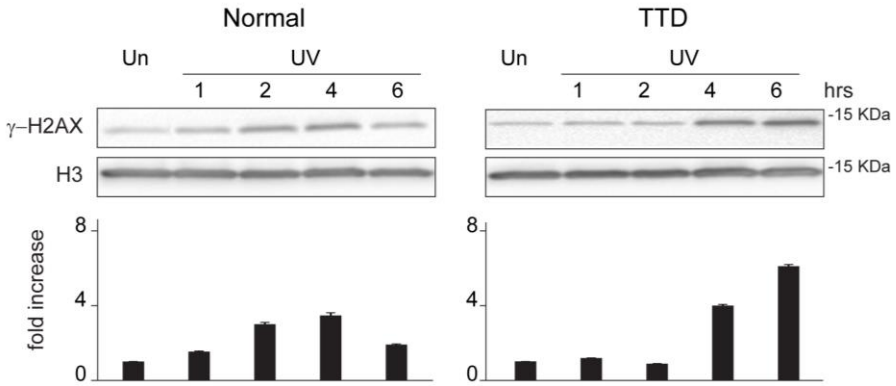

Figure 16. Intracellular levels of γ-H2AX in primary dermal fibroblasts. Immunoblot analysis of γ-H2AX in total lysates of normal donor and TTD patient fibroblasts, in basal conditions (Un) and 1, 2, 4, and 6 hours after UV irradiation. Protein levels were quantified and normalized to the amount of the loading control histone H3. The reported values represent the means of three independent experiments. Bars indicate the standard errors.

In normal cells the total amount of γ-H2AX increases and reaches the maximum level 4 hrs after UV-irradiation (Figure 16). At 6 hrs the level is reduced, likely because most of the DNA lesions have been already removed. In TTD fibroblasts,

where the UV-induced DNA-damage persists, the levels of γ-H2AX increase progressively at least up to 24 hrs after irradiation (data not shown).

Overall these results indicate that an accumulation of γ-H2AX protein in response to UV-irradiation might affect TTD cells, which fail to recover the normal chromatin status after UV-irradiation.

Emerging data indicate that epigenetic processes, such as DNA methylation and histone modifications, control gene expression by altering chromatin structure.
Starting from that notion, we asked whether changes in transcription regulation previously identified by RNAseq analysis in TTD fibroblasts are due to a persistence of unrepaired DNA lesions occurring at specific loci (hotspots) and to the subsequent interference with the transcriptional apparatus activity or whether they could be ascribed to a direct TFIIH-dependent transcriptional impairment caused by mutations typical of TTD.
To clarify this issue, we performed ChIPseq analysis using antibodies specific for the γ-H2AX histone modification in primary dermal fibroblasts from the TTD7PV patient and her healthy mother. Since the basal level of γ-H2AX in normal as well as in TTD cells was very low and not sufficient amount of DNA could be immunoprecipitated in untreated cells, the ChIPseq analysis was performed only following UV irradiation. In order to compare the γ-H2AX distribution by ChIPseq analysis with the expression profile by RNAseq, we maintained the same experimental conditions previously described. Thus, the samples were collected after 2hrs of recovery from the UV-irradiation and processed. The DNA fragments co-immunoprecipitated with anti-γ-H2AX were sequenced at the IGA Institute. The experiment was performed in triplicate, to reduce the variability due to stochastic variations.
Computational analyses of ChIPseq raw data were performed by Dr Roberta Carriero and Dr. Silvia Bione from the bioinformatic laboratory CABGEN (IGM-CNR, Pavia). The reads derived from the raw data were first mapped to a reference genome and the DNA regions with a significant enrichment of mapped reads (*peaks*) respect to the input, that highlights the sites of the genome tightly bound by γ-H2AX, were subsequently identified. Thus, the number of *peaks* in the actively transcribed and non-transcribed regions of the whole genome of UV-irradiated dermal fibroblasts from the healthy mother or TTD patient replicates, were detected. Several thousand of *peaks* were found in each sample, thus providing a profile of the random distribution of γ-H2AX along the genome. To identify possible hotspots of DNA damage in genomic regions that could be more exposed to UV irradiation, we isolated the *peaks* that are common to the three replicates of each cell strains. By so doing, we selected 282 and 260 *peaks* of γ-H2AX in the normal donor and TTD

patient, respectively (Figure 17).

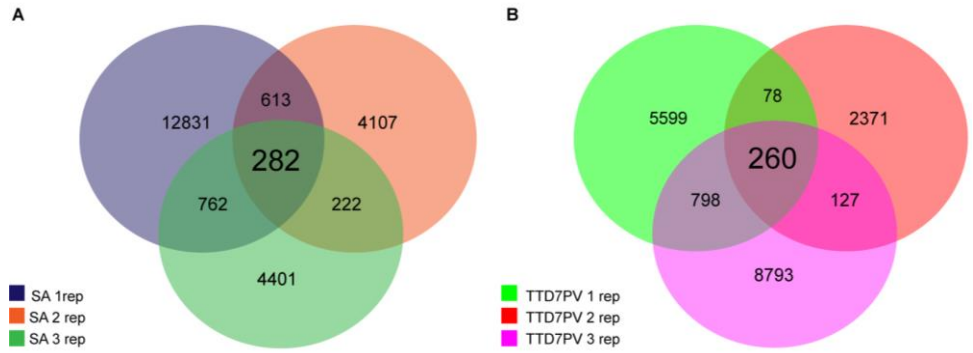

Figure 17. Venn diagram representing the number of γ-H2AX *peaks* from the ChIPseq analysis in the three replicates of control (TTD7PVmother) **(A)** and patient (TTD7PV) fibroblasts after UV-irradiation **(B).** The intersection indicates the common *picks* within the three replicates for each cell strain. In summary, 282 common *peaks* are found in normal fibroblasts, whereas 260 common *peaks* are found in TTD fibroblasts.

Among the 282 common *peaks* identified in the replicates from the fibroblasts of the healthy donor, the vast majority maps in gene-rich regions (55%) or intergenic regions (35%) located within 50Kb from the actively transcribed sites, which could contain transcriptional regulatory elements (enhancers, silencers or other cis-regulatory factors). A possible explanation to this finding is that transcribed genomic regions may be more exposed to DNA damage compared to not-transcribed regions because they are kept accessible to the transcriptional apparatus. In contrast, the compaction of euchromatin requires energy and time, given the complexity of the structure, to allow the positioning of the transcriptional machinery. A similar trend is found in TTD cells, with a distribution of *peaks* in the gene-rich regions and intergenic regions of about 51% and 39%, respectively.
By looking at the γ-H2AX *peaks* distribution over the chromosomes, it is evident that in NER-proficient cells 59% of *peaks* is located in intrachromosomal regions, whereas 31% map in the telomere-adjacent regions, which are known to be prone to replication-mediated DSBs caused by the stalling of replication forks in sub-telomeric regions (Zschenker et al., 2009). 10% of the remaining *peaks* sit in the regions flanking the centromere.
In contrast, the 260 *peaks* of γ-H2AX that are common to the three NER-deficient TTD7PV replicates mapped prevalently on the sub-telomeric regions (59%),

whereas a smaller amount (31%) are located in the large intrachromosomal regions (Figure 18).

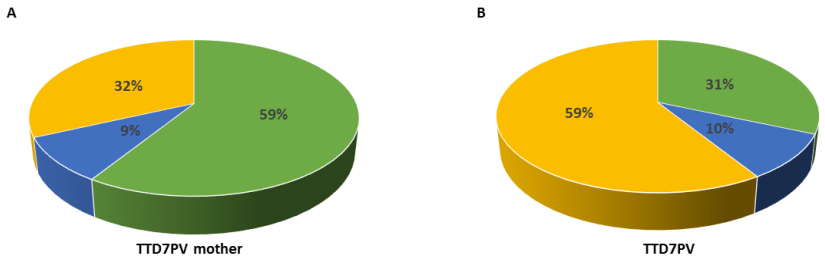

Figure 18. Pie chart representing the distribution along the chromosomes of the γ-H2AX *peaks* common to the three replicates of control (TTD7PVmother) **(A)** and patient (TTD7PV) fibroblasts after UV-irradiation **(B).** Each section represents a different region of the chromosome: sub-telomeric regions (*light green section*); pericentromeric regions (*blue section*); and intrachromosomal regions *(yellow section).*

To better understand whether the differential distribution of γ-H2AX *peaks* in TTD could account for the transcriptional deregulations identified by RNAseq analysis, we dissected the γ-H2AX *peaks* which were differentially enriched in TTD compared to the control fibroblasts. For that reason, we took advantage of the DiffBind, a tool directed to identify differentially enriched peaks between two sample groups in ChIPseq data. We found 122 *peaks* differentially enriched in TTD7PV patient fibroblasts compared to the healthy mother. Relevant of note, the differentially distributed γ-H2AX *peaks* were not located on the loci of the transcriptionally deregulated genes. None of them overlapped with the TTD-defective (82) or the TTD-specific (252) UV-responsive genes. These findings demonstrate that the hotspots of DNA damage along the genome of TTD cells do not correlate with the loci of differentially expressed genes, strengthening the hypothesis that TTD clinical features may be caused by the transcriptional impairment of specific subsets of genes rather than the accumulation of unrepaired DNA lesions in specific loci.

Overall, we found that *XPD* mutations associated with TTD result in a wide transcriptional impairment, both in basal condition as well as in response to UV-irradiation. We demonstrated that after UV exposure TTD fibroblasts fail to up-regulate the expression of particular sets of genes, whereas others are specifically deregulated in TTD. Finally, we showed the persistence of the epigenetic

modification γ-H2AX and its differentially distribution along the chromatin of TTD fibroblasts after UV-induced DNA damage, event likely caused by the accumulation of unrepaired DNA photolesions.

5.3 Gene expression deregulation in RNA pool from TTD/XP-D primary fibroblasts

In the attempt to identify transcription deregulations that might account for TTD clinical features, we focused our attention on the 82 genes that failed to be up-regulated in TTD fibroblasts following UV exposure and to the 718 and 502 genes that were deregulated in TTD cells before and after UV, respectively (5.2.2 paragraph). We took advantage of the Integrative Genomics Viewer (IGV) application, which allows the integration of a wide range of genomic data sets including RNAseq aligned sequence reads across several samples. At first, we excluded from further analysis all the genes showing very low expression levels in our samples as well as the genes that resulted significantly deregulated but displayed a heterogeneous expression among replicates. By this approach, we intended to minimize the number of false positive frequently caused by low expression levels or by a limited read length of RNASeq, which negatively affects the evaluation of gene expression. By so doing, we focused our attention on a reduced list of 176 deregulated genes, among which 92 were found deregulated both in basal condition and after UV irradiation, whereas the remaining 84 resulted deregulated only after UV-induced DNA damage. The selected 176 genes were further investigated by real time RT-PCR in primary dermal fibroblasts from four TTD patients, who carry different mutations in the *XPD* gene and are characterized by a severe phenotype. By so doing, we intend to identify those genes that are commonly deregulated in TTD patients. Therefore, we first performed the analysis on a pool of RNAs from the fibroblasts of four TTD patients and, as second step, in individual TTD cell strains.

5.3.1 Expression analysis of the deregulated genes in TTD patients with severe phenotypes and comparison with their healthy parents

A high-throughput gene expression profiling by RealTime Ready Custom Panels was applied to RNA pools obtained by mixing equal amounts of RNAs from dermal fibroblasts of either TTD patients (TTD pool) or the healthy parents (control pool). As reported in Table 8, we selected four TTD patients representative of different types and combinations of mutated *XPD* alleles (TTD/XP-D), including those resulting in the Arg112His and Arg722Trp changes that represent the most frequent alterations observed in TTD patients. For the control pool, we used the fibroblasts of

the parents of TTD7PV and of the siblings TTD12PV/TTD15PV.

Table 8. Clinical, cellular and molecular features of the 4 TTD/XP-D patients analyzed in this study

TTD PATIENT POOL				
Patient code	**Clinical severity**[a]	**alleles, aa changes**	**UDS levels**[b] **%** of normal	**TFIIH levels**[c] **%** of normal
TTD7PV	Severe	R722W/[L461V; V716_R730del]	15	56
TTD12PV[d]	Severe	R722W/C259Y	20	60
TTD15PV[d]	Severe	R722W/C259Y	20	60
TTD23PV	Severe	R112H/unexpressed	10	37

[a] In TTD, clinical severity refers to the degree of physical and mental impairment whereas in XP to the type and severity of skin lesions. For details, see the following references: Botta et al., 2002, 2009; Stefanini et al., 2010; Orioli et al., 2013 and references therein.
[b] UV-induced DNA repair synthesis (UDS) after irradiation with 10J/m2 observed in patient cells is expressed as percentage of the value found in normal cells analyzed in parallel.
[c] TFIIH levels in patient fibroblasts are expressed as percentages of the corresponding value in normal C3PV fibroblasts analyzed in parallel (Botta et al., 2002, unpublished data).
[d] Brothers.

By quantitative real time RT-PCR assays, we measured the transcript levels of the selected 176 genes in TTD patient pool and TTD control pool. These genes are listed in Table A (*see* Appendix). In parallel, we investigated the expression levels of three reference genes (*YWHAZ*, *G6PD* and *GAPDH*), which are stably expressed housekeeping genes. All the analyses were performed in duplicate, whereas a third replicate was done only for those genes showing a mild Cp variation between the biological replicates of TTD or control samples. The cycle threshold (Ct) of all the deregulated genes was normalized to the geometric mean of the reference genes transcript levels (ΔCt). For each gene, the mean Ct value of the replicates ± standard deviation (SD), the ΔCt and the fold change (FC), which represents the difference between the expression levels in the patient and corresponding control pools are reported in Tables B and C (*see* Appendix) in basal condition as well as after UV-irradiation, respectively. The result of the 176 genes investigated by qRT-PCR analysis in the RNA pool from TTD patient or parent fibroblasts are summarized in Figure 19.

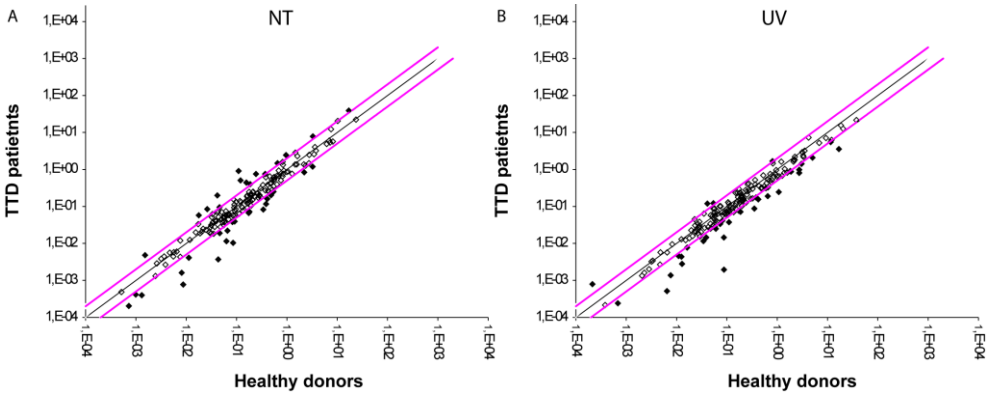

Figure 19. Fold changes of the 176 genes investigated by qRT-PCR analysis in the RNA pool from four TTD patients and compared with those obtained in the RNA pool from four TTD parents. Scatter plot representing the comparison of the 176 mRNA levels found in the RNA pool from patient and parent fibroblasts cultured in basal condition **(A)** and upon UV irradiation **(B)**. For each gene, the log2 fold change in TTD is plotted against the log2 fold change of the same gene in healthy donors. The black line indicates fold changes of 1 (= no expression deregulation), whereas the pink lines correspond to log2 fold changes ±|2|, respectively.
Black dots outside the pink lines indicate the transcripts with a fold-change greater than ±|2| whereas the black empty dots indicate the transcripts with a fold-change lower than ±|2|.

Among the 176 genes analyzed by qRT-PCR, 60 genes confirmed their expression deregulation in the RNA pool from TTD patients compared to the healthy parents, with a fold change (f.c.) value higher than ± |2|. Among all, *WISP2* resulted the most deregulated gene in TTD fibroblasts (f.c. -11,726 in basal condition; f.c.-45,203 after UV irradiation).
In summary, by extending the analysis to other TTD patients with different mutations in the *XPD* gene and the use of a different technical approach allowed us to reduce to 60 the number of differentially expressed genes.

5.4 Expression analysis of differentially expressed genes in individual TTD/XP-D and XP/XP-D fibroblast strains

Among the 60 genes deregulated in TTD fibroblasts, we selected the 40 with the highest f.c. values in TTD pool. Next we investigated them by individually analysing the fibroblasts of seven TTD patients, representative of distinct *XPD* mutations (Table 9) and six TTD parents.

Table 9. Clinical, cellular and molecular features of 3 additional TTD/XP-D patients (not included in the pool) and 5 XP/XP-D patients analyzed in this study

TTD PATIENT POOL				
Patient code	**Clinical severity**[a]	**alleles, aa changes**	**UDS levels**[b] **%** of normal	**TFIIH levels**[c] **%** of normal
TTD8PV	moderate	R112H/R112H	10	35
TTD11PV	severe	R112H/V121_E159del	10	44
TTD20PV	severe	R112H/[L461V; V716_R730del]	10	48
XP PATIENT POOL				
XP15PV[d]	mild	R683Q/R683Q	26	
XP16PV[d]	mild	R683Q/R683Q	25	108
XP17PV	mild	R683W/R616P	15	81
XP49PV	severe	R683W/[L461V;V716_R730del]	12	83
XP1BR	severe	R683W/R683W	30	84

[a] In TTD, clinical severity refers to the degree of physical and mental impairment whereas in XP to the type and severity of skin lesions. For details, see the following references: Botta et al., 2002, 2009; Stefanini et al., 2010; Orioli et al., 2013 and references therein.
[b] UV-induced DNA repair synthesis (UDS) after irradiation with 10J/m^2 observed in patient cells is expressed as percentage of the value found in normal cells analyzed in parallel.
[c] TFIIH levels in patient fibroblasts are expressed as percentages of the corresponding value in normal C3PV fibroblasts analyzed in parallel (Botta et al., 2002, unpublished data).
[d] Sisters.

Besides to TTD, *XPD* mutations have also been found in XP cases. To verify whether the identified transcription deregulations were specifically associated with the TTD phenotype or they should be generally ascribed to TFIIH malfunctioning, we extended our investigation to five XP patients and, as control, to the fibroblasts of four XP parents and two genetically unrelated healthy donors (C3PV and C5BO). As reported in Table 9, we selected five XP patients, representative of different types and combinations of mutated *XPD* alleles (XP/XP-D). Transcript levels were evaluated before and after UV irradiation by qRT-PCR using the same primers previously designed for RealTime Ready Custom Panels.
The genes selected are described by grouping them according to their functional role:

- *ID1* and *ID3* belong to the family of inhibitors of the DNA binding proteins and transcriptional activators.

• *C-Jun, JunD, c-Fos, FosB* encode proteins forming the transcription factor complex AP-1. They play a role in the regulation of cell proliferation, differentiation and cell transformation.

• *CSRP2*, *HAND2*, *HOXC10*, *HOXB7, LBH, GDF6* encode proteins involved in development, morphogenesis and cellular differentiation. Among them, the first five genes are transcriptional factors, the latest one is a secreted protein. In particular, *LBH* regulates cardiac gene expression by modulating the combinatorial activities of key cardiac transcription factors. *HAND2* is expressed in the developing ventricular chambers and plays an important role in the cardiac and aortic arch arteries morphogenesis. *CSRP2, HOXB7* and *HOXC10* are activated in the primary response during cell differentiation and proliferation. Finally, *GDF6* is required for normal formation of some bones and joints in the limbs, skull, and axial skeleton.

• *PTGIS, IL20RB, IL13RA2, APBB1IP, CCL1* and *ANGPTL4* encode proteins involved in the immunological response. In particular, *PTGIS* is a member of the prostanoids molecules, which catalyzes the conversion of prostaglandin H2 (PGH2)1 to prostacyclin (prostaglandin I2, PGI2); it is a potent vasodilator and inhibitor of platelet aggregation. *IL20RB* forms a heterodimeric receptor with IL20RA and IL22RA1, which can bind interleukin-20 (IL20). Relevant of note, IL20RB was shown to be over-expressed in psoriatic skin. Moreover, *IL13RA2* is a subunit of the interleukin 13 receptor complex; this cytokine is involved in several stages of B-cells maturation and down-regulates macrophage activity, thereby inhibits the production of pro-inflammatory cytokines and chemokines. *APBB1IP* increases the complement-mediated phagocytosis and mediates the recruitment of T cells in the site of inflammation. *CCL1* is a chemokine which is secreted by T cells and displays chemotactic activity for monocytes. Finally, *ANGPTL4* acts as an apoptosis survival factor for vascular endothelial cells and was shown to regulate glucose homeostasis, lipid metabolism and insulin sensitivity.

• *GADD45A, GADD45B, EGR1, IER3, GDF15, HERPUD1, CLU, HSPA2, GPX3* and *EIF4EBP1* encode proteins related to transcription regulation or translational repressor activity, stressful growth arrest conditions, oxidative stress response and apoptosis.

• *ADRA2, STMN2* and *PCDH10* are neuronal receptors. In particular, *ADRA2* is an adrenergic receptor, which has critical role in regulating neurotransmitter release from sympathetic nerves and from adrenergic neurons in the central nervous system. *STMN2* plays a regulatory role in neuronal growth and osteogenesis. Finally, *PCDH10* is a member of the protocadherin gene family; it is involved in the establishment of specific cell-cell connections in the brain.

• *GALNT2, GNG11, LRRC15* encode transmembrane receptor proteins related

to lipid metabolism as well as collagen and laminin binding.

- *TBX1*, *HAPLN3*, *POSTN* and *SFRP4* encode proteins known to play relevant functions in the development of skin fibroblasts, in the regulation of extracellular matrix homeostasis and cell migration.

- *WISP2* and *WNT4* genes are strictly connected. *WISP2* encodes a member of the WNT1 inducible signaling pathway (WISP) protein subfamily, which belongs to the connective tissue growth factor family (CTGF). *WNT4* is a member of a family of cysteine-rich, glycosylated signaling proteins, regulated by WISP, which has been implicated in oncogenesis and in several developmental processes.

Notably, 23 genes (out of the 40) that have been so far investigated in individual fibroblast strains, did not reveal any statistically significant expression deregulation in TTD cells neither in basal condition nor after UV irradiation. Therefore, the analysis of these genes was excluded from further characterization. The results of the analysis of the significantly deregulated genes in TTD, XP and healthy donors are reported below.

5.4.1 Expression deregulation of *ID*-transcriptional factors in TTD/XP-D and XP/XP-D patients

By real-time PCR assays we detected a significant reduction in the expression levels of *ID1* and *ID3* in TTD fibroblasts compared to the healthy controls, both in basal conditions and after UV irradiation (Figure 20). In contrast, no major differences are observed in XP fibroblasts since their expression levels are included within the range of expression variability observed in fibroblasts from healthy individuals, both in basal condition as well as after UV-irradiation.

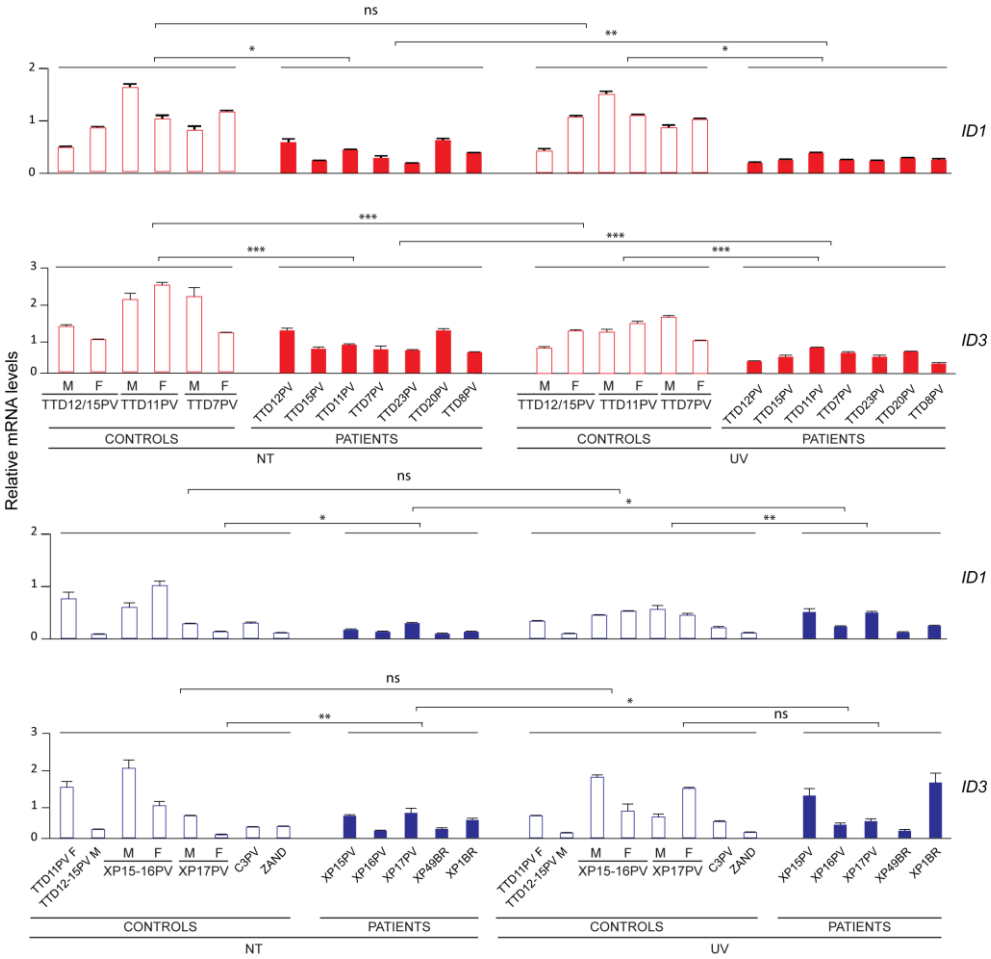

Figure 20. *ID1* and *ID3* transcript levels in primary dermal fibroblasts from TTD, XP and patient's parents. Real time quantification of *ID1* and *ID3* mRNA levels in fibroblasts from TTD healthy parents (TTD12PV-15PV parents, TTD11PV parents and TTD7PV parents, *red empty bars*), TTD/XP-D patients (TTD12PV, TTD15PV, TTD11PV, TTD7PV, TTD23PV, TTD20PV, TTD8PV, *red solid bars*), healthy donors (TTD11PV father, TTD12-15PV mother, XP15PV-16PV parents, XP17PV parents, C3PV and C5BO, *blue empty bars*) and XP/XP-D patients (XP15PV, XP-16PV, XP17PV, XP49BR and XP1BR *blue solid bars)* in basal condition (NT) and after UV irradiation (UV). The expression level of each gene was normalized to the expression of the *GAPDH* housekeeping gene and then to the expression level of an internal control sample (the TTD12-15PV father for TTD patients and the corresponding healthy parents or the XP15-16PV father for XP and the corresponding healthy parents). The reported values represent the means of at least two independent experiments (**P* <0.05, ***P* <0.01, ****P* <0.001; Student's t-test). Bars indicate the standard errors. M: mother, F: father.

5.4.2 Expression deregulation of cellular stress responsive-related genes in TTD/XP-D and XP/XP-D patients

As part of the early responsive genes, all the AP-1 transcription factors respond to the UV irradiation. The steady state levels of *c-Fos* transcripts and, to a lesser extent of *FosB* and *JunD*, tend to increase following the cellular stress induced by UV exposure whereas *c-Jun* appears down-regulated.

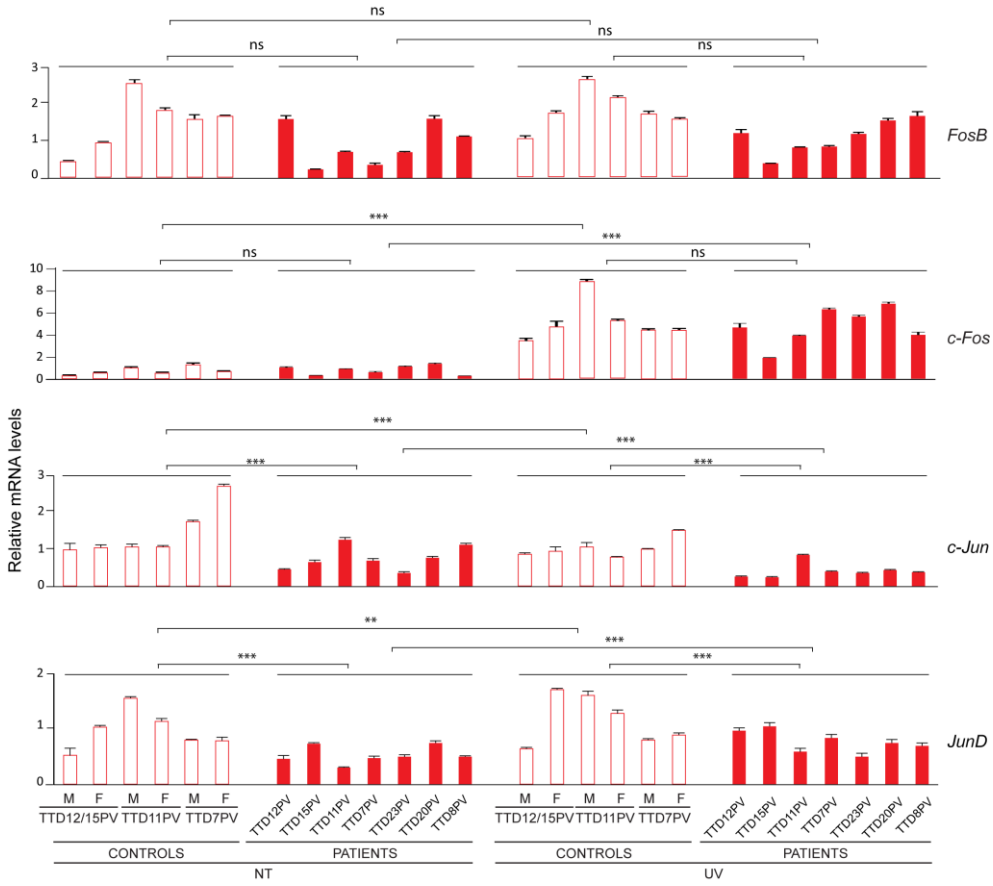

Figure 21. *FosB, c-Fos, c-Jun* and *JunD* transcript levels in primary dermal fibroblasts from TTD and patient's parents. Real time quantification of *FosB, c-Fos, c-Jun* and *JunD* mRNA levels in fibroblasts from TTD healthy parents (controls, *red empty bars*), TTD/XP-D patients (*red solid bars*). The expression level of each gene was normalized to the expression of the *GAPDH* housekeeping gene and then to the expression level of the healthy individual TTD12-15PV father. The reported values represent the means of at least two independent experiments (**P* <0.05, ***P* <0.01, ****P* <0.001; Student's t-test). Bars indicate the standard errors. M: mother, F: father.

In TTD cells the steady state levels of *JunD*, *c-Jun* and *FosB* are slightly reduced even though they respond normally to UV irradiation. Conversely, normal levels of *c-Fos* mRNA are found in TTD, both in basal condition and upon UV irradiation (Figure 21). Because of the mild reduction observed in TTD cells, even if statistically significant, we did not proceed with further analysis.

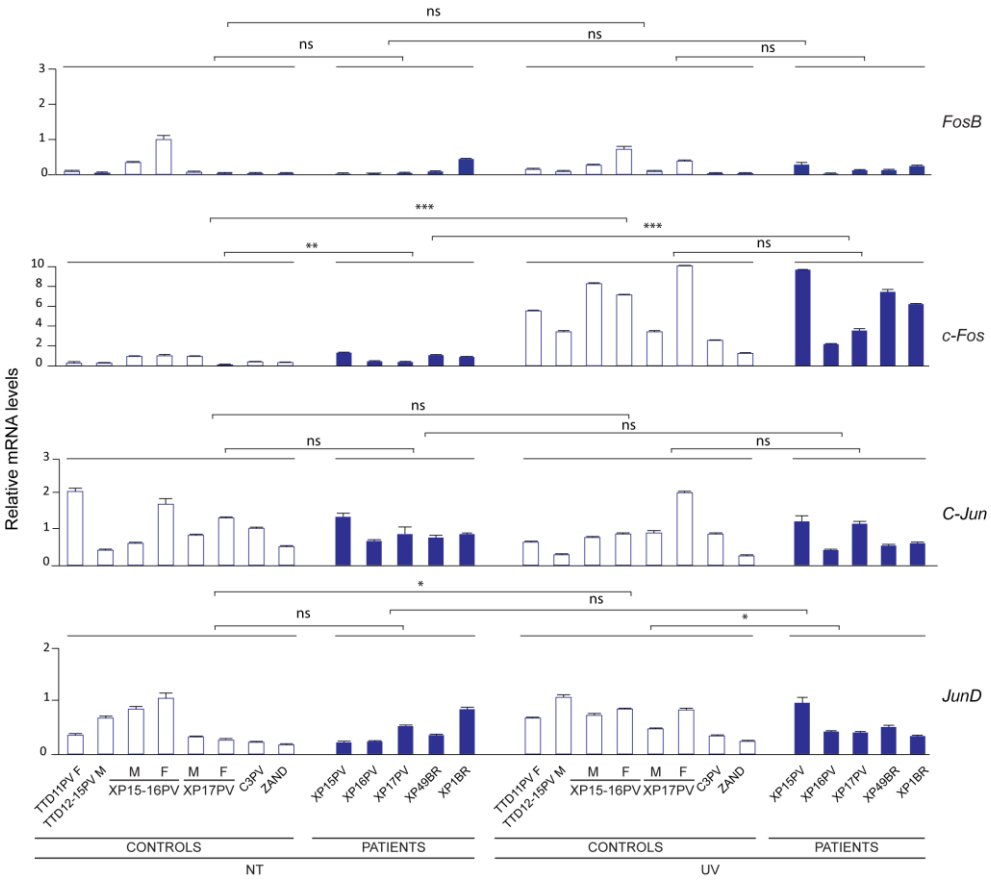

Figure 22. *FosB, c-Fos, c-Jun* and *JunD* transcript levels in primary dermal fibroblasts from XP and patient's parents. Real time quantification of *FosB*, *c-Fos*, *c-Jun* and *JunD* mRNA levels in fibroblasts from healthy donors (controls, *blue empty bars*) and XP/XP-D patients (*blue solid bars)* in basal condition (NT) and after UV irradiation (UV). The expression level of each gene was normalized to the expression of the *GAPDH* housekeeping gene and then to the expression levels of the healthy individual XP15-16PV father. The reported values represent the means of at least two independent experiments (**P* <0.05, ***P* <0.01, ****P* <0.001; Student's t-test). Bars indicate the standard errors. M: mother, F: father.

In addition, no statistically significant differences were observed in XP fibroblasts for all the analysed genes (Figure 22).

5.4.3 Expression deregulation of genes related to immunological response in TTD/XP-D and XP/XP-D patients

We observed that all TTD fibroblasts contain substantial reductions in the levels of *ANGPTL4*, *PTGIS*, *IL20RB* mRNAs compared to the control fibroblasts both in basal conditions and after UV irradiation (Figure 23). These results are in agreement with the finding that defects in lipid uptake, mitochondrial dysfunction and gluconeogenic pathway might be implicated in TTD clinical features (Compe et al., 2005; Traboulsi et al., 2014).

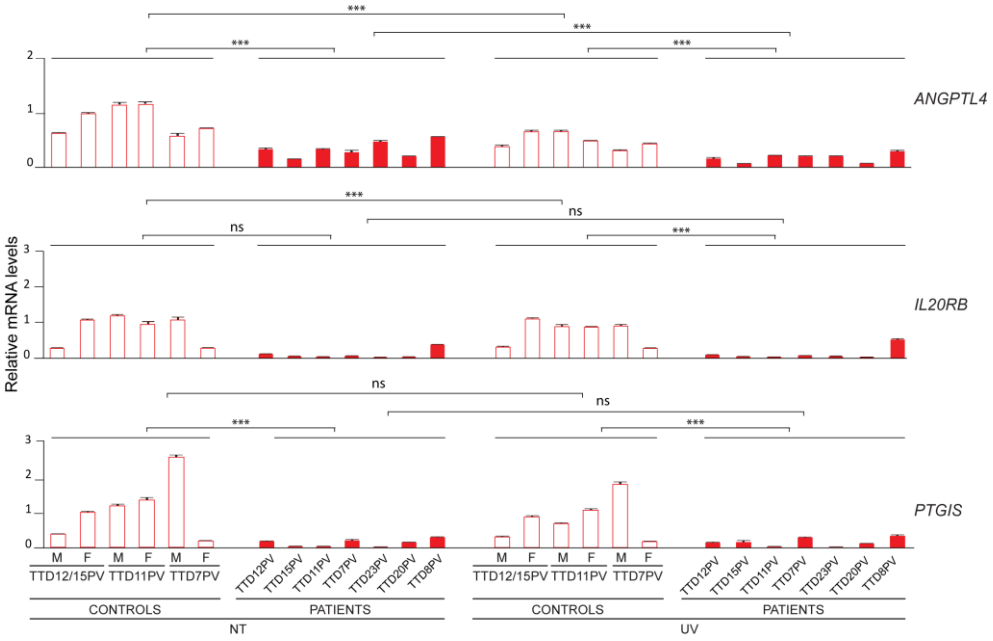

Figure 23. *ANGPTL4*, *IL20RB* and *PTGIS* transcript levels in primary dermal fibroblasts from TTD and patient's parents. Real time quantification of *ANGPTL4*, *IL20RB* and *PTGIS* mRNA levels in fibroblasts from TTD healthy parents (controls, *red empty bars*), TTD/XP-D patients (*red solid bars*). The expression level of each gene was normalized to the expression of the *GAPDH* housekeeping gene and then to the expression level of the healthy individual TTD12-15PV father. The reported values represent the means of at least two independent experiments (**P* <0.05, ***P* <0.01, ****P* <0.001; Student's t-test). Bars indicate the standard errors. M: mother, F: father.

Nevertheless, also the XP fibroblasts reveal reduced levels of *PTGIS* and, to some extent, of *ANGPTL4* after UV irradiation, thus indicating that their under-expression may not be strictly associated to the TTD phenotype but rather to a malfunctioning TFIIH. In contrast, the strong down-regulation of *IL20RB* appears to be more specific of TTD rather than XP fibroblasts (Figure 24). Considering the decreased expression levels observed in TTD, we intend to further investigate this expression deregulation at the protein level (section 5.5).

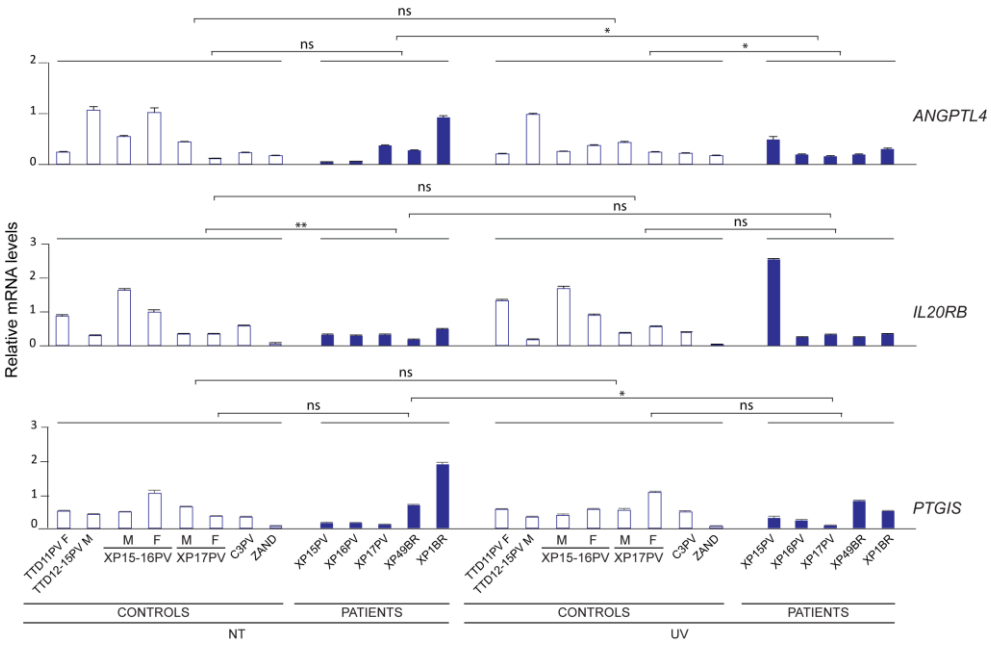

Figure 24. *ANGPTL4*, *IL20RB* and *PTGIS* transcript levels in primary dermal fibroblasts from XP and patient's parents. Real time quantification of *ANGPTL4*, *IL20RB* and *PTGIS* mRNA levels in fibroblasts from healthy donors (controls, *blue empty bars*) and XP/XP-D patients (*blue solid bars)* in basal condition (NT) and after UV irradiation (UV). The expression level of each gene was normalized to the expression of the *GAPDH* housekeeping gene and then to the expression level of healthy individual XP15-16PV father. The reported values represent the means of at least two independent experiments (**P* <0.05, ***P* <0.01, ****P* <0.001; Student's t-test). Bars indicate the standard errors. M: mother, F: father.

5.3.4 Expression deregulation of early responsive genes in the TTD/XP-D and XP/XP-D patients

In normal fibroblasts, *GADD45A*, *GADD45B*, *EGR1* and *IER3* genes respond to UV irradiation by increasing their expression levels. In contrast, no up-regulation is observed in TTD cells, which maintain a reduced level of basal transcription (Figure 25).

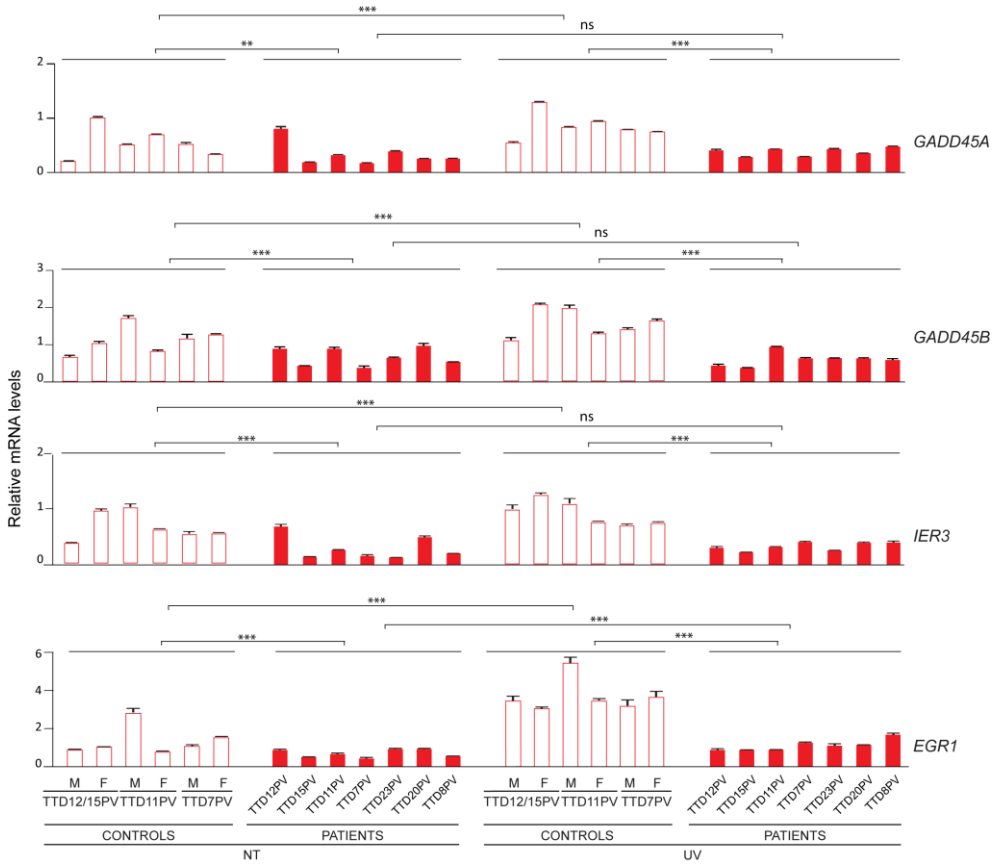

Figure 25. *GADD45A*, *GADD45B*, *IER3* and *EGR1* transcript levels in primary dermal fibroblasts from TTD and patient's parents. Real time quantification of *GADD45A*, *GADD45B*, *IER3* and *EGR1* mRNA levels in fibroblasts from TTD healthy parents (controls, *red empty bars*) and TTD/XP-D patients (*red solid bars*). The gene expression levels was normalized to the expression of the *GAPDH* housekeeping gene and to the expression level of the healthy individual TTD12-15PV father. The reported values represent the means of at least two independent experiments (**P* <0.05, ***P* <0.01, ****P* <0.001; Student's t-test). Bars indicate the standard errors. M: mother, F: father.

A normal response of *GADD45A*, *GADD45B*, *IER3* and *EGR1* to UV-irradiation is found in XP fibroblasts (Figure 26). Since *IER3* is an immediate early responsive gene, and *GADD45A*, *GADD45B* and *EGR1* are involved in the stress response, these findings suggest that TTD cells mutated in *XPD* might delay the activation of signalling events involved in the cellular stress response.

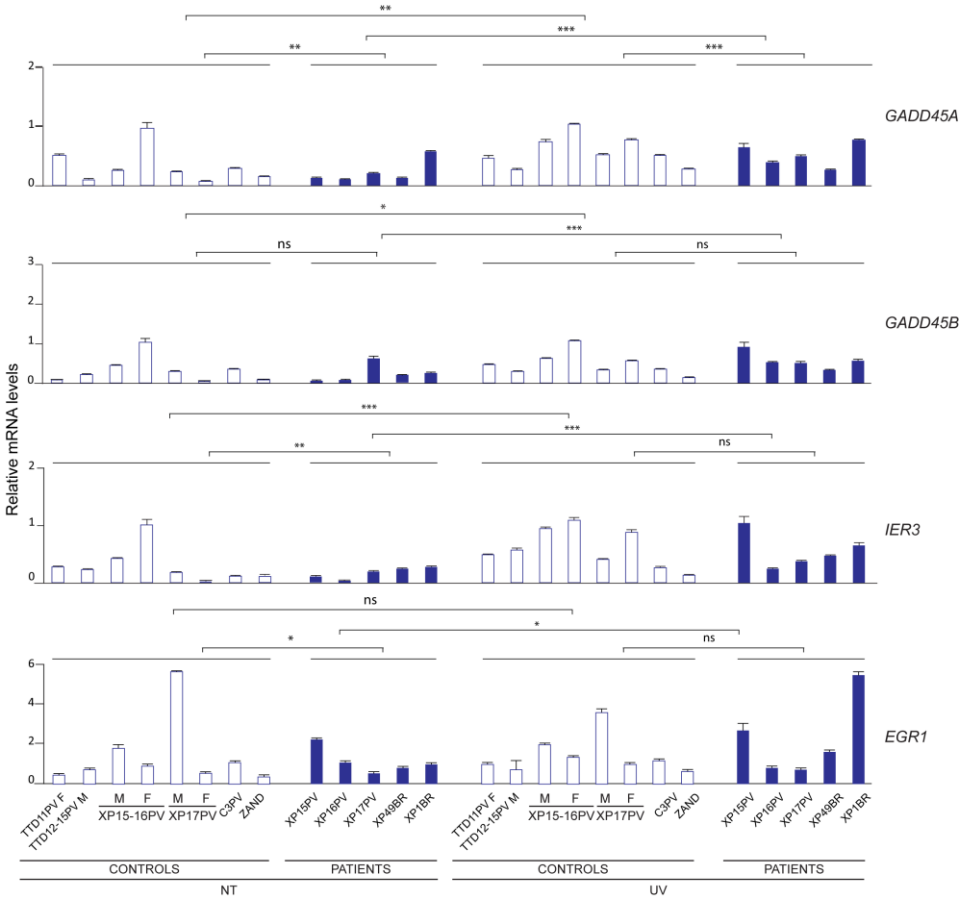

Figure 26. *GADD45A, GADD45B, IER3* and *EGR1* transcript levels in primary dermal fibroblasts from XP and patient's parents. Real time quantification of *GADD45A*, *GADD45B*, *IER3* and *EGR1* mRNA levels in fibroblasts from healthy donors (controls, *blue empty bars*) and XP/XP-D patients (*blue solid bars)* in basal condition (NT) and after UV irradiation (UV). The expression level of each gene was normalized to the expression of the *GAPDH* housekeeping gene and to the expression level of healthy individual XP15-16PV father. The reported values represent the means of at least two independent experiments (**P* <0.05, ***P* <0.01, ****P* <0.001; Student's t-test). Bars indicate the standard errors. M: mother, F: father.

5.4.5 Expression deregulation of *IL13RA2* and *PCDH10* in TTD/XP-D and XP/XP-D patients

We previously found that protocadherin *PCDH10* that acts in the cell-cell connection and cytokine *IL13RA2*, which is involved in the B-cell maturation, are up-regulated in TTD pool following UV-irradiation. In agreement, the individual analysis in TTD patients revealed a specific UV-induced increase in the expression of both genes in the TTD patients but not in the XP cases.

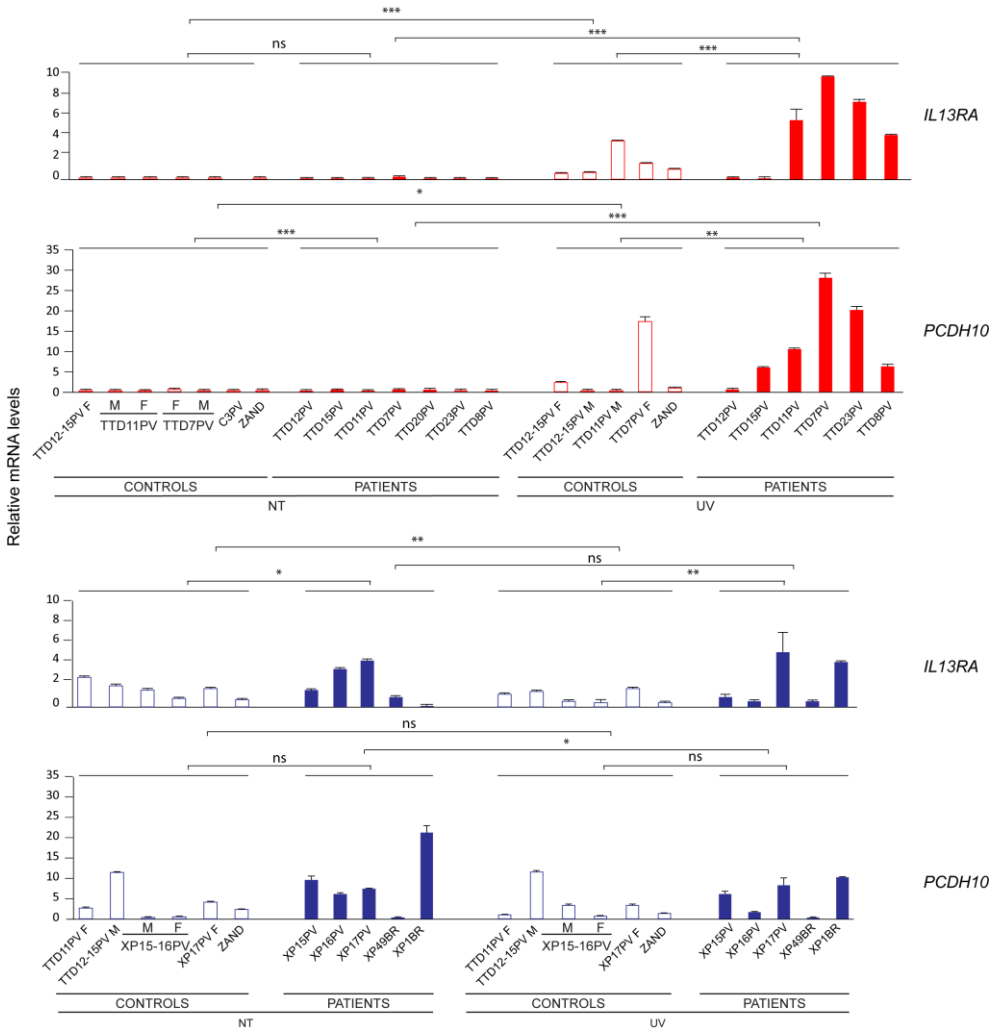

Figure 27. *IL13RA2* and *PCDH10* transcript levels in primary dermal fibroblasts from TTD, XP and patient's parents. Real time quantification of *IL13RA2* and *PCDH10* mRNA levels in fibroblasts from TTD healthy parents (TTD12-15PV parents, TTD11PV parents and TTD7PV parents, *red empty bars*), TTD/XP-D patients (TTD12PV, TTD15PV, TTD11PV, TTD7PV, TTD23PV, TTD20PV, TTD8PV, *red solid bars*), healthy donors (TTD11PV father TTD12-15PV mother, XP15PV-16PV parents, XP17PV father and the unrelated healthy individual C5BO, *blue empty bars*) and XP/XP-D patients (XP15PV, XP-16PV and XP17PV XP1BR, XP49BR, *blue solid bars)* in basal condition (NT) and after UV irradiation (UV). The expression level of each gene was normalized to the expression of the *GAPDH* housekeeping gene and then to the expression levels level of an internal control sample (the TTD12-15PV father for TTD patients and the corresponding healthy parents or the XP15-16PV father for XP and the corresponding healthy parents). The reported values represent the means of at least two independent experiments (**P* <0.05, ***P* <0.01, ****P* <0.001; Student's t-test). Bars indicate the standard errors. M: mother, F: father.

Conversely, XP fibroblasts showed expression levels similar to those of the controls pointing to a difference between TTD and XP patients (Figure 27). Therefore, *PCDH10* and *IL13RA2* over-expression after UV irradiation seems to distinguish the TTD from the XP response to UV-induced DNA damage.

5.4.6 Expression deregulation of *WISP2* and *WNT4* in TTD/XP-D and XP/XP-D patients

Also the expression analysis of *WISP2* and *WNT4* revealed a transcription down-regulation in the fibroblasts of all TTD patients, in basal condition as well as after UV irradiation. In addition, the transcription deregulation of *WISP2* appears specific of TTD and not XP fibroblasts (Figure 28).

Overall, this expression analysis supports the idea that *XPD* mutations associated with TTD phenotype result in a wide but specific transcriptional impairment. We define a transcriptional profile that characterize *XPD* mutated cells (both TTD and XP) as well as transcription deregulations that are specific of TTD fibroblasts. Among these, we observed a failure in transcription activation of specific early responsive as well as stress responsive genes after UV-induced DNA damage. We found a transcriptional impairment of genes involved in immunological pathways and the activation of subsets of genes such as *PCDH10* and *IL13RA2* that seem to characterize TTD phenotype.

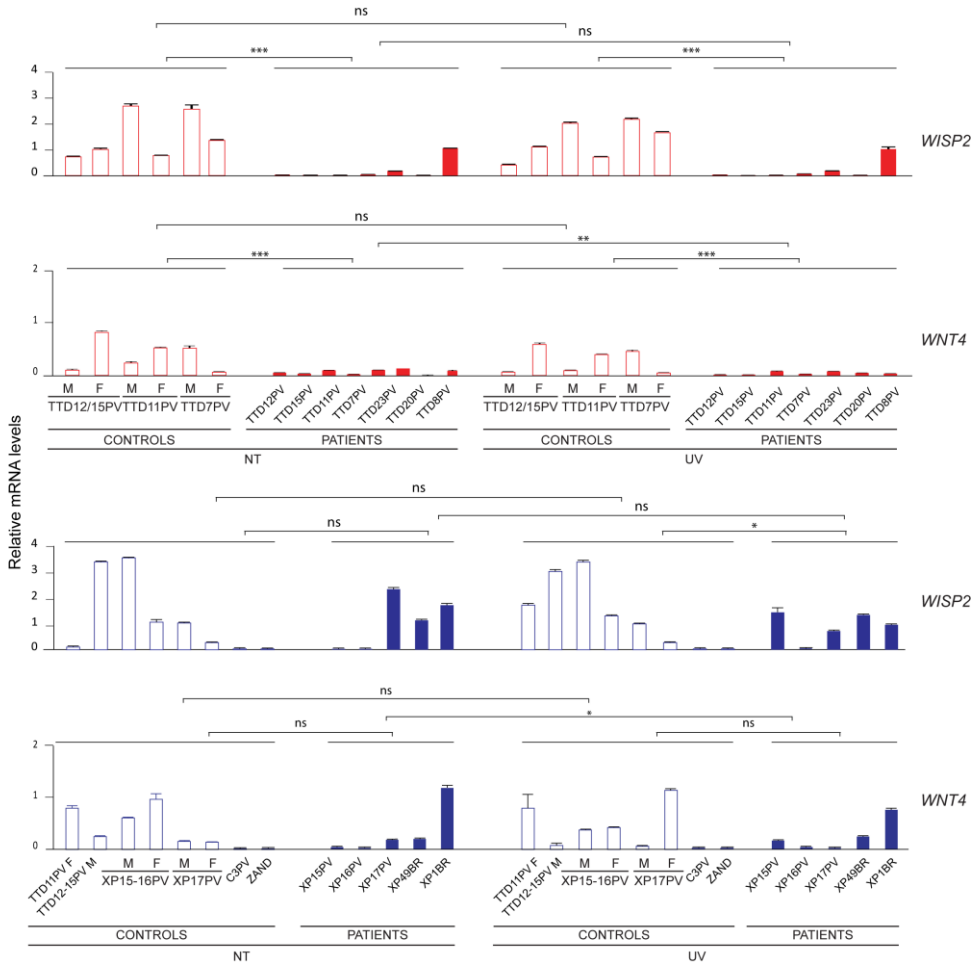

Figure 28. *WISP2* and *WNT4* transcript levels in primary dermal fibroblasts from TTD, XP and patient's parents. Real time quantification of *WISP2* and *WNT4* mRNA levels in fibroblasts from TTD healthy parents (TTD12PV-15PV parents, TTD11PV parents and TTD7PV parents, *red empty bars*), TTD/XP-D patients (TTD12PV, TTD15PV, TTD11PV, TTD7PV, TTD23PV, TTD20PV, TTD8PV, *red solid bars*), healthy donors (TTD11PV father, TTD12-15PV mother, XP15PV-16PV parents, XP17PV parents, C3PV and C5BO, *blue empty bars*) and XP/XP-D patients (XP15PV, XP-16PV, XP17PV, XP49BR and XP1BR *blue solid bars)* in basal condition (NT) and after UV irradiation (UV). The expression level of each gene was normalized to the expression of the *GAPDH* housekeeping gene and then to the expression levels of an internal control sample (the TTD12-15PV father for TTD patients and the corresponding healthy parents or the XP15-16PV father for XP and the corresponding healthy parents). The reported values represent the means of at least two independent experiments (**P* <0.05, ***P* <0.01, ****P* <0.001; Student's t-test). Bars indicate the standard errors. M: mother, F: father.

5.4.7 Several TTD-specific transcriptional deregulations are also found in TTD mouse embryonic fibroblasts

To gain further insight on the contribution of these genes to TTD phenotype, in collaboration with Dr. Emmanuel Compe (IGBMC/CNRS, Strasburg) we took advantage of the mouse embryonic fibroblasts (MEFs) from the TTD mouse model to investigate the correlation between TTD phenotype and specific gene expression deregulations. Therefore, the expression level of the differentially expressed genes (*WISP2*, *PTGIS*, *EGR1*, *PCDH10*, *WNT4*, *ANGPTL4*, *IL20RB* and *IL13RA2)* was investigated in MEFs isolated from either TTD mice or isogenic control mice (WT). Clearly, *WISP2*, *PTGIS*, *EGR1* and *PCDH10* are down-regulated in TTD cells, thus supporting their involvement in TTD phenotype (Figure 29). In contrast, *WNT4*, *ANGPTL4*, *IL20RB* and *IL13RA2* seemed not to be differentially expressed in TTD MEFs. This discrepancy could be explained by the diverse tissue derivation as well as the different developmental stage of the human and mouse TTD cells, according to the involvement that these genes have in pathways that are modulated during development. In addition, for specific genes such as *PCDH10* and *IL13RA2*, the expression deregulation should become evident only after UV-irradiation. Further studies are required to address this issue.

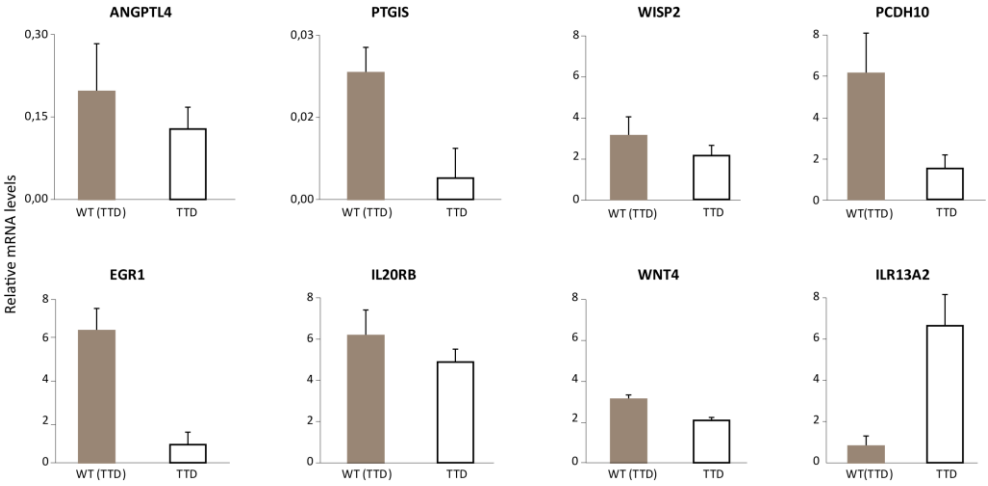

Figure 29. *ANGPTL4, PTGIS, WISP2, EGR1, IL20RB, WNT4* and *IL13RA2* expression levels in MEFs. Real time quantification of *ANGPTL4, PTGIS, WISP2, EGR1, IL20RB, WNT4* and *IL13RA2* mRNA levels in MEFs from wild type (WT) and TTD mice. The gene expression was normalized to the expression of the *rRNA 18S*. Bars indicate the standard errors. The reported values represent the means of at least two independent experiments (**P* <0.05, ***P* <0.01, ****P* <0.001; Student's t-test).

5.5 Impact of the gene expression deregulations on the corresponding protein levels in TTD dermal fibroblasts

To verify whether the transcriptional deregulations in TTD fibroblasts are paralleled by altered protein contents, we investigated the amounts of PTGIS, ANGPTL4, IL20RB, Il13RA2, WISP2, WNT4 and PCDH10 in whole extracts of primary fibroblasts from several XP-D patients (either TTD or XP) and healthy individuals. The analysis was performed by immunoblot in cells that were cultured in basal condition or after UV irradiation. No specific protein bands were detected for WNT4, IL20RB, IL13RA2 and PCDH10 as a result of malfunctioning antibodies or very low steady state levels in primary dermal fibroblasts. Indeed, it was previously shown that IL20RB receptor cooperates with IL20RA in the same heterodimeric complex and its amount increases after 24 hrs of treatment with cytokines (Keller et al., 2014). Immunoblot analysis revealed that the level of WISP2 varies among individuals and its variability is irrespective of the clinical phenotype. Furthermore, the protein cellular content is not significantly influenced by UV-treatment (Figure 30). Similar results are observed for ANGPTL4 protein amount in TTD, XP or control fibroblasts (Figure 31). Therefore, the severe transcription down-regulation of *ANGPTL4* and *WISP2* in TTD cells does not affect the corresponding protein levels, indicating that protein synthesis and/or protein stability can compensate for transcriptional impairments.

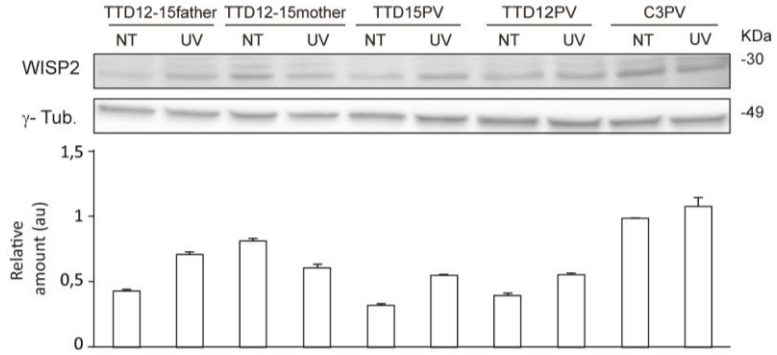

Figure 30. Intracellular amounts of WISP2 in primary dermal fibroblasts. Immunoblot analysis of WISP2 in total cell lysates of normal (C3PV, TTD12-15PV parents) and TTD/XP-D (TTD12PV, TTD15PV) fibroblasts cultured in basal condition (NT) or 2hrs after UV-irradiation (UV). γ tubulin was used as the loading control. The reported values are the mean of at least three independent experiments. Bars indicate standard errors. **Abbreviations**: NT, not treated; au, arbitrary unit.

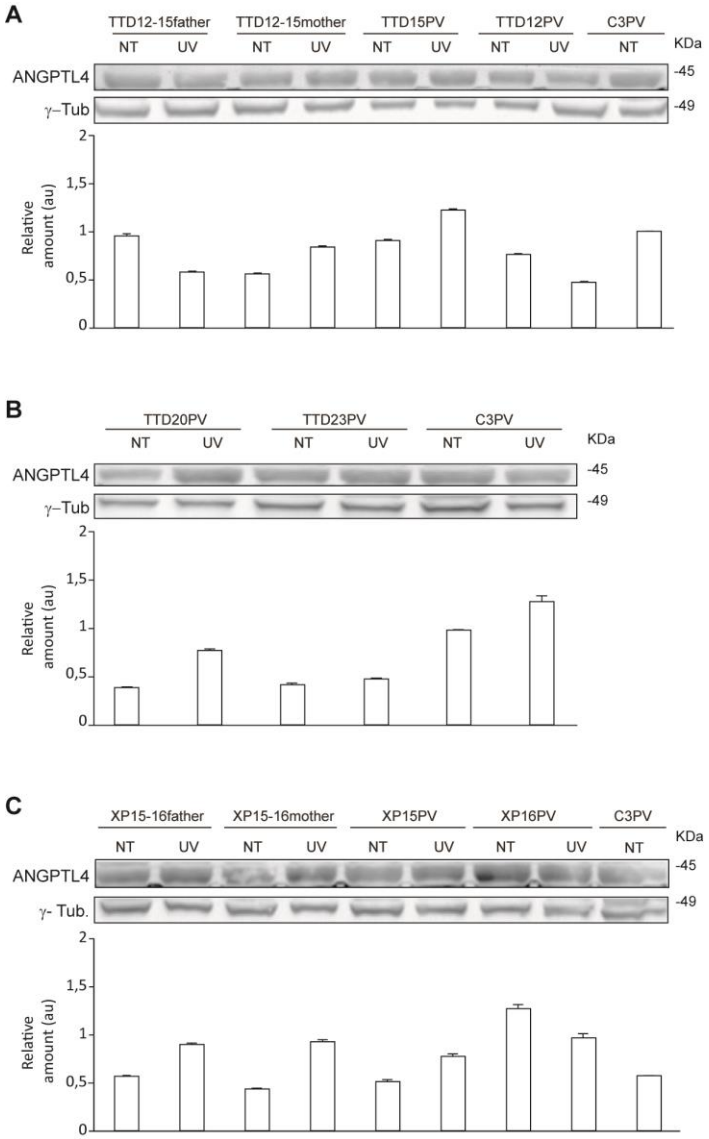

Figure 31. Intracellular amounts of ANGPTL4 in primary dermal fibroblasts. Immunoblot analysis of ANGPTL4 in total cell lysates of (**A-B**) normal (C3PV, TTD12-15PV parents) and TTD/XP-D fibroblasts (TTD12PV, TTD15PV; TTD20PV, TTD23PV); (**C**) normal (C3PV, mother and father of XP15-16PV siblings) and XP/XP-D (XP15PV, XP16PV) fibroblasts cultured in basal condition (NT) and 2 hrs after UV-irradiation (UV). γ tubulin was used as the loading control. The reported values are the mean of at least three independent experiments. Bars indicate standard errors. **Abbreviations**: NT, not treated; au, arbitrary unit.

Notably, we observed a drastic reduction of PTGIS amount in all the TTD/XP-D fibroblasts, in agreement with the transcriptional down-regulation detected in these cells (Figure 32). We also observed a slight reduction of PTGIS levels in XP/XP-D fibroblasts. This reduction is however less relevant compared to that of TTD cells.

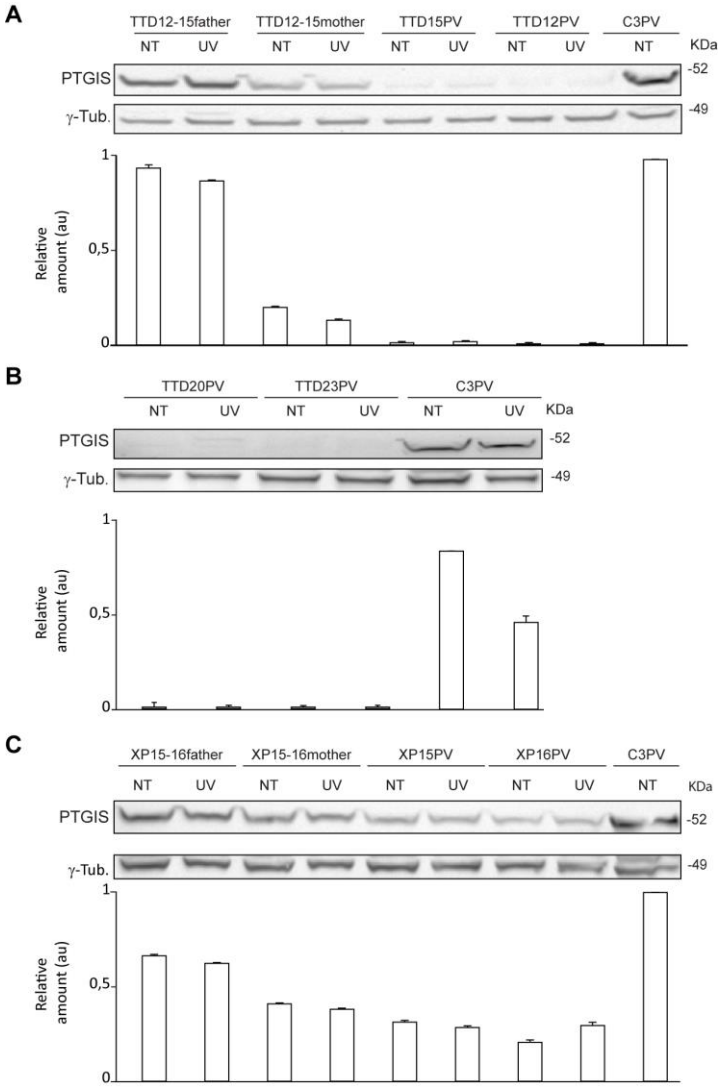

Figure 32. Intracellular amounts of PTGIS in primary dermal fibroblasts. Immunoblot analysis of PTGIS in total cell lysates of (**A-B**) normal (C3PV, TTD12-15PV parents) and TTD/XP-D fibroblasts

(TTD12PV, TTD15PV; TTD20PV, TTD23PV); (**C**) normal (C3PV, mother and father of XP15-16PV siblings) and XP/XP-D (XP15PV, XP16PV) fibroblasts cultured in basal condition (NT) and 2 hrs after UV-irradiation (UV). γ tubulin was used as the loading control. The reported values are the mean of at least three independent experiments. Bars indicate standard errors. **Abbreviations**: NT, not treated; au, arbitrary unit.

Overall, our results demonstrate a transcriptional deregulated profile specific of TTD primary dermal fibroblasts that was accomplished by an altered protein content of PTGIS, thus strengthening the differences between TTD and XP phenotypes. Further studies are required to fulfil the biological implications of PTGIS reduction in TTD patients. Nevertheless, this finding opens the possibility of novel biomarkers for this disorder.

6. Discussion and conclusions

The XPD helicase is a subunit of the transcription/repair factor IIH (TFIIH), an essential player in transcription initiation, gene expression regulation and nucleotide excision repair (NER). Mutations in *XPD* give rise to different ultraviolet (UV)-sensitive syndromes, including trichothiodystrophy (TTD) and xeroderma pigmentosum (XP) that, besides skin photosensitivity are characterized by different phenotypes. While XP patients exhibit freckle-like pigmentation and a greatly increased risk of sun-induced skin cancers, TTD patients have sulfur-deficient brittle hair, short stature, developmental delay and a variety of neuroectodermal symptoms. The dual role of TFIIH in NER and in basal/activated transcription could rationalize the different phenotypes by asserting that XP is caused by mutations that interfere mainly with DNA repair whereas TTD clinical features are due to additional impairment of transcription (Bootsma and Hoeijmakers, 1993, 1994).
Several lines of evidence have demonstrated *in vitro* and *in vivo* that TTD cells are characterized by transcriptional impairments which may account for some of the patient clinical features, including bone alterations (Orioli et al., 2013, Arseni et al., 2015), hypoplasia of adipose tissue (Compe et al., 2005), developmental and neurological defects (Compe et al., 2007; Traboulsi et al., 2014).
For this research study, we took advantage of next/generation sequencing technology to define the TTD gene expression profile and to search for global transcription alterations that might eventually explain other TTD clinical features. We found that 718 genes are transcriptionally deregulated in TTD7PV female patient compared to her healthy mother. Most of the differentially expressed genes are down-regulated, in agreement with the notion that a reduced transcriptional activity is responsible for the TTD phenotype. These events probably reflect the impact that TTD-specific mutations in *XPD* have on the structure and stability of the TFIIH complex, as attested by the reduced levels of TFIIH in TTD cells (Botta et al., 2002), as well as the reduced ability of TFIIH to phosphorylate and contribute to the transactivation mediated by specific transcription factors (Compe et al., 2007; Keriel et al., 2002). Moreover, the DAVID functional classification tool, based on the Gene Ontology analysis of the deregulated genes delineates a scenario in which “developmental processes”, “cell-cell signalling” and ‘cell adhesion’ categories are the most represented. This finding is in agreement with the observation that TTD is a multisystem disorder characterized by developmental defects and in which extracellular matrix alterations impair the wound healing and migration features of TTD fibroblasts cultured in basal conditions (Arseni et al, 2014).

Since TTD cells fail to repair UV-induced DNA lesions, we also investigated how DNA damage affects the gene expression profile. We found that 82 genes failed to be up-regulated in TTD7PV cells after UV irradiation. The lack of transcriptional up-regulation of this subset of genes could arise from the persistence of irreparable DNA photolesions that in turn leads to a block of transcription. However, it is also conceivable that the reduced levels of the mutated TFIIH cannot sustain the transcription of these 82 genes. In addition, 252 genes resulted deregulated in TTD7PV but not in control donor fibroblasts following UV-irradiation. The majority of these 252 genes are under-expressed in TTD cells and most of them are involved in transcription and gene expression regulation. This finding opens the possibility that the expression deregulation of the 252 genes may lead to a downstream cascade effect that alters the expression of a great number of target genes in term impacting on cell survival. Wide transcription deregulations together with the accumulation of unrepaired DNA lesions in the genome of TTD cells can likely explain the high cellular sensitivity of TTD fibroblasts to UV-irradiation.
Notably, no one of the transcriptional deregulated genes overlap with the γ–H2AX histone modification *peaks* differentially enriched in TTD compared to the healthy mother's dermal fibroblasts. These findings are in agreement with our hypothesis of TTD being a transcriptional disorder. Moreover, ChIPseq analysis revealed that the *peaks* of γ–H2AX in primary fibroblasts from healthy individuals are mainly localized in intrachromosomal regions of the chromosome and in the gene-enriched regions. On the contrary, in TTD dermal fibroblasts γ–H2AX accumulation sits prevalently on the sub-telomeric regions. These findings suggest that in TTD cells the intrachromosomal regions may be more protected than in the normal cells exposed to UV-irradiation. It is tempting to speculate that the stalling of the transcriptional machinery, due to a malfunctioning TFIIH, may protect from UV induced DNA damage or eventually interfere with the γ–H2AX accumulation on DNA-damage sites. This last hypothesis is supported by the delayed accumulation of γ–H2AX in TTD dermal fibroblasts exposed to UV irradiation at early time points (Figure 16).

The genome-wide analysis by RNAseq showed how one of the most typical TTD alterations in *XPD*, Arg722Trp, alters the transcriptional map of primary dermal fibroblasts. By extending the gene expression analysis to other TTD patients characterized by different combination of mutated *XPD* alleles, we could to reduce to 60 the number of differentially expressed genes, thus defining transcriptional alterations that hopefully characterize TTD fibroblasts. The use of cells from patients affected by the XP phenotype, further narrowed down the number of TTD-specific gene expression deregulations and discerned them from those caused by the XP-typical mutations in *XPD*. From this analysis, only few genes resulted deregulated

in XP fibroblasts, whereas the majority is specifically altered in TTD fibroblasts cultured in basal condition or after UV-irradiation.
It is important to remark that by comparing patients with corresponding parents we wanted to reduce the expression variability caused by different genetic backgrounds. Nevertheless, this type of comparison may even result in an increased variability due to the different ages of the investigated individuals (child patients versus adult parents). The above-cited limitation should be overcome by the comparison between TTD and XP patients, who show similar ages.

Gene expression analysis revealed that TTD fibroblasts are characterized by a decreased expression of early responsive genes and cellular stress-responsive genes, suggesting that TTD may be characterized by delayed DNA damage responses, as also evinced a delay in γ-H2AX histone modification following UV irradiation (Figure 16).
Moreover, in TTD fibroblasts, *WISP2* resulted to be the most deregulated gene (fold change -45,203 after UV irradiation). WISP2 is a downstream target of the WNT signaling pathway, which mediates various developmental processes. WISP2 exerts dual actions: the secreted form of WISP2 activates the canonical WNT protein and maintains the cells in an undifferentiated state, whereas, in the adipose tissue WISP2 induced spontaneous differentiation of fibroblasts to become committed to the adipocytes (Grünberg et al., 2014; Hammarsted et al., 2013). Therefore, WISP2 deregulation may play a role in TTD ethiopatogenesis even if we were unable to detect any reduction at the protein level in whole cell extracts of TTD skin fibroblasts. It might however be that in other tissues this transcriptional impairment impact on protein amount. It will be interesting to investigate WISP2 amount in the patient adipose tissue or in the mouse model.

Some of the genes down-regulated in TTD fibroblasts both in basal condition and after UV-irradiation are involved in the immunological response. This finding reminds us of the immunological defects of TTD patients, including the frequently multiple infections as well as the β-thalassemia and reduced synthesis of β-globin, which characterise TTD clinical features.
Notably, we identified a strong reduction of *PTGIS* both at the transcript and at the protein level. PTGIS belongs to the family of prostacyclin and is secreted by various cell types in adipose tissue. It is involved in the regulation of the inflammatory response as well as in adipocyte functioning. In particular, PTGIS catalyzes the conversion of prostaglandin H2 (PGH2)1 to prostacyclin (prostaglandin I2, PGI2), a potent mediator of vasodilation and inhibitor of platelet aggregation (Baenziger et al., 1979; Cebola et al., 2015). In addition, prostaglandins (PGs) are also lipid mediators that promote the differentiation of adipocyte-precursor cells to adipose

cells via activation of the expression of C/EBP β and δ (Michaud et al., 2014). These proteins are important transcription factors in the activation of the early phase of adipogenesis differentiation. According to its role in adipocyte metabolism it is tempting to speculate that the deregulation of PTGIS could account for the defects in low subcutaneous fat content that is implicated in TTD clinical features (Traboulsi, 2014). Interestingly, a recent study demonstrated that the induction of *PTGIS* under hypoxic conditions is responsible of the increased expression of *VEGF* in human fibroblasts, leading to an increased angiogenesis (Wang et al., 2013). It is worthwhile mentioning that tumour cells need a rich and highly vascularized local microenvironment, or niche, in which it can establish and develop. A decreased angiogenesis, due to the down-regulation of PTGIS could inhibit the tumour growth capacity. Moreover, tumours are associated with chronic inflammation to the maintenance of microenvironment; thus the highly reactive nitrogen and oxygen species released from inflammatory cells, interacts with DNA in proliferating cells resulting in permanent genomic alterations, that induce tumour proliferation. The reduced amount of PTGIS could be insufficient to exert its pro-inflammatory function, leading to the decreasing growth of tumours cells. Relevant of note, it is worthwhile remembering that TTD patients do not develop skin cancer. Since the biological role of PTGIS needs to be further characterized, it could be interesting to investigate the protein amount in other tissues as well as in the mouse model.

Perspectives

In summary, this study identifies a distinctive transcriptional profile for TTD patients with mutations in the *XPD* gene and demonstrates a relevant reduction of PTGIS protein in TTD dermal fibroblasts.The clinical diagnosis of TTD is at present provided following the microscopic hair examination for tiger tail banding and hair shaft abnormalities. The discovery of other markers, such as *PTGIS* down-regulation in all TTD patients, could be useful for TTD diagnostic and therapeutic strategies.

In addition, since TTD is characterized by defects affecting several tissue and organs, it would be interesting to perform a similar gene expression profile analysis in different cell types derived from TTD patients. This approach will allow to better understand the mechanisms underlying the multisystem nature of TTD disorder. Moreover, it will be useful to extend the analysis to the non-photosensitive TTD patients, who share with the photosensitive TTD most of the clinical features but not skin photosensitivity.

Overall, the transcriptional alterations that we identified in this study together with the other alterations previously described in TTD likely contribute to explain the TTD ethiopatogenesis.

7. References

Abdulrahman W, Iltis I, Radu L, Braun C, Maglott-Roth A, Giraudon C, Egly JM, Poterszman A (2013). ARCH domain of XPD, an anchoring platform for CAK that conditions TFIIH DNA repair and transcription activities. Proc Natl Acad Sci U S A, 110:E633-42.

Aguilar-Fuentes J, Valadez-Graham V, Reynaud E, Zurita M (2006).TFIIH trafficking and its nuclear assembly during early Drosophila embryo development. J Cell Sci, 119:3866-75.

Aguilar-Fuentes J, Fregoso M, Herrera M, Reynaud E, Braun C, Egly JM, Zurita M (2008). p8/TTDA overexpression enhances UV-irradiation resistance and suppresses TFIIH mutations in a Drosophila trichothiodystrophy model. PLoS Genet, 4:e1000253.

Akoulitchev S, Chuikov S, Reinberg D (2000). TFIIH is negatively regulated by cdk8-containing mediator complexes. Nature, 407:102-6.

Alekseev S, Coin F (2015). Orchestral maneuvers at the damaged sites in nucleotide excision repair. Cell Mol Life Sci, 72:2177–2186.

Andressoo JO, Weeda G, de Wit J, Mitchell JR, Beems RB, van Steeg H, van der Horst GT, Hoeijmakers JH (2009). An Xpb Mouse Model for Combined Xeroderma Pigmentosum and Cockayne Syndrome Reveals Progeroid Features upon Further Attenuation of DNA Repair. Mol Cell Bio, 29:1276-90.

Arseni L, Lanzafame M, Compe E, Fortugno P, Afonso-Barroso A, Peverali FA, Lehmann AR, Zambruno G, Egly JM, Stefanini M, Orioli D (2015). TFIIH-dependent MMP-1 overexpression in trichothiodystrophy leads to extracellular matrix alterations in patient skin. Proc Natl Acad Sci U S A, 2015 112:1499-504.

Assfalg R, Lebedev A, Gonzalez OG, Schelling A, Koch S, Iben S (2012). TFIIH is an elongation factor of RNA polymerase I. Nucleic Acids Res, 40:650-9.

Baenziger NL, Becherer PR, Majerus PW (1979). Characterization of prostacyclin synthesis in cultured human arterial smooth muscle cells, venous endothelial cells and skin fibroblasts. Cell. 16:967-74.

Barreto G, Schäfer A, Marhold J, Stach D, Swaminathan SK, Handa V, Döderlein G, Maltry N, Wu W, Lyko F, Niehrs C (2007). Gadd45a promotes epigenetic gene activation by repair-mediated DNA demethylation. Nature, 445:671-675.

Battistella PA, Peserico A (1996). Central nervous system dysmyelination in PIBI(D)S syndrome: a further case. Childs Nerv Syst. 12:110-113.

Bedez F, Linard B, Brochet X, Ripp R, Thompson JD, Moras D, Lecompte O, Poch O (2013). Functional insights into the core-TFIIH from a comparative survey. Genomics, 101:178-86.

Bernardes de Jesus BM, Bjoras M, Coin F, Egly JM (2008). Dissection of the molecular the highly conservation of histones among species, many organisms produce several variant histones defects caused by pathogenic mutations in the DNA repair factor XPC. Mol Cell Biol, 28:7225-7235.

Bootsma D (1978). DNA repair defects in genetic diseases in man. Biochimie 60:1173-4.

Bootsma D, Hoeijmakers JH (1993). DNA repair. Engagement with transcription. Nature, 363:114-5.

Botta E, Nardo T, Broughton BC, Marinoni S, Lehmann AR, Stefanini M (1998). Analysis of mutations in the *XPD* gene in Italian patients with trichothiodystrophy: Site of mutation correlates with repair deficiency, but gene dosage appears to determine clinical severity. American Journal of Human Genetics 63:1036-1048.

Botta E, Nardo T, Lehmann AR, Egly JM, Pedrini AM, Stefanini M (2002). Reduced level of the repair/transcription factor TFIIH in trichothiodystrophy. Hum Mol Genet, 11:2919-28.

Botta E, Nardo T, Orioli D, Guglielmino R, Ricotti R, Bondanza S, Benedicenti F, Zambruno G, Stefanini M (2009). Genotype-phenotype relationships in trichothiodystrophy patients with novel splicing mutations in the *XPD* gene. Human Mutation 30:438-445.

Bour G, Plassat JL, Bauer A, Lalevee S, Rochette-Egly C (2005). Vinexin beta interacts with the non-phosphorylated AF-1 domain of retinoid receptor gamma (RAR gamma) and represses RAR gamma-mediated transcription. J Biol Chem, 280:17027-17037.

Boyle J, Ueda T, Oh KS, Imoto K, Tamura D, Jagdeo J, Khan SG, Nadem C, Digiovanna JJ, Kraemer KH (2008). Persistence of repair proteins at unrepaired DNA damage distinguishes diseases with ERCC2 (XPD) mutations: cancer-prone xeroderma pigmentosum vs. non-cancer-prone trichothiodystrophy. Hum Mutat, 29:1194-1208.

Broughton BC, Berneburg M, Fawcett H, Taylor EM, Arlett CF, Nardo T, Stefanini M, Menefee E, Price VH, Queille S, Sarasin A, Bohnert E, Krutmann J, Davidson R, Kraemer KH, Lehmann AR (2001). Two individuals with features of both xeroderma pigmentosum and trichothiodystrophy highlight the complexity of the clinical outcomes of mutations in the XPD gene. Hum Mol Genet. 10:2539-47.

Cebola I, Custodio , Muñoz M, Díez-Villanueva A, Paré L, Prieto P5, Aussó S, Coll-Mulet L, Boscá L, Moreno V, Peinado MA (2015). Epigenetics override pro-

inflammatory PTGS transcriptomic signature towards selective hyperactivation of PGE2 in colorectal cancer. Clin Epigenetics. 7:74.

Chang WH and Kornberg RD (2000). Electron crystal structure of the transcription factor and DNA repair complex, core TFIIH. Cell 102:609–613.

Chebaro Y, Amal I, Rochel N, Rochette-Egly C, Stote RH, Dejaegere A (2013). Phosphorylation of the retinoic acid receptor alpha induces a mechanical allosteric regulation and changes in internal dynamics. PLoS Comput Biol, 9:e1003012.

Chen J, Larochelle S, Li X, Suter B (2003). Xpd/Ercc2 regulates CAK activity and mitotic progression. Nature, 424:228-32.

Chymkowitch P, Le May N, Charneau P, Compe E, Egly JM (2011). The phosphorylation of the androgen receptor by TFIIH directs the ubiquitin/proteasome process. EMBO J, 30:468-79.

Cleaver JE (1968). Defective repair replication of DNA in xeroderma pigmentosum. Nature 218:652-656.

Clement FC, Kaczmarek N, Mathieu N, Tomas M, Leitenstorfer A, Ferrando-May E, Naegeli H (2010). Dissection of the xeroderma pigmentosum group C protein function by site-directed mutagenesis. Antioxid Redox Signal, 15;14:2479-90.

Coin F, Marinoni JC, Rodolfo C, Fribourg S, Pedrini AM, Egly JM (1998). Mutations in the XPD helicase gene result in XP and TTD phenotypes, preventing interaction between XPD and the p44 subunit of TFIIH. Nat Genet. 20:184-8.

Coin F, Auriol J, Tapias A, Clivio P, Vermeulen W, Egly JM (2004). Phosphorylation of XPB helicase regulates TFIIH nucleotide excision repair activity. EMBO J, 23:4835-46.

Coin F, Proietti De Santis L, Nardo T, Zlobinskaya O, Stefanini M, Egly JM (2006). p8/TTD-A as a repair-specific TFIIH subunit. Mol Cell, 21:215-226.

Coin F, Oksenych V, Egly JM (2007). Distinct roles for the XPB/p52 and XPD/p44 subcomplexes of TFIIH in damaged DNA opening during nucleotide excision repair. Mol Cell, 26:245-56.

Coin F, Oksenych V, Mocquet V, Groh S, Blattner C, Egly JM (2008). Nucleotide excision repair driven by the dissociation of CAK from TFIIH. Mol Cell, 31:9-20.

Coin F, Egly JM (2015). Revisiting the Function of CDK7 in Transcription by Virtue of a Recently Described TFIIH Kinase Inhibitor. Mol Cell, 59:513-4.

Collins CS, Hong JY, Sapinoso L, Zhou YY, Liu Z, Micklash K, Schultz PG, Hampton GM (2006). A small interfering RNA screen for modulators of tumor cell motility identifies MAP4K4 as a promigratory kinase. Proc Natl Acad Sci U S A, 103:3775-3780.

Compe E, Drane P, Laurent C, Diderich K, Braun C, Hoeijmakers JH, Egly JM (2005). Dysregulation of the peroxisome proliferator-activated receptor target genes by XPD mutations. Mol Cell Biol, 25:6065-6076.

Compe E, Malerba M, Soler L, Marescaux J, Borrelli E, Egly JM (2007). Neurological defects in trichothiodystrophy reveal a coactivator function of TFIIH. Nat Neurosci, 10:1414-1422.

Compe E, Egly JM (2012). TFIIH: when transcription met DNA repair. Nat Rev Mol Cell Biol, 13:343-54.

Compe E, Egly JM (2016). Nucleotide Excision Repair and Transcriptional Regulation: TFIIH and Beyond. Annu Rev Biochem. 85:265-90.

Conaway RC, Conaway JW (1989). An RNA polymerase II transcription factor has an associated DNA-dependent ATPase (dATPase) activity strongly stimulated by the TATA region of promoters. Proc Natl Acad Sci U S A, 86:7356-7360.

Conaway RC, Conaway JW (2011). Origins and activity of the mediator complex. Semin Cell Dev Biol, 22:729-734.

Cowling VH, Cole MD (2007). The Myc Transactivation Domain Promotes Global Phosphorylation of the RNA Polymerase II Carboxy-Terminal Domain Independently of Direct DNA Binding. Mol Cell Biol, 27:2059-73.

Dantuma NP, Heinen C, Hoogstraten D (2009). The ubiquitin receptor Rad23: at the crossroads of nucleotide excision repair and proteasomal degradation. DNA Repair (Amst), 8:449-460.

de Boer J, Donker I, de Wit J, Hoeijmakers JH, Weeda G (1998). Disruption of the mouse xeroderma pigmentosum group D DNA repair/basal transcription gene results in preimplantation lethality. Cancer Res, 58:89-94.

de Laat WL, Jaspers NG, Hoeijmakers JH (1999). Molecular mechanism of nucleotide excision repair. Genes Dev, 13:768-85.

Di Lello P, Miller Jenkins LM, Mas C, Langlois C, Malitskaya E, Fradet-Turcotte A, Archambault J, Legault P, Omichinski JG (2008). p53 and TFIIEalpha share a common binding site on the Tfb1/p62 subunit of TFIIH. PNAS, 105:106-11.

de Weerd-Kastelein EA, Kleijer WJ, Sluyter ML, Keijzer W (1973). Repair replication in heterokaryons deprived from different repair-deficient xeroderma pigmentosum strains. Mutation research 19:237-243.

Diderich KE, Nicolaije C, Priemel M, Waarsing JH, Day JS, Brandt RM, Schilling AF, Botter SM, Weinans H, van der Horst GT, Hoeijmakers JH, van Leeuwen JP (2012). Bone fragility and decline in stem cells in prematurely aging DNA repair deficient trichothiodystrophy mice. Age (Dordr), 34:845-61.

Dijk M, Typas D, Mullenders L, Pines A (2014). Insight in the multilevel regulation of NER. Exp Cell Res, 329:116-23.

Drané P, Compe E, Catez P, Chymkowitch P, Egly JM (2004). Selective regulation of vitamin D receptor-responsive genes by TFIIH. Mol Cell, 16:187-197.

Dubaele S, Proietti De Santis L, Bienstock RJ, Keriel A, Stefanini M, Van Houten B, Egly JM (2003). Basal transcription defect discriminates between xeroderma pigmentosum and trichothiodystrophy in XPD patients. Mol Cell, 11:1635-1646.

Egloff S, O'Reilly D, Chapman RD, Taylor A, Tanzhaus K, Pitts L, Eick D, Murphy S (2007). Serine-7 of the RNA polymerase II CTD is specifically required for snRNA

Emmert S, Slor H, Busch DB, Batko S, Albert RB, Coleman D, Khan SG, Abu-Libdeh B, DiGiovanna JJ, Cunningham BB, Lee MM, Crollick J, Inui H, Ueda T, Hedayati M, Grossman L, Shahlavi T, Cleaver JE, Kraemer KH (2002). Relationship of neurologic degeneration to genotype in three xeroderma pigmentosum group G patients. Journal of Investigative Dermatology 118:972-982.

Esnault C, Ghavi-Helm Y, Brun S, Soutourina J, Van Berkum N, Boschiero C, Holstege F, Werner M (2008). Mediator-dependent recruitment of TFIIH modules in preinitiation complex. Mol Cell, 31:337-346.

Fagbemi AF, Orelli B, Schärer OD (2011). Regulation of endonuclease activity in human nucleotide excision repair. DNA Repair (Amst),10:722-9.

Fan L, Arvai AS, Cooper PK, Iwai S, Hanaoka F, Tainer JA (2006). Conserved XPB core structure and motifs for DNA unwinding: implications for pathway selection of transcription or excision repair. Mol Cell, 22:27-37.

Fassihi H, Sethi M, Fawcett H, Wing J, Chandler N, Mohammed S, Craythorne E, Morley AM, Lim R, Turner S, Henshaw T, Garrood I, Giunti P, Hedderly T, Abiona A, Naik H, Harrop G, McGibbon D, Jaspers NG, Botta E, Nardo T, Stefanini M, Young AR, Sarkany RP, Lehmann AR (2016). Deep phenotyping of 89 xeroderma pigmentosum patients reveals unexpected heterogeneity dependent on the precise molecular defect. Proc Natl Acad Sci U S A. 113:E1236-45.

Feaver WJ, Gileadi O, Kornberg RD (1991). Purification and characterization of yeast rna polymerase-ii transcription factor-b. J Biol Chem. 266:19000-19005.

Feltes BC, Bonatto D (2015). Overview of xeroderma pigmentosum proteins architecture, mutations and post-translational modifications. Mutat Res Rev Mutat Res, 763:306-20.

Fishburn J, Tomko E, Galburt E, Hahn S (2015). Double-stranded DNA translocase activity of transcription factor TFIIH and the mechanism of RNA polymerase II open complex formation. Proc Natl Acad Sci U S A. 112:3961-6.

Fisher RP (2005). Secrets of a double agent: CDK7 in cell-cycle control and transcription. J Cell Sci, 118:5171-5180.

Fisher RP (2012). The CDK Network: Linking Cycles of Cell Division and Gene Expression. Genes Cancer, 3:731-8.

Fitch ME, Nakajima S, Yasui A, Ford JM (2003). In vivo recruitment of XPC to UV-induced cyclobutane pyrimidine dimers by the DDB2 gene product. J Biol Chem, 278:46906-46910.

Fousteri M, Mullenders LH (2008). Transcription-coupled nucleotide excision repair in mammalian cells: molecular mechanisms and biological effects. Cell Res, 18:73-84.

Fregoso M, Lainé JP, Aguilar-Fuentes J, Mocquet V, Reynaud E, Coin F, Egly JM, Zurita M (2007). DNA repair and transcriptional deficiencies caused by mutations in the Drosophila p52 subunit of TFIIH generate developmental defects and chromosome fragility. Mol Cell Biol. 27:3640-50.

Fribourg S, Kellenberger E, Rogniaux H, Poterszman A, Van Dorsselaer A, Thierry JC, Egly JM, Moras D, Kieffer B (2000). Structural characterization of the cysteine-rich domain of TFIIH p44 subunit. J Biol Chem, 275:31963-71.

Fuss JO, Tainer JA (2011). XPB and XPD helicases in TFIIH orchestrate DNA duplex opening and damage verification to coordinate repair with transcription and cell cycle via CAK kinase. DNA Repair (Amst), 10:697-713.

Ganuza M, Sáiz-Ladera C, Cañamero M, Gómez G, Schneider R, Blasco MA, Pisano D, Paramio JM, Santamaría D, Barbacid M (2012). Genetic inactivation of Cdk7 leads to cell cycle arrest and induces premature aging due to adult stem cell exhaustion. EMBO J, 31:2498-510.

Garrett S, Barton WA, Knights R, Jin P, Morgan DO, Fisher RP (2001). Reciprocal activation by cyclin-dependent kinases 2 and 7 is directed by substrate specificity determinants outside the T loop. Mol Cell Biol, 21:88-99.

Gdowicz-Klosok A, Widel M, Rzeszowska-Wolny J (2013). The influence of XPD, APE1, XRCC1, and NBS1 polymorphic variants on DNA repair in cells exposed to X-rays. Mutat Res, 755:42-48.

Gentile M, Latonen L, Laiho M (2003). Cell cycle arrest and apoptosis provoked by UV radiation-induced DNA damage are transcriptionally highly divergent responses. Nucleic Acids Res. 31:4779-90.

Gerard M, Fischer L, Moncollin V, Chipoulet JM, Chambon P, Egly JM (1991). Purification and interaction properties of the human RNA polymerase-b(II) general transcription factor BTF2. J Biol Chem, 266:20940-20945.

Ghamari A, van de Corput MPC, Thongjuea S, van Cappellen WA, van Ijcken W, van Haren J, Soler E, Eick D, Lenhard B, Grosveld FG (2013). In vivo live imaging of RNA polymerase II transcription factories in primary cells. Genes Dev, 27:767-777.

Giglia-Mari G, Coin F, Ranish JA, Hoogstraten D, Theil A, Wijgers N, Jaspers NGJ, Raams A, Argentini M, van der Spek PJ, Botta E, Stefanini M, Egly JM, Aebersold R, Hoeijmakers JH, Vermeulen W. 2004. A new, tenth subunit of TFIIH is responsible for the DNA repair syndrome trichothiodystrophy group A. Nature Genetics 36:714-719.

Giglia-Mari G, Miquel C, Theil AF, Mari PO, Hoogstraten D, Ng JM, Dinant C, Hoeijmakers JH, Vermeulen W (2006). Dynamic interaction of TTDA with TFIIH is stabilized by nucleotide excision repair in living cells. PLoS Biol, 4:e156.

Giglia-Mari G, Theil AF, Mari PO, Mourgues S, Nonnekens J, Andrieux LO, de Wit J, Miquel C, Wijgers N, Maas A, Fousteri M, Hoeijmakers JH, Vermeulen W (2009). Differentiation driven changes in the dynamic organization of basal transcription initiation. PLoS Biol, 7:e1000220.

Glover-Cutter K, Larochelle S, Erickson B, Zhang C, Shokat K, Fisher RP, Bentley DL (2009). TFIIH-associated Cdk7 kinase functions in phosphorylation of C-terminal domain Ser7 residues, promoter-proximal pausing, and termination by RNA polymerase II. Mol Cell Bio, 29:5455-64.

Godon C, Mourgues S, Nonnekens J, Mourcet A, Coin F, Vermeulen W, Mari P-O, Giglia-Mari G. 2012. Generation of DNA single-strand displacement by compromised nucleotide excision repair. Embo Journal 31:3550-3563.

Grünberg JR, Hammarstedt A, Hedjazifar S, Smith U (2014). The Novel Secreted Adipokine WNT1-inducible Signaling Pathway Protein 2 (WISP2) Is a Mesenchymal Cell Activator of Canonical WNT. J Biol Chem. 289:6899-907.

Hammarstedt A, Hedjazifar S, Jenndahl L, Gogg S, Grünberg J, Gustafson B, Klimcakova E, Stich V, Langin D, Laakso M, Smith U (2013). WISP2 regulates preadipocyte commitment and PPARγ activation by BMP4. Proc Natl Acad Sci. 11:2563-8.

Hanawalt PC, Spivak G (2008). Transcription-coupled DNA repair: two decades of progress and surprises. Nat Rev Mol Cell Biol, 9:958-970.

Hannah J, Zhou P (2009). Regulation of DNA damage response pathways by the cullin-RING ubiquitin ligases. DNA Repair (Amst), 8:536-43.

Happle R, Traupe H, Grobe H, Bonsmann G. 1984. The Tay syndrome (congenital ichthyosis with trichothiodystrophy). European journal of pediatrics 141:147-52.

Hashimoto S, Egly JM (2009). Trichothiodystrophy view from the molecular basis of DNA repair/transcription factor TFIIH. Hum Mol Genet, 18:R224-R230.

He Y, Fang J, Taatjes DJ, Nogales E (2013). Structural visualization of key steps in human transcription initiation. Nature, 495:481-488.

Held JM, Britton DJ, Scott GK, Lee EL, Schilling B, Baldwin MA, Gibson BW, Benz CC (2012). Ligand binding promotes CDK-dependent phosphorylation of ER-alpha on hinge serine 294 but inhibits ligand-independent phosphorylation of serine 305. Mol Cancer Res, 10:1120-32.

Helenius K, Yang Y, Alasaari J, Mäkelä TP (2009). Mat1 inhibits peroxisome proliferator-activated receptor gamma-mediated adipocyte differentiation. Mol Cell Biol, 29:315-23.

Helenius K, Yang Y, Tselykh TV, Pessa HK, Frilander MJ, Mäkelä TP (2011). Requirement of TFIIH kinase subunit Mat1 for RNA Pol II C-terminal domain Ser5 phosphorylation, transcription and mRNA turnover. Nucleic Acids Res, 39:5025-35.

Hirai Y, Kodama Y, Moriwaki S-I, Noda A, Cullings HM, MacPhee DG, Kodama K, Mabuchi K, Kraemer KH, Land CE, Nakamura N (2006). Heterozygous individuals bearing a founder mutation in the XPA DNA repair gene comprise nearly 1% of the Japanese population. Mutation Research-Fundamental and Molecular Mechanisms of Mutagenesis 601:171-178.

Iben S, Tschochner H, Bier M, Hoogstraten D, Hozak P, Egly JM, Grummt I (2002). TFIIH plays an essential role in RNA polymerase I transcription. Cell, 109:297-306.

Ito S, Tan LJ, Andoh D, Narita T, Seki M, Hirano Y, Narita K, Kuraoka I, Hiraoka Y, Tanaka K (2010). MMXD, a TFIIH-independent XPD-MMS19 protein complex involved in chromosome segregation. Mol Cell, 39:632-40.

Jia N, Nakazawa Y, Guo C, Shimada M, Sethi M, Takahashi Y, Ueda H, Nagayama Y, Ogi T (2015). A rapid, comprehensive system for assaying DNA repair activity and cytotoxic effects of DNA-damaging reagents. Nat Protoc. 10:12-24.

Kayaselcuk F, Erkanli S, Bolat F, Seydaoglu G, Kuscu E, Demirhan B (2006). Expression of cyclin H in normal and cancerous endometrium, its correlation with other cyclins, and association with clinicopathologic parameters. Int J Gynecol Cancer, 16:402-408.

Kellenberger E, Dominguez C, Fribourg S, Wasielewski E, Moras D, Poterszman A, Boelens R, Kieffer B (2005). Solution structure of the C-terminal domain of TFIIH P44 subunit reveals a novel type of C4C4 ring domain involved in protein-protein interactions. J Biol Chem, 280:20785-92.

Keller KE, Yang YF, Sun YY, Sykes R, Gaudette ND, Samples JR, Acott TS, Wirtz MK (2014). Interleukin-20 receptor expression in the trabecular meshwork and its implication in glaucoma. J Ocul Pharmacol Ther. 30:267-76.

Keriel A, Stary A, Sarasin A, Rochette-Egly C, Egly JM (2002). XPD mutations prevent TFIIH-dependent transactivation by nuclear receptors and phosphorylation of RARalpha. Cell, 109:125-135.

Kinner A, Wu W, Staudt C, Iliakis G (2008). γ-H2AX in recognition and signaling of DNA double-strand breaks in the context of chromatin. Nucleic Acids Res. 36: 5678–5694.

Kim KK, Chamberlin HM, Morgan DO, Kim SH (1996). Three-dimensional structure of human cyclin H, a positive regulator of the CDK-activating kinase. Nat Struct Biol, 3:849-55.

Kim JS, Saint-André C, Lim HS1, Hwang CS, Egly JM, Cho Y (2015). Crystal structure of the Rad3/XPD regulatory domain of Ssl1/p44. J Biol Chem, 290:8321-30.

Ko LJ, Shieh SY, Chen X, Jayaraman L, Tamai K, Taya Y, Prives C and Pan ZQ (1997). p53 is phosphorylated by CDK7-cyclin H in a p36MAT1-dependent manner. Mol Cell Biol, 17:7220-7229.

Komarnitsky P, Cho EJ, Buratowski S (2000). Different phosphorylated forms of RNA polymerase II and associated mRNA processing factors during transcription. Genes Dev, 14:2452-2460.

Kornberg RD (2007). The molecular basis of eucaryotic transcription. Cell Death Differ, 14:1989-97.

Korsisaari N, Rossi DJ, Paetau A, Charnay P, Henkemeyer M, Makela TP (2002). Conditional ablation of the Mat1 subunit of TFIIH in Schwann cells provides evidence that Mat1 is not required for general transcription. J Cell Sci, 115:4275-4284.

Kraemer KH, Coon HG, Petinga RA, Barrett SF, Rahe AE, Robbins JH (1975a). Genetic heterogeneity in xeroderma pigmentosum: complementation groups and their relationship to DNA repair rates. Proc Natl Acad Sci USA. 72:59-63.

Kraemer KH, De Weerd-Kastelein EA, Robbins JH, Keijzer W, Barrett SF, Petinga RA, Bootsma D (1975b). Five complementation groups in xeroderma pigmentosum. Mutation research 33:327-340.

Kraemer KH, Lee MM, Scotto J (1987). Xeroderma pigmentosum. Cutaneous, ocular, and neurologic abnormalities in 830 published cases. Archives of dermatology 123:241-250.

Kraemer KH (1994). Nucleotide excision-repair genes involved in xeroderma-pigmentosum. Japanese Journal of Cancer Research 85:COV2-COV2.

Kraemer KH, Patronas NJ, Schiffmann R, Brooks BP, Tamura D, Digiovanna JJ (2007). Xeroderma pigmentosum, trichothiodystrophy and Cockayne syndrome: A complex genotype-phenotype relationship. Neuroscience, 145:1388-1396.

Krempler A, Kartarius S, Günther J, Montenarh M (2005). Cyclin H is targeted to the nucleus by C-terminal nuclear localization sequences. Cell Mol Life Sci, 62:1379-87.

Kuper J, Braun C, Elias A, Michels G, Sauer F, Schmitt DR, Poterszman A, Egly JM, Kisker C (2014). In TFIIH, XPD helicase is exclusively devoted to DNA repair. PLoS Biol, 12:e1001954.

Kuschal C, Botta E, Orioli D, Digiovanna JJ, Seneca S, Keymolen K, Tamura D, Heller E, Khan SG, Caligiuri G, Lanzafame M, Nardo T, Ricotti R, Peverali FA, Stephens R, Zhao Y, Lehmann AR, Baranello L, Levens D, Kraemer KH, Stefanini M (2016). GTF2E2 Mutations Destabilize the General Transcription Factor Complex TFIIE in Individuals with DNA Repair-Proficient Trichothiodystrophy. Am J Hum Genet. 98:627-42.

Lafrance-Vanasse J, Arseneault G, Cappadocia L, Chen HT, Legault P, Omichinski JG (2012). Structural and functional characterization of interactions involving the Tfb1 subunit of TFIIH and the NER factor Rad2. Nucleic Acids Res, 40:5739-50.

Lafrance-Vanasse J, Arseneault G, Cappadocia L, Legault P, Omichinski JG (2013). Structural and functional evidence that Rad4 competes with Rad2 for binding to the Tfb1 subunit of TFIIH in NER. Nucleic Acids Res, 41:2736-45.

Lainé JP1, Egly JM (2006). When transcription and repair meet: a complex system. Trends Genet. 22:430-6.

Langlois C, Mas C, Di Lello P, Jenkins LM, Legault P, Omichinski JG (2008). NMR structure of the complex between the Tfb1 subunit of TFIIH and the activation domain of VP16: structural similarities between VP16 and p53. J Am Chem Soc, 130:10596-604.

Larochelle S, Chen J, Knights R, Pandur J, Morcillo P, Erdjument-Bromage H, Tempst P, Suter B, Fisher RP (2001). T-loop phosphorylation stabilizes the CDK7-cyclin H-MAT1 complex in vivo and regulates its CTD kinase activity. EMBO J, 20:3749-59.

Larochelle S, Amat R, Glover-Cutter K, Sansó M, Zhang C, Allen JJ, Shokat KM, Bentley DL, Fisher RP (2012). Cyclin-dependent kinase control of the initiation-to-elongation switch of RNA polymerase II. Nat Struct Mol Biol, 19:1108-15.

Le May N, Mota-Fernandes D, Vélez-Cruz R, Iltis I, Biard D, Egly JM (2010). NER factors are recruited to active promoters and facilitate chromatin modification for transcription in the absence of exogenous genotoxic attack. Mol Cell, 38:54-66.

Leclerc V, Raisin S, Léopold P (2000). Dominant-negative mutants reveal a role for the Cdk7 kinase at the mid-blastula transition in Drosophila embryos. EMBO J, 19:1567-75.

Lehmann, A.R. (1995). Nucleotide excision repair and the link with transcription. Trends Biochem. Sci., 20, 402–405.

Lehmann AR1, McGibbon D, Stefanini M (2011). Xeroderma pigmentosum. Orphanet J Rare Dis. 1;6:70.

Lindenbaum Y, Dickson D, Rosenbaum P, Kraemer K, Robbins I, Rapin I (2001). Xeroderma pigmentosum/cockayne syndrome complex: first neuropathological study and review of eight other cases. Eur J Paediatr Neurol, 5:225-242.

Liu JH, He LS, Collins I, Ge H, Libutti D, Li JF, Egly JM, Levens D (2000). The FBP interacting repressor targets TFIIH to inhibit activated transcription. Mol Cell, 5:331-341.

Liu JH, Akoulitchev S, Weber A, Ge H, Chuikov S, Libutti D, Wang XW, Conaway JW, Harris CC, Conaway RC, Reinberg D, Levens D (2001). Defective interplay of activators and repressors with TFIIH in xeroderma pigmentosum. Cell, 104:353-363.

Liu J, Fang H, Chi Z, Wu Z, Wei D, Mo D, Niu K, Balajee AS, Hei TK, Nie L, Zhao Y (2014). XPD localizes in mitochondria and protects the mitochondrial genome from oxidative DNA damage. Nucleic Acids Res, 43:5476-88.

Liu X, Kraus WL, Bai X (2015). Ready, pause, go: regulation of RNA polymerase II pausing and release by cellular signaling pathways. Trends Biochem Sci, 40:516-25.

Livak KJ, Schmittgen TD (2001). Analysis of relative gene expression data using real-time quantitative PCR and the 2(T)(-Delta Delta C) method. Methods 25:402-408.

Lolli G, Lowe ED, Brown NR, Johnson LN (2004). The crystal structure of human CDK7 and its protein recognition properties. Structure, 12:2067-79.

Lossaint G, Besnard E, Fisher D, Piette J, Dulić V (2011). Chk1 is dispensable for G2 arrest in response to sustained DNA damage when the ATM/p53/p21 pathway is functional. Oncogene, 30:4261-74.

Lu H, Fisher RP, Bailey P, Levine AJ (1997). The CDK7-cycH-p36 complex of transcription factor IIH phosphorylates p53, enhancing its sequence-specific DNA binding activity in vitro. Mol Cell Biol, 17:5923-5934.

Malumbres M (2014). Cyclin-dependent kinases. Genome Biol, 15:122.

Mariani E, Facchini A, Honorati MC, Lalli E, Berardesca E, Ghetti P, Marinoni S, Nuzzo F, Astaldi Ricotti GC, Stefanini M (1992). Immune defects in families and

patients with xeroderma pigmentosum and trichothiodystrophy. Clin. Exp. Immunol. 88:376-382.

Marteijn JA, Lans H1, Vermeulen W2, Hoeijmakers JH (2014). Understanding nucleotide excision repair and its roles in cancer and ageing. Nat Rev Mol Cell Biol. 15:465-81.

Mason AC, Rambo RP, Greer B, Pritchett M, Tainer JA, Cortez D, Eichman BF (2014). A structure-specific nucleic acid-binding domain conserved among DNA repair proteins. Proc Natl Acad Sci U S A, 111:7618-23.

Mathieu N, Kaczmarek N, Rüthemann P, Luch A, Naegeli H (2013). DNA quality control by a lesion sensor pocket of the xeroderma pigmentosum group D helicase subunit of TFIIH. Curr Biol, 23:204-12.

Messaoud O, Ben Rekaya M, Ouragini H, Benfadhel S, Azaiez H, Kefi R, Gouider-Khouja N, Mokhtar I, Amouri A, Boubaker MS, Zghal M, Abdelhak S. 2012. Severe phenotypes in two Tunisian families with novel XPA mutations: evidence for a correlation between mutation location and disease severity. Archives of Dermatological Research 304:171-176.

Michaud A, Lacroix-Pépin N, Pelletier M, Daris M, Biertho L, Fortier MA, Tchernof A (2014). Expression of genes related to prostaglandin synthesis or signaling in human subcutaneous and omental adipose tissue: depot differences and modulation by adipogenesis. Mediators Inflamm. 451620. doi: 10.

Min J-H, Pavletich NP (2007). Recognition of DNA damage by the Rad4 nucleotide excision repair protein. Nature, 449:570-577.

Mitchell NC, Johanson TM, Cranna NJ, Er ALJ, Richardson HE, Hannan RD, Quinn LM (2010). Hfp inhibits Drosophila myc transcription and cell growth in a TFIIH/Hay-dependent manner. Development, 137:2875-2884.

Mocquet V, Kropachev K, Kolbanovskiy M, Kolbanovskiy A, Tapias A, Cai Y, Broyde S, Geacintov NE, Egly JM (2007). The human DNA repair factor XPC-HR23B distinguishes stereoisomeric benzo a pyrenyl-DNA lesions. EMBO J, 26:2923-2932.

Moisan A, Larochelle C, Guillemette B, Gaudreau L (2004). BRCA1 can modulate RNA polymerase II carboxy-terminal domain phosphorylation levels. Mol Cell Biol, 24:6947-56.

Moriel-Carretero M, Tous C, Aguilera A (2011). Control of the function of the transcription and repair factor TFIIH by the action of the cochaperone Ydj1. Proc Natl Acad Sci U S A, 108:15300-15305.

Moriwaki S, Kraemer KH (2001). Xeroderma pigmentosum - bridging a gap between clinic and laboratory. Photodermatology Photoimmunology & Photomedicine 17:47-54.

Moslehi R, Signore C, Tamura D (2010). Adverse effects of trichothiodystrophy DNA repair and transcription gene disorder on human fetal development. Clin Genet 77: 365–373.

Moslehi R, Kumar A, Mills JL, Ambroggio X, Signore C, Dzutsev A (2012). Phenotype-specific adverse effects of XPD mutations on human prenatal development implicate impairment of TFIIH-mediated functions in placenta. Eur J Hum Genet, 20:626-631.

Moslehi R, Ambroggio X, Nagarajan V, Kumar A, Dzutsev A (2014) Nucleotide excision repair/transcription gene defects in the fetus and impaired TFIIH-mediated function in transcription in placenta leading to preeclampsia. BMC Genomics, 15:373.

Murakami K, Gibbons BJ, Davis RE, Nagai S, Liu X, Robinson PJ, Wu T, Kaplanb CD, Kornberga RD (2012). Tfb6, a previously unidentified subunit of the general transcription factor TFIIH, facilitates dissociation of Ssl2 helicase after transcription initiation. PNAS, 109:4816-21.

Nakabayashi K, Amann D, Ren Y, Saarialho-Kere U, Avidan N, Gentles S, MacDonald JR, Puffenberger EG, Christiano AM, Martinez-Mir A, Salas-Alanis JC, Rizzo R, Vamos E, Raams A, Les C, Seboun E, Jaspers NG, Beckmann JS, Jackson CE, Scherer SW (2005). Identification of *C7orf11* (*TTDN1*) gene mutations and genetic heterogeneity in nonphotosensitive trichothiodystrophy. Am J Hum Genet. 76:510-516.

Nilson KA, Guo J, Turek ME, Brogie JE, Delaney E, Luse DS, Price DH (2015). THZ1 Reveals Roles for Cdk7 in Co-transcriptional Capping and Pausing. Mol Cell, 59:576-87.

Nonnekens J, Cabantous S, Slingerland J, Mari PO, Giglia-Mari G (2013). In vivo interactions of TTDA mutant proteins within TFIIH. J Cell Sci, 126:3278-83.

Nouspikel T (2009). DNA repair in mammalian cells: Nucleotide excision repair: variations on versatility. Cell Mol Life Sci, 66:994-1009.

O'Gorman W, Thomas B, Kwek KY, Furger A, Akoulitchev A (2005). Analysis of U1 small nuclear RNA interaction with cyclin H. J Biol Chem, 280:36920-5.

Orioli D, Compe E, Nardo T, Mura M, Giraudon C, Botta E, Arrigoni L, Peverali FA, Egly JM, Stefanini M (2013). XPD mutations in trichothiodystrophy hamper collagen VI expression and reveal a role of TFIIH in transcription derepression. Hum Mol Genet, 22:1061-1073.

Østergaard JR, Christensen T. (1996) The central nervous system in Tay syndrome. Neuropediatrics, 27:326–30.

Pannucci NL, Li D, Sahay S, Thomas EK, Chen R, Tala I, Hu T, Ciccarelli BT, Megjugorac NJ, Adams HC III, Rodriguez PL, Fitzpatrick ER, Lagunoff D, Williams DA, Whitehead IP (2013). Loss of the xeroderma pigmentosum group B protein binding site impairs p210 BCR/ABL1 leukemogenic activity. Blood Cancer J, 3:e135.

Park JY, Cho M, Leonard S, Calder B, Mian IS, Kim WO, Wijnhoven S, Van Steeg H, Mitchell J, Van der Horst GTJ, Hoeijmakers J, Cohen P, Vijg J, Suh Y (2008). Homeostatic imbalance between apoptosis and cell renewal in the liver of premature aging xpdTTD mice. PLoS one, 3:e2346.

Patel SA, Simon MC (2010). Functional analysis of the Cdk7.cyclin H.Mat1 complex in mouse embryonic stem cells and embryos. J Biol Chem, 285:15587-98.

Pillai P, Desai S, Patel R, Sajan M, Farese R, Ostrov D, Acevedo-Duncan M (2011). A novel PKC-ι inhibitor abrogates cell proliferation and induces apoptosis in neuroblastoma. Int J Biochem Cell Biol, 43:784-94.

Pollitt RJ, Jenner FA, Davies M. 1968. Sibs with mental and physical retardation and trichorrhexis nodosa with abnormal amino acid composition of the hair. Archives of disease in childhood 43:211-216.

Portal MM (2011). MicroRNA-27a regulates basal transcription by targeting the p44 subunit of general transcription factor IIH. Proc Natl Acad Sci U S A, 108:8686-8691.

Qadri I, Conaway JW, Conaway RC, Schaack J, Siddiqui A (1996). Hepatitis B virus transactivator protein, HBx, associates with the components of TFIIH and stimulates the DNA helicase activity of TFIIH. Proc Natl Acad Sci U S A, 93:10578-10583.

Rabut G, Le Dez G, Verma R, Makhnevych T, Knebel A, Kurz T, Boone C, Deshaies RJ, Peter M (2011). The TFIIH subunit Tfb3 regulates cullin neddylation. Mol Cell, 43:488-95.

Rapin I, Lindenbaum Y, Dickson DW, Kraemer KH, Robbins JH (2000). Cockayne syndrome and xeroderma pigmentosum - DNA repair disorders with overlaps and paradoxes. Neurology 55:1442-1449.

Rosales J, Han B, Lee KY (2003). Cdk7 functions as a cdk5 activating kinase in brain. Cell Physiol Biochem, 13:285-96.

Rossi DJ, Londesborough A, Korsisaari N, Pihlak A, Lehtonen E, Henkemeyer M, Mäkelä TP (2001). Inability to enter S phase and defective RNA polymerase II CTD phosphorylation in mice lacking Mat1. EMBO J, 20:2844-56.

Roy R, Adamczewski JP, Seroz T, Vermeulen W, Tassan JP, Schaeffer L, Nigg EA, Hoeijmakers JHJ, Egly JM (1994). The MO15 cell-cycle kinase is associated with the tfiih transcription dna-repair factor. Cell, 79:1093-1101.

Sass JO1, Skladal D, Zelger B, Romani N, Utermann B (2004). Trichothiodystrophy: quantification of cysteine in human hair and nails by application of sodium azide-dependent oxidation to cysteic acid. Arch Dermatol Res., 296:188-91.

Sainsbury S, Bernecky C, Cramer P (2015). Structural basis of transcription initiation by RNA polymerase II. Nat Rev Mol Cell Biol, 16:129-43.

Sano M, Izumi Y, Helenius K, Asakura M, Rossi DJ, Xie M, Taffet G, Hu L, Pautler RG, Wilson CR, Boudina S, Abel ED, Taegtmeyer H, Scaglia F, Graham BH, Kralli A, Shimizu N, Tanaka H, Mäkelä TP, Schneider MD (2007). Menage-a-trois 1 is critical for the transcriptional function of PPAR gamma coactivator 1. Cell Metab, 5:129-142.

Schachter MM, Merrick KA, Larochelle S, Hirschi A, Zhang C, Shokat KM, Rubin SM, Fisher RP (2013). A Cdk7-Cdk4 T-loop phosphorylation cascade promotes G1 progression. Mol Cell, 50:250-60.

Schmitt DR, Kuper J, Elias A, Kisker C (2014). The structure of the TFIIH p34 subunit reveals a von Willebrand factor A like fold. PLoS One, 9:e102389.

Schneider E, Montenarh M, Wagner P (1998). Regulation of CAK kinase activity by p53. Oncogene, 17:2733-41.

Schneider E, Kartarius S, Schuster N, Montenarh M (2002). The cyclin H/cdk7/Mat1 kinase activity is regulated by CK2 phosphorylation of cyclin H. Oncogene, 21:5031-7.

Schultz P, Fribourg S, Potersman A, Mallouh V, Moras D, Egly JM (2000). Molecular structure of human TFIIH. Cell, 102:599-607.

Sethi M, Lehmann A, Robson A, McGibbon D, Sarkany R, Fassihi H (2013). Patients with xeroderma pigmentosum complementation groups C, E and V do not have abnormal sunburn reactions. British Journal of Dermatology 169:60-60.

Shin S, Kim J, Kim Y, Sun JY, Yoo JH, Lee K-A (2013). Analysis of mutations in the XPD gene in a patient with brittle hair. Ann Clin Lab Sci, 43:323-327.

Sidwell RU, Sandison A, Wing J, Fawcett HD, Seet JE, Fisher C, Nardo T, Stefanini M, Lehmann AR, Cream JJ. 2006. A novel mutation in the *XPA* gene associated with unusually mild clinical features in a patient who developed a spindle cell melanoma. British Journal of Dermatology 155:81-88.

Singh A, Compe E, Le May N, Egly JM (2015). TFIIH subunit alterations causing xeroderma pigmentosum and trichothiodystrophy specifically disturb several steps during transcription. Am J Hum Genet, 96:194-207.

Sontz PA, Mui TP, Fuss JO, Tainer JA, Barton JK (2012). DNA charge transport as a first step in coordinating the detection of lesions by repair proteins. Proc Natl Acad Sci U S A, 109:1856-61.

Spies M (2014). Two steps forward, one step back: determining XPD helicase mechanism by single-molecule fluorescence and high-resolution optical tweezers. DNA Repair (Amst), 20:58-70.

Spivak G (2016). Transcription-coupled repair: an update. Arch Toxicol. 90:2583-2594.

Stefanini M, Giliani S, Nardo T, Marinoni S, Nazzaro V, Rizzo R, Trevisan G (1992). DNA repair investigations in nine Italian patients affected by trichothiodystrophy. Mutat Res 273:119-125.

Stefanini M, Lagomarsini P, Giliani S, Nardo T, Botta E, Peserico A, Kleijer WJ, Lehmann AR and Sarasin A (1993a). Genetic heterogeneity of the excision repair defect associated with trichothiodystrophy. Carcinogenesis 14:1101-1105.

Stefanini M, Kraemer KH (2008). Xeroderma pigmentosum, in: M. Ruggieri, I. Pascual-Castroviejo, C. Di Rocco. Neurocutaneous Diseases, Springer-Verlag, New York Wien, 771-792.

Stefanini M, Botta E, Lanzafame M, Orioli D (2010). Trichothiodystrophy: from basic mechanisms to clinical implications. DNA Repair, 9:2-10.

Stefanini, M, Ruggieri,M (2008). Cockayne syndrome. In: Ruggieri M. Pascual-Castroviejo I., Di Rocco C. (Eds.), Neurocutaneous Disorders: Phakomatoses and Hamartoneoplastic Syndromes. Springer, New York, pp. 793–820.

Sugasawa K, Okamoto T, Shimizu Y, Masutani C, Iwai S, Hanaoka F (2001). A multistep damage recognition mechanism for global genomic nucleotide excision repair. Genes Dev, 15:507-521.

Takagi Y, Masuda CA, Chang WH, Komori H, Wang D, Hunter T, Joazeiro CA, Kornberg RD (2005). Ubiquitin ligase activity of TFIIH and the transcriptional response to DNA damage. Mol Cell, 18:237-43.

Takayama K, Salazar EP, Lehmann A, Stefanini M, Thompson LH, Weber CA (1995). Defects in the DNA repair and transcription gene *ERCC2* in the cancer-prone disorder xeroderma pigmentosum group D. Cancer Res. 55:5656-5663.

Talukder AH, Mishra SK, Mandal M, Balasenthil S, Mehta S, Sahin AA, Barnes CJ, Kumar R (2003). MTA1 interacts with MAT1, a cyclin-dependent kinase-activating kinase complex ring finger factor, and regulates estrogen receptor transactivation functions. J Biol Chem, 278:11676-11685.

Tamura D, Khan SG, Merideth M, DiGiovanna JJ, Tucker MA, Goldstein AM, Oh K-S, Ueda T, Boyle J, Sarihan M, Kraemer KH. 2012. Effect of mutations in

XPD(ERCC2) on pregnancy and prenatal development in mothers of patients with trichothiodystrophy or xeroderma pigmentosum. European Journal of Human Genetics 20:1308-1310.

Tay CH. 1971. Ichthyosiform erythroderma, hair shaft abnormalities, and mental and growth retardation. A new recessive disorder. Archives of dermatology 104:4-13.

Taylor EM, Broughton BC, Botta E, Stefanini M, Sarasin A, Jaspers NG, Fawcett H, Harcourt SA, Arlett CF, Lehmann AR (1997). Xeroderma pigmentosum and trichothiodystrophy are associated with different mutations in the XPD (ERCC2) repair/transcription gene. PNAS, 94:8658-63.

Theil AF, Nonnekens J, Steurer B, Mari PO, de Wit J, Lemaitre C, Marteijn JA, Raams A, Maas A, Vermeij M, Essers J, Hoeijmakers JH, Giglia-Mari G, Vermeulen W (2013). Disruption of TTDA results in complete nucleotide excision repair deficiency and embryonic lethality. PLoS Genet, 9:e1003431.

Toelle SP1, Valsangiacomo E, Boltshauser E (2001). Trichothiodystrophy with severe cardiac and neurological involvement in two sisters. Eur J Pediatr. 160:728-31.

Tong X, Wang F, Thut CJ, Kieff E (1995). The epstein-barr-virus nuclear-protein-2 acidic domain can interact with tfiib, TAF40, and RPA70 but not with tata-binding protein. J Virol, 69:585-588.

Traboulsi H, Davoli S, Catez P, Egly JM, Compe E (2014). Dynamic partnership between TFIIH, PGC-1α and SIRT1 is impaired in trichothiodystrophy. PLoS Genet, 10:e1004732.

Tremeau-Bravard A, Perez C, Egly JM (2001). A role of the C-terminal part of p44 in the promoter escape activity of transcription factor IIH. J Biol Chem, 276:27693-7.

Vashisht AA, Yu CC, Sharma T, Ro K, Wohlschlegel JA (2015). The Association of the Xeroderma Pigmentosum Group D DNA Helicase (XPD) with Transcription Factor IIH Is Regulated by the Cytosolic Iron-Sulfur Cluster Assembly Pathway. J Biol Chem. 290:14218-25.

Vermeulen W, Bergmann E, Auriol J, Rademakers S, Frit P, Appeldoorn E, Hoeijmakers JH, Egly JM (2000). Sublimiting concentration of TFIIH transcription/DNA repair factor causes TTD-A trichothiodystrophy disorder. Nat Genet, 26:307-13.

Vermeulen W, Fousteri M (2013). Mammalian transcription-coupled excision repair. Cold Spring Harb Perspect Biol, 5:a012625.

Villicana C, Cruz G, Zurita M (2013). The genetic depletion or the triptolide inhibition of TFIIH in p53-deficient cells induces a JNK-dependent cell death in Drosophila. J Cell Sci, 126:2502-2515.

Viprakasit V, Gibbons RJ, Broughton BC, Tolmie JL, Brown D, Lunt P, Winter RM, Marinoni S, Stefanini M, Brueton L, Lehmann AR, Higgs DR (2001). Mutations in the general transcription factor TFIIH result in beta-thalassaemia in individuals with trichothiodystrophy. Hum Mol Genet 10:2797-2802.

Wakeling EL1, Cruwys M, Suri M, Brady AF, Aylett SE, Hall C (2004). Central osteosclerosis with trichothiodystrophy. Pediatr Radiol. 34:541-6.

Wallenfang MR, Seydoux G (2002). cdk-7 Is required for mRNA transcription and cell cycle progression in Caenorhabditis elegans embryos. Proc Natl Acad Sci U S A, 99:5527-32.

Wang QE, Zhu QZ, Wani G, Chen JM, Wani AA (2004). UV radiation-induced XPC translocation within chromatin is mediated by damaged-DNA binding protein, DDB2. Carcinogenesis 25:1033-1043.

Wang Y, Liu F, Mao F, Hang Q, Huang X, He S, Wang Y, Cheng C, Wang H, Xu G, Zhang T, Shen A (2013). Interaction with cyclin H/cyclin-dependent kinase 7 (CCNH/CDK7) Stabilizes c-terminal binding protein 2 (ctBP2) and promotes cancer cell migration. J Biol Chem, 288:9028-9034.

Wang J, Ikeda R, Che XF, Ooyama A, Yamamoto M, Furukawa T, Hasui K, Zheng CL, Tajitsu Y, Oka T, Tabata S, Nishizawa Y, Eizuru Y, Akiyama S (2013). VEGF expression is augmented by hypoxia-induced PGIS in human fibroblasts. Int J Oncol. 43:746-54.

Weber A, Chung HJ, Springer E, Heitzmann D, Warth R (2010). The TFIIH subunit p89 (XPB) localizes to the centrosome during mitosis. Cell Oncol, 32:121-130.

Xiao H, Pearson A, Coulombe B, Truant R, Zhang S, Regier JL, Triezenberg SJ, Reinberg D, Flores O, Ingles CJ, Greenblatt J (1994). Binding of basal transcription factor tfiih to the acidic activation domains of VP16 and p53. Mol Cell Biol, 14:7013-7024.

Yakovchuk P, Goodrich JA, Kugel JF (2009). B2 RNA and Alu RNA repress transcription by disrupting contacts between RNA polymerase II and promoter DNA within assembled complexes. Proc Natl Acad Sci U S A, 106:5569-5574.

Yoon HK1, Sargent MA, Prendiville JS, Poskitt KJ (2005). Cerebellar and cerebral atrophy in trichothiodystrophy. Pediatr Radiol. 35(10):1019-23.

Zhovmer A, Oksenych V, Coin F (2010). Two sides of the same coin: TFIIH complexes in transcription and DNA repair. ScientificWorldJournal, 10:633-643.

Zhu Q, Wani G, Sharma N, Wani A (2012). Lack of CAK complex accumulation at DNA damage sites in XP-B and XP-B/CS fibroblasts reveals differential regulation of CAK anchoring to core TFIIH by XPB and XPD helicases during nucleotide excision repair. DNA Repair (Amst), 11:942-50.

Zschenker O, Kulkarni A, Miller D, Reynolds GE, Granger-Locatelli M, Pottier G, Sabatier L, Murnane JP (2009). Increased sensitivity of subtelomeric regions to DNA double-strand breaks in a human cancer cell line. DNA Repair (Amst). 8:886-900.

Appendix

Table **A**. Description of the 176 deregulated genes and the 3 reference genes analyzed by RealTime Ready Custom Panels in the RNA pools from primary dermal fibroblasts of 4 TTD/XP-D patients (TTD pool), 4 healthy TTD parents (control pool).

Gene Symbol	**Gene Description**	Source: HGNC Symbol; Acc
ACOT1	acyl-CoA thioesterase 1	41
ADM	myeloid-associated differentiation marker	359
ADRA2A	adrenergic, alpha-2A- receptor	281
AHR	aryl hydrocarbon receptor	348
AKAP2	A kinase (PRKA) anchor protein 2	372
AKR1C2	aldo-keto reductase family 1, member C2 (dihydrodiol dehydrogenase 2	385
ALDH1A3	aldehyde dehydrogenase 1 family, member A3	409
ALDH1B1	aldehyde dehydrogenase 1 family, member B1	407
ALDH3B1	aldehyde dehydrogenase 3 family, member B1	410
ANGPTL4	angiopoietin-like 4	16039
ANP32A	acidic (leucine-rich) nuclear phosphoprotein 32 family, member A	13233
ANTXR1	anthrax toxin receptor 1	21014
AP1S2	adaptor-related protein complex 1, sigma 2 subunit	560
APBB1IP	amyloid beta (A4) precursor protein-binding, family B, member 1 interacting protein	17379
ARHGAP23	Rho GTPase activating protein 23	29293
ASS1	argininosuccinate synthase 1	758
ATF5	activating transcription factor 5	790
ATP13A3	ATPase type 13A3	24113
C15orf39	Uncharacterized protein C15orf39	-
C16orf72	PF0472 protein C16orf72	-
C1orf198	Uncharacterized protein C1orf198	-
C8orf58	Uncharacterized protein C8orf58	-
CABLES1	Cdk5 and Abl enzyme substrate 1	25097
CAMK2N1	calcium/calmodulin-dependent protein kinase II inhibitor 1	24190
CCDC8	coiled-coil domain containing 8	25367
CCRL1	chemokine (C-C motif) receptor-like 1	1611
CLEC3B	C-type lectin domain family 3, member B	11891
CLGN	calmegin	2060
CLIC3	chloride intracellular channel 3	2064
CLU	clusterin	2095
CNN1	calponin 1, basic, smooth muscle	2155
COL4A1	collagen, type IV, alpha 1	2202
CRABP2	cellular retinoic acid binding protein 2	2339

Gene Symbol	Gene Description	Source: HGNC Symbol; Acc
CRLF1	cytokine receptor-like factor 1	2364
CRYAB	crystallin, alpha B	2389
CRYZ	crystallin, zeta (quinone reductase)	2419
CSRP2	cysteine and glycine-rich protein 2	2470
CTGF	connective tissue growth factor	2500
CTSC	cathepsin C	2528
CTSK	cathepsin K	2536
CYR61	cysteine-rich, angiogenic inducer, 61	2654
DCAF4	DDB1 and CUL4 associated factor 4	20229
DDIT3	DNA-damage-inducible transcript 3	2726
DDIT4	DNA-damage-inducible transcript 4	24944
DNAJB1	DnaJ (Hsp40) homolog, subfamily B, member 1	5270
DPP4	dipeptidyl-peptidase 4	3009
DSP	desmoplakin	3052
DUSP1	dual specificity phosphatase 1	3064
EGR1	early growth response 1	3238
EIF4EBP1	eukaryotic translation initiation factor 4E binding protein 1	3288
EPDR1	ependymin related protein 1	17572
EPS8L2	EPS8-like 2	21296
F2R	coagulation factor II (thrombin) receptor	3537
FAM118A	family with sequence similarity 118, member A	1313
FAM43A	family with sequence similarity 43, member A	26888
FBXO32	F-box protein 32	16731
FGF7	fibroblast growth factor 7	3685
FNDC4	fibronectin type III domain containing 4	20239
FOSB	FBJ murine osteosarcoma viral oncogene homolog B	3797
FOXO3	forkhead box O3	3821
GADD45A	growth arrest and DNA-damage-inducible, alpha	4095
GADD45B	growth arrest and DNA-damage-inducible, beta	4096
GALNTL2	UDP-N-acetyl-alpha-D-galactosamine:polypeptide N-acetylgalactosaminyltransferase-like 2	21531
GAS1	growth arrest-specific 1	4165
GAS5	small nucleolar RNA, C/D box 44	10183
GAS6	growth arrest-specific 6	4168
GDF15	growth differentiation factor 15	30142
GDF6	growth differentiation factor 6	4221
GLRX	glutaredoxin (thioltransferase)	4330
GNG11	guanine nucleotide binding protein (G protein), gamma 11	4403
GYPC	glycophorin C (Gerbich blood group)	4704
HAND2	heart and neural crest derivatives expressed 2	4808
HAPLN3	hyaluronan and proteoglycan link protein 3	21446

Gene Symbol	**Gene Description**	Source: HGNC Symbol; Acc
HERPUD1	homocysteine-inducible, endoplasmic reticulum stress-inducible, ubiquitin-like domain member 1	13744
HIST2H2BE	histone cluster 2, H2be	4760
HMOX1	heme oxygenase (decycling) 1	5013
HNRNPA1	heterogeneous nuclear ribonucleoprotein A1	5031
HOXB7	homeobox B7	5118
HOXC10	homeobox C10	5122
HOXC9	homeobox C9	5130
HS3ST3A1	heparan sulfate (glucosamine) 3-O-sulfotransferase 3A1	5196
HSD3B7	hydroxy-delta-5-steroid dehydrogenase, 3 beta- and steroid delta-isomerase 7	18324
HSPA2	heat shock 70kDa protein 2	5235
HSPB7	heat shock 27kDa protein family, member 7	5249
ID1	inhibitor of DNA binding 1, dominant negative helix-loop-helix protein	5360
ID3	inhibitor of DNA binding 3, dominant negative helix-loop-helix protein	5362
IER3	Radiation-inducible immediate-early gene IEX-1 (Immediate early protein GLY96)(Immediate early response 3 protein)	P46695
IGFBP4	insulin-like growth factor binding protein 4	5473
IL13RA2	interleukin 13 receptor, alpha 2	5975
IL20RB	interleukin 20 receptor beta	6004
IL6	interleukin 6 (interferon, beta 2)	6018
IRF2BP2	interferon regulatory factor 2 binding protein 2	21729
IRS2	insulin receptor substrate 2	6126
JUN	jun proto-oncogene	6204
JUND	jun D proto-oncogene	6206
KCNE4	potassium voltage-gated channel, Isk-related family, member 4	6244
KRT34	keratin 34	6452
KRTAP1-5	keratin associated protein 1-5	16777
LBH	limb bud and heart development homolog (mouse)	29532
LDOC1	leucine zipper, down-regulated in cancer 1	6548
LGALS3BP	lectin, galactoside-binding, soluble, 3 binding protein	6564
LGR4	leucine-rich repeat-containing G protein-coupled receptor 4	13299
LIF	leukemia inhibitory factor (cholinergic differentiation factor)	6596
LMCD1	LIM and cysteine-rich domains 1	6633
LMO7	LIM domain 7	6646
LRRC15	leucine rich repeat containing 15	20818
MFAP5	microfibrillar associated protein 5	29673
MIDN	midnolin	16298
MMP1	matrix metallopeptidase 1 (interstitial collagenase)	7155
MMS19	MMS19 nucleotide excision repair homolog (S. cerevisiae)	13824
MOXD1	monooxygenase, DBH-like 1	21063
MT1E	metallothionein 1L (gene/pseudogene)	7404

Gene Symbol	Gene Description	Source: HGNC Symbol; Acc
MT2A	metallothionein 2A	7406
MUC1	mucin 1, cell surface associated	7508
MYADM	myeloid-associated differentiation marker	7544
MYC	v-myc myelocytomatosis viral oncogene homolog (avian)	7553
MYL9	myosin, light chain 9, regulatory	15754
MYLK	myosin light chain kinase	7590
NBL1	neuroblastoma, suppression of tumorigenicity 1	7650
NQO1	NAD(P)H dehydrogenase, quinone 1	2874
PAM	peptidylglycine alpha-amidating monooxygenase	8596
PCDH10	protocadherin 10	13404
PHGDH	phosphoglycerate dehydrogenase	8923
PIK3IP1	phosphoinositide-3-kinase interacting protein 1	24942
PLEKHO2	pleckstrin homology domain containing, family O member 2	30026
PLXNB1	plexin B1	9103
PMP22	peripheral myelin protein 22	9118
POSTN	periostin, osteoblast specific factor	16953
PPP1R3C	protein phosphatase 1, regulatory (inhibitor) subunit 3C	9293
PRSS23	Serine protease 23 Precursor (EC 3.4.21.-)(Putative secreted protein Zsig13)	560
PSG1	pregnancy specific beta-1-glycoprotein 1	9514
PSG4	pregnancy specific beta-1-glycoprotein 4	9521
PTGES	prostaglandin E synthase	9599
PTGIS	prostaglandin I2 (prostacyclin) synthase	9603
PTGS1	prostaglandin-endoperoxide synthase 1 (prostaglandin G/H synthase and cyclooxygenase)	9604
QPCT	glutaminyl-peptide cyclotransferase	9753
RAB3B	RAB3B, member RAS oncogene family	9778
RPL22L1	ribosomal protein L22-like 1	27610
RPL36A	ribosomal protein L36a	135255
RPS21	ribosomal protein S21	10409
RPS3	ribosomal protein S3	10420
RSPO3	R-spondin 3 homolog (Xenopus laevis)	20866
SERINC2	serine incorporator 2	23231
SERPINH1	serpin peptidase inhibitor, clade H (heat shock protein 47), member 1, (collagen binding protein 1)	1546
SFRP4	secreted frizzled-related protein 4	10778
SGK1	serum/glucocorticoid regulated kinase 1	10810
SH3BGR	SH3 domain binding glutamic acid-rich protein	10822
SLC16A3	solute carrier family 16, member 3 (monocarboxylic acid transporter 4)	10924
SLC2A1	solute carrier family 2 (facilitated glucose transporter), member 1	11005
SMAD7	SMAD family member 7	6773

Gene Symbol	**Gene Description**	Source: HGNC Symbol; Acc
SOCS1	suppressor of cytokine signaling 1	19383
SPON2	spondin 2, extracellular matrix protein	11253
STBD1	starch binding domain 1	24854
STC2	stanniocalcin 2	11374
STMN2	stathmin-like 2	10577
SYNPO2	synaptopodin 2	17732
TBX1	T-box 1	11592
TFPI2	"tissue factor pathway inhibitor 2	11761
TGM2	transglutaminase 2 (C polypeptide, protein-glutamine-gamma-glutamyltransferase)	11778
THBS1	thrombospondin 1	11785
THBS2	thrombospondin 2	11786
TM4SF1	transmembrane 4 L six family member 1	11853
TNFRSF12A	tumor necrosis factor receptor superfamily, member 12A	18152
TOB1	transducer of ERBB2, 1	11979
TSC22D3	TSC22 domain family, member 3	3051
UCHL1	ubiquitin carboxyl-terminal esterase L1 (ubiquitin thiolesterase)	12513
WISP2	WNT1 inducible signaling pathway protein 2	12770
WNT5B	wingless-type MMTV integration site family, member 5B	16265
XG	Xg pseudogene, Y-linked 2	34022
ZNF503	zinc finger protein 503	23589
REFERENCE GENES		
G6PD	glucose-6-phosphate dehydrogenase	4057
GAPDH	glyceraldehyde-3-phosphate dehydrogenase	4141
YWHAZ	tyrosine 3-monooxygenase/tryptophan 5-monooxygenase activation protein, zeta polypeptide	12855

Table B. Expression levels of 176 deregulated genes in the TTD pool and the Control pool in basal condition

Gene Symbol	TTD pool		Control pool		Fold Change[b]
	C_t Mean±SD	ΔC_t[a]	C_t Mean±SD	ΔC_t[a]	
TM4SF1	25,57±0,08	0,15	27,42±0,21	3,19	8,253
PCDH10	27,76±0,23	2,33	28,82±0,25	4,59	4,790
PSG1	26,41±0,01	0,98	27,29±0,19	3,06	4,238
CLGN	29,54±0,25	4,12	30,04±0,23	5,82	3,253
SOCS1	28,81±0,13	3,57	29,29±0,27	5,25	3,223
GNG11	33,13±0,03	7,71	33,59±0,13	9,36	3,157
IL13RA2	25,83±0,14	0,41	26,26±0,30	2,04	3,099
HSPA2	26,42±0,14	1,18	26,71±0,43	2,67	2,809
TFPI2	24,14±0,25	-1,29	24,28±0,39	0,06	2,534
MP1	22,46±0,17	-2,97	22,51±0,55	-1,72	2,370
RPL36A	19,96±0,00	-5,28	19,94±0,07	-4,09	2,276
CCRL1	24,68±0,15	-0,57	24,66±0,51	0,62	2,274
ADRA2A	26,75±0,21	1,32	26,64±0,20	2,42	2,139
HOXC10	28,82±0,01	3,40	28,68±1,20	4,45	2,078
TOB1	25,65±0,27	0,41	25,47±0,30	1,43	2,033
RPS21	20,89±0,19	-4,36	20,68±0,13	-3,36	1,998
FAM43A	24,57±0,16	-0,67	24,32±0,47	0,28	1,936
UCHL1	23,73±0,23	-1,51	23,48±0,38	-0,56	1,932
CRYAB	30,34±0,86	4,92	30,08±0,55	5,85	1,912
FOSB	29,26±0,09	4,02	28,95±0,70	4,91	1,860
ARHGAP23	28,98±0,11	3,74	28,58±0,74	4,55	1,755
C4orf49	28,14±0,11	2,72	27,73±0,13	3,51	1,731
PIK3IP1	29,31±0,12	3,88	28,80±1,21	4,58	1,621
ID1	21,63±0,14	-3,61	21,12±0,11	-2,91	1,621
AP1S2	26,13±0,33	0,71	25,62±0,18	1,39	1,608
CRABP2	25,01±0,06	-0,41	24,48±1,16	0,26	1,593
PTGES	29,72±0,08	4,30	29,18±1,12	4,96	1,582
JUND	31,63±0,06	6,39	31,08±0,60	7,04	1,569
GLRX	25,87±0,24	0,63	25,16±0,31	1,13	1,411
PAM	24,05±0,36	-1,20	23,34±0,35	-0,70	1,409
CLEC3B	29,26±0,11	3,83	28,53±1,25	4,31	1,392
MALL	27,45±0,10	2,03	26,72±1,36	2,49	1,380
LGR4	28,15±0,04	2,91	27,39±1,28	3,35	1,360
ZNF503	25,52±0,11	0,10	24,76±0,25	0,53	1,355

Gene Symbol	TTD pool		Control pool		Fold Change[b]
	C_t Mean±SD	ΔC_t[a]	C_t Mean±SD	ΔC_t[a]	
EPS8L2	30,89±0,29	5,65	30,06±0,87	6,02	1,297
ADM	28,41±0,21	3,17	27,50±1,18	3,47	1,233
CAMK2N1	33,25±0,32	7,82	32,33±0,54	8,10	1,214
MYLK	29,17±0,27	3,75	28,25±0,95	4,02	1,213
CTSC	27,58±0,07	2,34	26,65±0,90	2,61	1,209
PPP1R3C	28,08±0,19	2,84	27,14±1,17	3,11	1,207
SYNPO2	33,46±0,16	8,03	32,53±1,00	8,30	1,206
MALAT1	32,72±0,13	7,48	31,77±1,04	7,73	1,196
CNN1	29,51±0,21	4,27	28,55±1,32	4,51	1,184
IRF2BP2	27,24±0,01	2,00	26,27±1,01	2,23	1,176
RSPO3	27,29±0,06	2,05	26,30±0,83	2,26	1,163
LDOC1	30,76±0,08	5,33	29,76±1,06	5,53	1,149
KRTAP1-5	27,86±0,16	2,44	26,86±1,17	2,63	1,145
ASS1	26,83±0,09	1,40	25,81±1,09	1,58	1,133
C16orf72	27,43±0,37	2,19	26,40±0,25	2,36	1,129
FGF7	23,41±0,11	-2,02	22,38±0,39	-1,85	1,121
IGFBP4	26,16±0,11	0,73	25,11±0,46	0,88	1,110
MOXD1	26,11±0,08	0,68	25,06±1,02	0,83	1,110
KCNE4	33,69±0,32	8,45	32,62±1,26	8,58	1,101
SH3BGR	30,18±0,18	4,76	29,12±0,43	4,89	1,101
ANGPTL4	29,86±0,10	4,62	28,76±0,96	4,73	1,077
CCDC8	28,17±0,52	2,93	27,06±0,57	3,03	1,073
MT1E	25,35±0,35	0,11	24,24±0,43	0,20	1,064
NQO1	25,98±0,04	0,56	24,87±0,82	0,64	1,063
COL4A1	30,06±0,13	4,64	28,94±0,88	4,72	1,058
HIST2H2BE	27,58±0,11	2,34	26,45±0,79	2,41	1,056
CRYZ	31,75±0,14	6,33	30,63±0,54	6,40	1,056
JUN	26,17±0,40	0,92	25,03±0,23	0,99	1,046
NBL1	28,85±0,27	3,43	27,71±0,72	3,48	1,039
SPON2	27,69±0,08	2,27	26,53±1,13	2,30	1,025
ALDH1A3	27,12±0,06	1,70	25,95±1,00	1,73	1,022
FOXO3	32,68±0,06	7,44	31,50±1,25	7,46	1,020
HOXC9	31,02±0,07	5,60	29,84±1,08	5,61	1,010
DNAJB1	29,89±0,11	4,65	28,70±1,05	4,66	1,009
SLC16A3	27,74±0,05	2,31	26,54±1,33	2,32	1,005
MMS19	30,23±0,09	4,99	29,03±1,14	4,99	1,003
FAM118A	30,98±0,13	5,74	29,76±0,82	5,73	-1,009
RAB3B	30,44±0,13	5,02	29,22±0,89	4,99	-1,017
EGR1	26,12±0,03	0,88	24,88±0,92	0,84	-1,028
THBS2	26,01±0,20	0,59	24,77±0,83	0,54	-1,032
ALDH3B1	29,72±0,08	4,29	28,44±1,03	4,21	-1,055
DDIT4	29,36±0,06	4,12	28,07±0,91	4,03	-1,058

Table B. ***(continued)*** **Expression levels of 176 deregulated genes in the TTD pool and the Control pool in basal condition.**

Gene Symbol	TTD pool		Control pool		Fold Change[b]
	C_t Mean±SD	ΔC_t[a]	C_t Mean±SD	ΔC_t[a]	
THBS1	20,77±0,16	-4,48	19,48±1,25	-4,56	-1,061
PLEKHO2	30,67±0,11	5,43	29,38±0,75	5,34	-1,061
TGM2	36,44±0,32	11,01	35,15±1,51	10,92	-1,062
ANTXR1	26,20±0,04	0,96	24,90±1,01	0,87	-1,067
CABLES1	32,62±0,00	7,38	31,31±1,14	7,28	-1,074
HSPB7	26,80±0,19	1,37	25,49±0,94	1,27	-1,074
DUSP1	24,80±0,00	-0,44	23,48±1,08	-0,56	-1,084
ANP32A	27,77±0,08	2,53	26,45±0,98	2,41	-1,087
PLXNB1	28,24±0,16	2,81	26,91±0,82	2,69	-1,089
KRT34	29,32±0,05	4,08	27,99±1,00	3,95	-1,091
TNFRSF12A	25,62±0,01	0,38	24,29±0,93	0,25	-1,092
FNDC4	29,90±0,02	4,47	28,56±1,28	4,34	-1,097
QPCT	30,43±0,01	5,19	29,08±0,88	5,04	-1,107
ACOT1	29,88±0,05	4,45	28,53±1,01	4,30	-1,110
C1orf198	26,68±0,05	1,25	25,33±1,29	1,10	-1,110
MUC1	29,53±0,03	4,29	28,16±1,13	4,13	-1,120
MFAP5	23,94±0,30	-1,31	22,56±0,48	-1,48	-1,126
XG	27,53±0,06	2,11	26,16±0,43	1,93	-1,129
HS3ST3A1	28,81±0,02	3,57	27,42±1,08	3,38	-1,134
HNRNPA1	29,25±0,49	4,01	27,86±0,43	3,82	-1,137
ID3	24,79±0,05	-0,46	23,38±1,12	-0,65	-1,147
RPS3	22,66±0,06	-2,59	21,24±0,84	-2,80	-1,158
STBD1	28,03±0,21	2,79	26,61±0,69	2,57	-1,165
GAS6	25,66±0,10	0,24	24,24±1,34	0,01	-1,166
LMO7	23,73±0,25	-1,70	22,30±0,57	-1,92	-1,171
MIDN	27,44±0,16	2,20	25,99±0,95	1,96	-1,180
AKAP2	25,42±0,18	0,18	23,97±0,79	-0,07	-1,186
C8orf58	29,36±0,30	4,12	27,86±0,75	3,82	-1,228
STC2	29,15±0,25	3,73	27,65±1,22	3,43	-1,230
GADD45B	33,06±0,57	7,82	31,53±1,31	7,50	-1,251
LMCD1	25,86±0,13	0,62	24,32±1,15	0,28	-1,258
MYL9	23,14±0,03	-2,29	21,59±1,22	-2,63	-1,273
AHR	27,69±0,02	2,45	26,13±0,86	2,09	-1,279
GAS1	28,58±0,07	3,34	27,02±1,04	2,98	-1,280
C15orf39	30,41±0,36	5,17	28,80±0,68	4,76	-1,321
HSD3B7	28,46±0,12	3,03	26,84±0,80	2,61	-1,338
SMAD7	28,28±0,24	2,86	26,66±1,23	2,43	-1,343
CTSK	23,87±0,10	-1,37	22,24±0,99	-1,80	-1,344
CYR61	22,82±0,16	-2,42	21,19±1,04	-2,85	-1,347

Gene Symbol	TTD pool		Control pool		Fold Change[b]
	C_t Mean±SD	ΔC_t[a]	C_t Mean±SD	ΔC_t[a]	
MYC	27,13±0,21	1,89	25,46±0,71	1,42	-1,380
ALDH1B1	30,16±0,21	4,73	28,49±1,15	4,26	-1,382
LIF	27,56±0,11	2,32	25,88±0,79	1,85	-1,384
EPDR1	28,43±0,18	3,00	26,76±1,00	2,53	-1,385
WNT5B	28,18±0,13	2,75	26,50±1,19	2,27	-1,392
CRLF1	28,85±0,11	3,42	27,17±1,27	2,94	-1,392
AP000654.2	27,55±0,08	2,31	25,84±0,86	1,81	-1,417
MT2A	22,73±0,20	-2,51	21,00±0,82	-3,04	-1,441
GAS5	33,98±0,04	8,56	32,24±0,70	8,02	-1,452
DCAF4	30,91±0,05	5,67	29,15±1,33	5,11	-1,469
GYPC	29,55±0,01	4,13	27,79±1,01	3,57	-1,473
HMOX1	26,22±0,04	0,98	24,43±1,27	0,40	-1,498
SLC2A1	29,95±0,01	4,71	28,15±1,24	4,12	-1,509
LRRC32	29,90±0,21	4,48	28,07±0,98	3,85	-1,546
PSG4	26,94±0,15	1,51	25,10±0,17	0,88	-1,551
AKR1C2	27,14±0,02	1,90	25,28±1,17	1,25	-1,567
PMP22	27,97±0,06	2,54	26,12±1,11	1,89	-1,569
SERPINH1	24,78±0,01	-0,46	22,92±1,24	-1,12	-1,580
IRS2	26,57±0,30	1,33	24,69±0,52	0,66	-1,595
LGALS3BP	29,55±0,06	4,12	27,65±1,22	3,43	-1,617
IL6	29,44±0,23	4,20	27,53±0,77	3,49	-1,636
SERINC2	31,18±0,36	5,75	29,27±1,30	5,04	-1,636
SGK1	25,63±0,06	0,39	23,69±1,03	-0,34	-1,662
C14orf4	30,98±0,01	5,74	29,03±1,23	4,99	-1,672
DSP	27,92±0,13	2,50	25,96±0,84	1,73	-1,695
ATP13A3	27,41±0,14	1,99	25,44±1,10	1,21	-1,707
GADD45A	30,08±0,49	4,84	28,10±0,93	4,06	-1,707
TSC22D3	30,41±0,11	5,17	28,43±1,28	4,39	-1,717
F2R	29,15±0,12	3,72	27,15±1,14	2,92	-1,741
RPL22L1	33,28±0,10	7,86	31,26±0,17	7,04	-1,763
DDIT3	28,68±0,21	3,44	26,65±0,58	2,61	-1,774
PHGDH	29,40±0,27	3,98	27,36±1,41	3,14	-1,788
FBXO32	30,25±0,04	5,01	28,20±0,95	4,16	-1,798
DPP4	27,24±0,28	1,81	25,19±1,01	0,96	-1,803
CLIC3	34,99±0,33	9,57	32,91±1,64	8,68	-1,847
IER3	24,90±0,02	-0,35	22,80±1,07	-1,23	-1,851
ATF5	28,68±0,03	3,26	26,58±1,20	2,36	-1,864
CTGF	24,69±0,49	-0,56	22,58±0,68	-1,46	-1,873
MYADM	31,02±0,21	5,78	28,87±1,43	4,83	-1,927
EIF4EBP1	27,24±0,08	2,00	24,92±1,02	0,89	-2,163
GALNTL2	30,15±0,05	4,72	27,82±0,98	3,59	-2,184
SFRP4	30,10±0,10	4,68	27,68±0,55	3,45	-2,338
GDF15	36,48±0,31	11,24	34,02±1,21	9,98	-2,395
LBH	27,55±0,04	2,31	25,08±1,04	1,04	-2,398

Gene Symbol	TTD pool		Control pool		Fold Change[b]
	C_t Mean±*SD*	**ΔC_t[a]**	**C_t Mean±**SD	**ΔC_t[a]**	
HAPLN3	31,15±0,15	5,72	28,67±1,19	4,44	-2,428
LRRC15	29,22±0,16	3,79	26,69±1,25	2,47	-2,502
POSTN	28,07±0,08	2,64	25,52±1,05	1,29	-2,543
PTGS1	29,34±0,21	3,91	26,75±1,21	2,52	-2,615
STMN2	25,68±0,30	0,26	23,08±0,61	-1,15	-2,642
CLU	25,18±0,03	-0,24	22,53±1,19	-1,70	-2,742
APBB1IP	33,36±0,22	7,93	30,70±1,03	6,47	-2,745
HAND2	30,93±0,04	5,50	28,15±1,05	3,93	-2,976
HOXB7	36,54±0,66	11,30	33,62±1,11	9,58	-3,294
CSRP2	28,53±0,14	3,11	25,60±0,61	1,37	-3,321
GPX3	37,69±0,29	12,26	34,66±1,34	10,43	-3,555
PTGIS	29,02±0,17	3,60	25,79±1,15	1,56	-4,098
TBX1	34,70±0,57	9,28	31,17±0,92	6,95	-5,022
HERPUD1	31,69±0,34	6,45	28,03±0,87	3,99	-5,489
IL20RB	32,02±0,16	6,60	27,78±1,10	3,55	-8,234
GDF6	35,58±0,21	10,34	30,88±0,85	6,84	-11,249
WISP2	33,51±0,00	8,09	28,76±0,20	4,53	-11,726

Table C. Expression levels of 176 deregulated genes in the TTD pool and the Control pool after UV-irradiation

Gene Symbol	TTD pool		Control pool		Fold Change[b]
	Ct Mean±SD	ΔC_t[a]	Ct Mean±SD	ΔC_t[a]	
HOXB7	34,71±0,98	10,31	37,43±3,64	12,20	3,702
HOXC10	27,66±1,14	3,07	30,04±0,21	4,61	2,891
PCDH10	27,62±0,22	3,03	29,64±0,24	4,21	2,266
CRABP2	23,85±1,20	-0,74	25,74±0,25	0,31	2,063
QPCT	28,87±1,01	4,47	30,69±0,60	5,46	1,979
ARHGAP23	28,37±1,12	3,97	30,07±0,02	4,84	1,821
CCRL1	23,86±0,58	-0,54	25,51±0,34	0,28	1,761
MMP1	21,72±0,50	-2,87	23,36±0,47	-2,07	1,737
TM4SF1	26,38±0,05	1,79	27,93±0,06	2,50	1,636
ASS1	25,82±1,24	1,23	27,33±0,16	1,90	1,582
CLEC3B	28,14±1,32	3,55	29,64±0,23	4,21	1,578
MALL	26,69±1,37	2,10	28,18±0,05	2,75	1,564
PIK3IP1	28,10±1,25	3,51	29,56±0,04	4,13	1,537
HSPA2	25,76±0,37	1,36	27,17±0,40	1,94	1,498
KRTAP1-5	26,70±1,29	2,11	28,05±0,18	2,62	1,427
IL13RA2	25,54±0,28	0,95	26,89±0,11	1,46	1,416
DDIT4	27,70±1,00	3,30	29,02±0,12	3,79	1,400
TFPI2	23,89±0,56	-0,70	25,16±0,46	-0,28	1,343
CLGN	29,30±0,33	4,71	30,56±0,35	5,13	1,338
LGR4	27,72±1,41	3,32	28,96±0,03	3,73	1,332
HOXC9	29,62±0,94	5,03	30,85±0,16	5,42	1,303
MOXD1	25,13±1,16	0,54	26,35±0,26	0,92	1,300
CTSC	26,50±0,99	2,10	27,70±0,38	2,47	1,289
PTGES	29,47±1,25	4,88	30,67±0,04	5,24	1,283
RSPO3	26,49±0,83	2,09	27,67±0,12	2,44	1,273
MUC1	28,23±1,25	3,83	29,36±0,27	4,13	1,234
GAS1	27,35±1,17	2,95	28,47±0,32	3,24	1,216
FNDC4	28,71±1,47	4,12	29,82±0,28	4,39	1,206
PPP1R3C	27,36±1,42	2,96	28,46±0,04	3,23	1,203
CABLES1	31,84±1,26	7,44	32,94±0,01	7,71	1,199
C1orf198	26,05±1,42	1,46	27,14±0,20	1,71	1,186
PSG1	26,44±0,08	1,85	27,52±0,21	2,09	1,180
MALAT1	31,12±1,21	6,72	32,16±0,25	6,93	1,154
MYADM	29,86±1,62	5,46	30,90±0,25	5,67	1,154

Gene Symbol	TTD pool		Control pool		Fold Change[b]
	C_t Mean±SD	ΔC_t[a]	C_t Mean±SD	ΔC_t[a]	
MYLK	28,38±1,21	3,79	29,38±0,16	3,95	1,113
AKR1C2	25,74±1,17	1,34	26,68±0,14	1,45	1,077
ADM	27,48±1,13	3,08	28,41±0,20	3,18	1,069
HIST2H2BE	26,90±1,23	2,50	27,82±0,09	2,59	1,063
ACOT1	28,77±1,17	4,18	29,70±0,20	4,27	1,062
ANP32A	26,69±1,09	2,29	27,58±0,24	2,35	1,040
NQO1	25,00±0,79	0,41	25,89±0,31	0,46	1,033
CRYZ	30,87±0,74	6,28	31,75±0,61	6,32	1,030
MMS19	29,47±1,40	5,07	30,35±0,16	5,12	1,029
AP000654.2	26,36±1,16	1,96	27,23±0,17	2,00	1,028
LDOC1	29,77±1,14	5,18	30,64±0,25	5,21	1,021
FOXO3	32,68±1,42	8,28	33,53±0,11	8,30	1,010
SYNPO2	32,79±1,15	8,20	33,64±0,20	8,21	1,009
GAS6	24,65±1,49	0,06	25,50±0,18	0,07	1,006
UCHL1	23,26±0,57	-1,14	24,06±0,35	-1,17	-1,021
CNN1	28,55±1,25	4,15	29,35±0,16	4,12	-1,025
ALDH1A3	26,47±1,10	1,88	27,28±0,08	1,85	-1,027
ALDH3B1	28,61±1,25	4,02	29,38±0,14	3,95	-1,050
RAB3B	29,81±1,11	5,22	30,57±0,19	5,14	-1,058
EPS8L2	29,93±1,15	5,53	30,66±0,11	5,43	-1,072
PMP22	27,08±1,36	2,49	27,82±0,16	2,39	-1,074
LMO7	23,04±0,59	-1,55	23,77±0,44	-1,66	-1,077
ADRA2A	26,34±0,18	1,75	27,06±0,21	1,63	-1,084
IL6	27,68±1,09	3,28	28,39±0,28	3,16	-1,093
C14orf4	29,94±1,53	5,54	30,64±0,09	5,41	-1,096
CTSK	22,72±1,09	-1,68	23,42±0,16	-1,82	-1,098
AHR	26,86±1,13	2,46	27,55±0,14	2,32	-1,104
KCNE4	31,86±1,38	7,46	32,50±0,06	7,27	-1,142
DNAJB1	28,79±1,18	4,39	29,43±0,22	4,20	-1,147
FOSB	28,25±1,06	3,85	28,88±0,05	3,65	-1,155
PLXNB1	27,29±0,84	2,70	27,91±0,34	2,48	-1,162
PLEKHO2	30,07±1,09	5,67	30,68±0,13	5,45	-1,171
SLC16A3	27,13±1,23	2,54	27,74±0,21	2,31	-1,173
STC2	28,16±1,38	3,57	28,76±0,10	3,33	-1,181
DUSP1	23,56±1,27	-0,84	24,14±0,30	-1,10	-1,191
THBS1	20,45±1,43	-3,95	21,02±0,07	-4,21	-1,195
CRYAB	30,21±0,36	5,62	30,79±0,33	5,36	-1,202
SPON2	26,86±1,08	2,27	27,43±0,18	2,00	-1,210
LMCD1	25,89±1,28	1,49	26,43±0,23	1,20	-1,227
ANTXR1	25,31±1,11	0,91	25,85±0,09	0,62	-1,230
PAM	23,54±0,31	-0,86	24,07±0,35	-1,16	-1,231
JUND	30,75±0,92	6,35	31,27±0,03	6,04	-1,243
STBD1	27,45±0,71	3,05	27,95±0,25	2,72	-1,258
AKAP2	24,85±0,95	0,45	25,32±0,33	0,08	-1,285

Table C. ***(continued)*** **Expression levels of 176 deregulated genes in the TTD pool and the Control pool after UV-irradiation**

Gene Symbol	TTD pool		Control pool		Fold Change[b]
	C_t Mean±SD	ΔC_t[a]	C_t Mean±SD	ΔC_t[a]	
SERPINH1	23,70±1,34	-0,70	24,16±0,02	-1,08	-1,300
MYL9	22,20±1,20	-2,39	22,66±0,02	-2,78	-1,309
FAM118A	30,58±0,85	6,18	31,03±0,01	5,80	-1,309
DCAF4	30,39±1,40	5,99	30,82±0,13	5,59	-1,320
RPS3	21,59±1,01	-2,81	22,01±0,28	-3,23	-1,330
HNRNPA1	28,32±0,54	3,92	28,74±0,23	3,51	-1,332
MIDN	27,03±1,16	2,63	27,45±0,06	2,22	-1,336
F2R	28,21±1,42	3,62	28,63±0,19	3,20	-1,343
CCDC8	28,17±0,48	3,77	28,57±0,37	3,34	-1,350
HSD3B7	27,27±0,93	2,68	27,67±0,29	2,24	-1,358
LIF	27,16±1,19	2,76	27,55±0,05	2,32	-1,358
IRF2BP2	27,14±1,24	2,74	27,53±0,19	2,30	-1,364
TOB1	25,05±0,31	0,65	25,43±0,23	0,20	-1,366
C4orf49	27,83±0,13	3,24	28,22±0,37	2,79	-1,368
SGK1	24,36±1,25	-0,04	24,73±0,11	-0,50	-1,379
COL4A1	29,84±1,16	5,25	30,21±0,13	4,78	-1,382
SMAD7	29,46±1,29	4,87	29,84±0,18	4,41	-1,384
EPDR1	27,48±1,16	2,89	27,86±0,23	2,43	-1,384
MFAP5	23,16±0,54	-1,24	23,51±0,33	-1,72	-1,398
GLRX	25,39±0,32	0,99	25,72±0,20	0,49	-1,411
GNG11	33,55±0,22	8,96	33,89±0,24	8,46	-1,417
DSP	27,43±1,25	2,84	27,77±0,13	2,34	-1,417
SERINC2	30,31±1,58	5,72	30,65±0,35	5,22	-1,417
CLIC3	33,87±1,61	9,28	34,20±0,08	8,77	-1,421
LRRC32	29,18±1,28	4,59	29,52±0,36	4,09	-1,422
WNT5B	27,58±1,32	2,99	27,91±0,21	2,48	-1,429
NBL1	28,14±1,01	3,55	28,47±0,12	3,04	-1,429
AP1S2	25,82±0,11	1,23	26,13±0,31	0,70	-1,444
KRT34	28,52±1,20	4,12	28,82±0,08	3,59	-1,444
CRLF1	28,03±1,52	3,44	28,34±0,32	2,91	-1,446
ATP13A3	27,38±1,33	2,79	27,67±0,14	2,24	-1,464
HMOX1	26,02±1,28	1,62	26,27±0,04	1,04	-1,504
SOCS1	28,27±0,38	3,87	28,51±0,40	3,28	-1,509
HERPUD1	30,02±1,30	5,62	30,25±0,85	5,02	-1,516
THBS2	25,54±0,90	0,95	25,78±0,08	0,35	-1,519
DPP4	26,21±1,26	1,62	26,45±0,17	1,02	-1,519
PHGDH	28,37±1,34	3,78	28,60±0,34	3,17	-1,523
TNFRSF12A	25,03±1,05	0,63	25,25±0,24	0,02	-1,530
GDF15	33,95±1,26	9,55	34,16±0,12	8,93	-1,539

Gene Symbol	TTD pool		Control pool		Fold Change[b]
	C_t Mean±SD	ΔC_t[a]	C_t Mean±SD	ΔC_t[a]	
HSPB7	26,27±1,13	1,68	26,49±0,20	1,06	-1,540
FBXO32	29,58±1,20	5,18	29,79±0,07	4,56	-1,540
FGF7	23,48±0,54	-1,11	23,69±0,48	-1,74	-1,548
GYPC	28,62±1,31	4,03	28,81±0,16	3,38	-1,573
MYC	25,92±0,79	1,52	26,09±0,30	0,86	-1,589
RPS21	20,74±0,12	-3,66	20,88±0,28	-4,35	-1,613
C8orf58	29,08±0,84	4,68	29,20±0,05	3,97	-1,638
IGFBP4	25,73±0,98	1,14	25,83±0,22	0,40	-1,680
ZNF503	25,21±0,30	0,62	25,30±0,20	-0,13	-1,686
C16orf72	27,91±0,17	3,51	27,96±0,34	2,73	-1,717
FAM43A	24,72±0,43	0,32	24,76±0,24	-0,47	-1,725
RPL36A	19,97±0,04	-4,43	20,00±0,17	-5,23	-1,737
SH3BGR	29,61±0,27	5,02	29,66±0,28	4,23	-1,739
HS3ST3A1	29,25±1,18	4,85	29,28±0,04	4,05	-1,743
CAMK2N1	33,13±0,49	8,54	33,17±0,70	7,74	-1,747
TGM2	36,78±1,61	12,19	36,78±0,16	11,35	-1,786
LGALS3BP	28,67±1,28	4,08	28,67±0,17	3,24	-1,786
LBH	27,03±1,14	2,63	26,97±0,23	1,74	-1,853
ID3	24,97±1,18	0,57	24,90±0,15	-0,34	-1,868
ATF5	27,57±1,30	2,98	27,49±0,15	2,06	-1,899
SLC2A1	29,72±1,40	5,32	29,63±0,04	4,40	-1,899
C15orf39	30,43±0,76	6,03	30,33±0,54	5,10	-1,907
EIF4EBP1	26,09±1,08	1,69	25,98±0,24	0,75	-1,919
CYR61	21,75±1,21	-2,65	21,64±0,13	-3,60	-1,930
MT1E	24,69±0,40	0,29	24,57±0,37	-0,66	-1,932
DDIT3	27,69±0,77	3,29	27,56±0,29	2,33	-1,948
GADD45A	28,24±1,05	3,84	28,11±0,15	2,88	-1,957
POSTN	27,19±1,37	2,60	27,05±0,09	1,62	-1,979
GALNTL2	29,21±1,17	4,62	29,06±0,33	3,63	-1,982
IRS2	26,01±0,55	1,61	25,85±0,36	0,62	-1,993
EGR1	24,55±1,15	0,15	24,37±0,14	-0,86	-2,009
ALDH1B1	29,76±1,29	5,17	29,55±0,00	4,12	-2,066
GAS5	31,61±0,74	7,02	31,37±0,23	5,94	-2,114
MT2A	21,95±0,86	-2,45	21,70±0,29	-3,54	-2,126
CLU	24,09±1,25	-0,50	23,83±0,21	-1,61	-2,151
XG	27,11±0,38	2,52	26,83±0,14	1,40	-2,168
TSC22D3	29,30±1,44	4,90	29,00±0,09	3,77	-2,191
LRRC15	28,31±1,45	3,72	27,96±0,18	2,53	-2,276
APBB1IP	32,36±1,37	7,77	31,94±0,08	6,51	-2,389
HAND2	29,92±1,04	5,33	29,48±0,47	4,05	-2,423
IER3	23,34±1,22	-1,06	22,90±0,12	-2,34	-2,426
PTGS1	28,40±1,23	3,81	27,85±0,17	2,42	-2,615
HAPLN3	30,71±1,25	6,12	30,11±0,14	4,68	-2,707

Gene Symbol	TTD pool		Control pool		Fold Change[b]
	C_t Mean±SD	ΔC_t[a]	C_t Mean±SD	ΔC_t[a]	
CSRP2	27,28±0,70	2,69	26,68±0,53	1,25	-2,729
STMN2	24,61±0,49	0,02	23,97±0,31	-1,46	-2,796
GPX3	36,61±1,58	12,02	35,95±0,00	10,52	-2,828
GADD45B	32,24±1,35	7,84	31,55±0,62	6,32	-2,868
SFRP4	29,33±0,62	4,74	28,61±0,35	3,18	-2,949
ANGPTL4	30,83±1,06	6,43	30,10±0,06	4,87	-2,966
CTGF	24,72±0,83	0,32	23,77±0,14	-1,46	-3,434
JUN	26,81±0,12	2,41	25,86±0,26	0,63	-3,438
PTGIS	28,10±1,33	3,51	26,94±0,07	1,51	-4,009
PSG4	26,62±0,13	2,03	25,33±0,42	-0,10	-4,382
RPL22L1	33,07±0,32	8,48	31,71±0,19	6,28	-4,611
ID1	22,57±0,06	-1,83	21,16±0,06	-4,08	-4,729
TBX1	34,10±1,24	9,51	32,46±0,18	7,03	-5,592
IL20RB	30,70±1,36	6,11	28,95±0,21	3,52	-6,028
GDF6	35,33±1,00	10,93	32,51±0,04	7,28	-12,568
WISP2	33,59±0,27	9,00	28,94±0,15	3,51	-45,203